PLANT EVAPOTRANSPIRATION IN A GREENHOUSE ON MARS

By

ERIN GEORGETTE WILKERSON

A DISSERTATION PRESENTED TO THE GRADUATE SCHOOL
OF THE UNIVERSITY OF FLORIDA IN PARTIAL FULFILLMENT
OF THE REQUIREMENTS FOR THE DEGREE OF
DOCTOR OF PHILOSOPHY

UNIVERSITY OF FLORIDA

2005

Dedicated to the memory of my grandmother, Elsie Bell Wilkerson, whose sweet spirit and strong faith will always challenge and encourage me

ACKNOWLEDGMENTS

I thank the engineers and scientists who took time from their busy schedules to invest in my professional development and my work. My major professor, Dr. Ray Bucklin, was a patient advisor and source of wisdom. He gave me freedom to explore my research topic, yet was readily available when problems arose. My committee, Dr. Khe Chau, Dr. Dennis McConnell, Dr. Jim Jones, and Dr. Charles Beatty, very kindly challenged me to be a better engineer and researcher. Dr. Ray Wheeler, Dr. Phil Fowler, and Dr. John Sager welcomed me to the Space Life Sciences Lab and took me under their wings while I learned the ropes at KSC. Dr. Hyeon-Hye Kim and the folks from Dynamac taught me how to grow radishes and always had answers to my many questions. The KSC Prototype Shop guys built some beautiful bases for me in exchange for a few cookies.

I may have learned a lot of math, biology, and physics these past three years, but I have learned so much more about myself and the wonderful people in my life. Dr. Stephanie Reeder may have grown up in Florida, but she was destined to find her way to the mountains and my life. The most beautiful engineers I know, Dr. Czarena Crofcheck, Dr. Mari Chinn, and Dr. Grace Danao, are the best colleagues and friends a girl could ask for. Jennifer DeFoe and Angela Archer have supported me for many years. I'm so blessed to have two such amazing cheerleaders in my corner! My beautiful, awesome "big sis" Kathy has enriched my life in so many ways. I always wanted a sister and I sure picked a good one! Newman Webb has very patiently put up with my fussing and

complaining the past couple of years, all the while reminding me what I was here for and all that I have to look forward to. And my wonderful family, Daddy, Momma, and Wesley, have loved and supported me unconditionally. They have taught me how to work hard and how to treat people right.

TABLE OF CONTENTS

LIST OF TABLES

LIST OF FIGURES

Abstract of Dissertation Presented to the Graduate School
of the University of Florida in Partial Fulfillment of the
Requirements for the Degree of Doctor of Philosophy

PLANT EVAPOTRANSPIRATION IN A GREENHOUSE ON MARS

By

Erin Georgette Wilkerson

December 2005

Chair: Ray A. Bucklin
Major Department: Agricultural and Biological Engineering

Successful crop production is vital to manned missions to Mars. Plants play integral roles in conceptual life-support systems as sources of food, oxygen, and waste treatment. Constraints of building a structure on the Martian surface to withstand Earth-similar interior air pressures make it necessary to develop plant growth systems capable of operating in air pressures as low as 0.1 to 0.3 atm (10 – 30 kPa). Research has shown that plants are capable of surviving in such environments, but have increased rates of water loss. The enormous costs associated with launching a manned mission to Mars make it crucial that plants be not only capable of survival, but also of producing fruit and seed. Plant growth and development, and thus, performance of a biological life-support system are highly dependent on plant environmental responses. Therefore, it is important that the interactions between plants and the environment of a Mars greenhouse are well understood.

A model was used to predict the rate of evapotranspiration in response to changes in pressure, CO_2, and light. The model was compared to empirical data obtained in experiments performed in a system of three small-scale low pressure controlled environment chambers built for this research. The system provided control of pressure, CO_2 concentration, air temperature, and relative humidity and measured plant weight and leaf temperature.

The rate of evapotranspiration changed little when pressure was 33 kPa and greater, but increased significantly at 12 kPa. Plants quickly wilted when pressure was 12 kPa and CO_2 was 40 Pa. Reduced pressure increased the rate of evapotranspiration by decreasing resistances to sensible and latent heat loss as well as reducing the effectiveness of convection. However, when CO_2 concentration was increased from 40 to 150 Pa, stomata closed and evapotranspiration decreased even at the lowest pressure. Thus, plants are capable of growing at extreme low pressures, but are more sensitive to changes in other environmental parameters. In a low pressure Mars greenhouse, failure of the control system will likely result in crop failure.

CHAPTER 1
GENERAL INTRODUCTION

For a long-term manned mission in space (~ 3 years), the costs of transporting and storing consumable resources (e.g. food, oxygen) are not feasible and resources must be produced in situ. Preliminary strategies for a manned mission to Mars include a greenhouse for the production of vascular plants. Growing plants provide essential life support functions such as food production, oxygen production and waste treatment (Drysdale et al., 1999) and psychological benefits associated with the sensory value of fresh food and of nurturing plants (Corey et al., 2002).

Figure 1-1. Artist's conception of a future Mars colony. The settlement includes an inflated greenhouse for food and production, oxygen production, and waste treatment.

Low-Pressure, Inflatable Greenhouse

One possible concept, currently being developed by researchers at the University of Florida and the Kennedy Space Center, is an inflatable greenhouse system. Such a system would be autonomous and could be deployed during an unmanned mission 100 to 120 days prior to the crew's arrival (Fowler et al., 2001). The purpose of a greenhouse on Mars is no different than on Earth - to overcome "climatic adversity" (Hanan, 1998). However, the Martian climate presents several new and interesting challenges. Reductions in gravity, atmospheric pressure, light levels, and temperature all significantly affect the design and control of a greenhouse (Bucklin et al., 2004). The climatic factor of greatest concern for plant growth and development is pressure.

The atmospheric pressure on Mars varies greatly with location, but is always less than one-hundredth that of Earth sea level (101.3 kPa) and for structural design purposes can be considered equal to zero (Bucklin et al., 2004). It is possible to build a structure capable of withstanding a pressure differential of 100 kPa as would result for a greenhouse maintaining Earth-similar pressures on Mars. However, the costs associated with such a massive structure are prohibitive. Also, it is desirable for the structure to be transparent in order to make use of the sun's radiant energy for plant photosynthesis as well as heating (Corey at al., 2002; Ferl et al., 2002). Consequently, it is important to minimize the pressure differential across the structure surface by maintaining a low atmospheric pressure within. No official decisions have been made regarding the internal pressure of a Mars greenhouse. Present strategies call for less than one-third the atmospheric pressure of Earth (Bucklin et al. 2004; Fowler et al., 2001).

Growing Plants in Reduced Pressures

Based on the results of previous studies, avoiding excessive water losses and subsequent dehydration is likely to be a challenge in maintaining productivity of plants in a low atmosphere Mars greenhouse (0.1 – 0.2 atm). Large reductions in atmospheric pressure have been shown to significantly increase the rate of evapotranspiration (Andre and Massimino, 1992; Corey at al., 1997; Daunicht and Brinkjans, 1992; Goto et al., 1995; Goto et al., 1996; Goto et al., 2002; Massimino and Andre, 1999; Rule and Staby, 1981; Rygalov et al., 2002). The most likely explanation for these increases is the inversely proportional relationship between pressure and mass diffusivity. As the mass diffusivities of CO_2 and water increase, so do the boundary layer and stomatal conductances to CO_2 and water exchange (Nobel, 1999; Monteith and Unsworth, 1990).

Because evapotranspiration is increased at low pressure, the health and productivity of plants grown at low pressures depends on their ability to maintain turgidity in an environment with a high transpirational load. In their studies on tomato plants, Daunicht and Brinkjans (1992), showed slight decreases (<10%) in biomass and leaf area and a slight increase (10%) in the dry weight of plants grown at 40 kPa versus 100 kPa (≈ Earth atmospheric pressure). On the last day of their study, the photosynthesis and transpiration rates were 12 and 39% higher, respectively, for the plants grown at the lower pressure. They concluded that, in spite of having a higher photosynthesis rate, plants grown at the lower pressure were most significantly affected by the increase in transpiration rate, which they considered to be the cause of reduced growth. In experiments by Goto et al. (2002) vegetative rice plants were grown in one of three total pressure environments: 34, 50, and 100 kPa. Growth, as measured by plant height and

dry weight, were statistically similar for 50 and 100 kPa, but significantly reduced at 34 kPa. They also concluded that this growth inhibition at extreme low pressures was caused by water stress. This is a reasonable conclusion based on earlier studies by the same research group in which rates of transpiration for maize were approximately four times higher at 10 kPa than at 100 kPa (Goto et al, 1996). Experiments to measure the open water surface evaporation by Rygalov et al. (2002) showed marked increases at total pressures less than 25 kPa. These low pressures ($\leq$ 25 kPa) correspond to the design internal pressure range currently being considered for the Mars greenhouse (Bucklin et al., 2004).

Increases in mass diffusivity may not be the only reason for increases in evapotranspiration at low pressures. Goto et al. (1996) incorporated a simple model for the changes in stomatal and boundary layer resistances at low pressures to predict transpiration rate as a function of vapor pressure deficit (VPD) and resistance to water vapor transfer. In this model, the resistances were adjusted proportional to changes in mass diffusivity as pressure decreased. In other words, it was assumed that the stomatal opening remained the same at all pressures and changes in stomatal resistance were caused only by an increase in the mass diffusivity of water vapor. With their assumptions that stomatal and boundary layer resistances were affected only by pressure and VPD remained constant, the measured transpiration rates showed smaller incremental increases than simulated rates. Goto et al. (1996) hypothesized that stomatal control might also be affected by pressure changes. Decreases in stomatal aperture at low pressures, but constant VPD, seem likely considering the increases in evaporation rate and recent research claiming that stomatal control is a function of the rate of water loss rather than

humidity (Monteith, 1995). It was also shown in work by Paul et al. (2004) that Arabidopsis plants subjected to reduced pressures show gene expressions as if they are in drought stress despite no visible signs of desiccation. Stomatal controls, and consequently transpiration and photosynthesis rates, are also affected by CO_2 concentration, VPD, and photosynthetically active radiation (PAR) (Jarvis, 1976). The effects of interaction between pressure and these variables have not been explored.

Evapotranspiration Model

The Penman-Monteith evapotranspiration model (Monteith, 1965) has been used extensively over the past several decades to predict plant water loss rates in field and greenhouse conditions. Based on work by Penman (1948) and later modified by Monteith, the model predicts the evapotranspiration of plants as driven by convective and radiative forces and incorporates the resistances of the crop canopy to water vapor loss.

Derivation of the Penman-Monteith evapotranspiration model begins with a steady-state energy balance of the plant canopy (equation 1-1).

$$R_n - H - LE = 0 \tag{1-1}$$

where: R_n = net radiation, W m^{-2}

H = sensible heat flux, W m^{-2}

LE = latent heat flux, W m^{-2}

Sensible heat flux, H, is estimated by equation 1-2.

$$H = \frac{\rho_a c_p (T_{leaf} - T_{air})}{r_h} \tag{1-2}$$

where: ρ_a = density of air, kg m^{-3}

c_p = specific heat of air at constant pressure, J kg^{-1} $^oC^{-1}$

T_{leaf} = leaf temperature, ^oC

T_{air} = air temperature, ^oC

r_h = external resistance for sensible heat transfer by convection, s m^{-1}

Equation 1-3 gives the estimation for the latent heat flux, LE.

$$LE = \frac{\rho_a c_p VPD_{leaf-air}}{\gamma(r_s - r_h)} \quad (1\text{-}3)$$

where: $VPD_{leaf\text{-}air}$ = leaf to air vapor pressure deficit, kPa

$$VPD_{leaf-air} = (e_{sleaf} - e_a) \quad (1\text{-}4)$$

e_{sleaf} = saturation vapor pressure at leaf temperature, kPa

e_a = vapor pressure, kPa

γ = psychrometric constant, Pa $^oC^{-1}$

$$\gamma = \frac{Pc_p}{0.622\lambda} \quad (1\text{-}5)$$

λ = latent heat of vaporization, kJ kg^{-1}

P = pressure, Pa

r_s = surface resistance of canopy to water vapor transfer, s m^{-1}

Calculation of the sensible and latent heat fluxes of equations 1-2 and 1-3 requires surface temperature, a variable that is typically unknown. Penman (1948) incorporated a simplifying assumption to eliminate leaf temperature from the model. Equation 1-6 shows an approximation for $VPD_{leaf\text{-}air}$ calculated from air vapor pressure deficit (VPD_{air}), the leaf to air temperature difference, and the slope of the saturation vapor pressure curve (Δ).

$$VPD_{leaf-air} \approx VPD_{air} + \Delta(T_{leaf} - T_{air}) \quad (1\text{-}6)$$

An example is shown in Figure 1-2. Consider a leaf whose surface temperature is 20 ^oC in a 24 ^oC airstream. Saturation vapor pressure at a given temperature, T, is calculated by equation 1-7.

$$e_s(T) = 0.61078 * 10^{\frac{7.5T}{237.3+T}} \quad (1\text{-}7)$$

where: $e_s(T)$ = saturation vapor pressure at temperature T, kPa

T = temperature, C

In Figure 1-2 the dashed line is a straight line with slope equal to the saturation vapor pressure curve at the air temperature, 24 ^{o}C. The difference between the actual $VPD_{leaf\text{-}air}$ and the estimation from equation 1-6 is only 0.08 kPa.

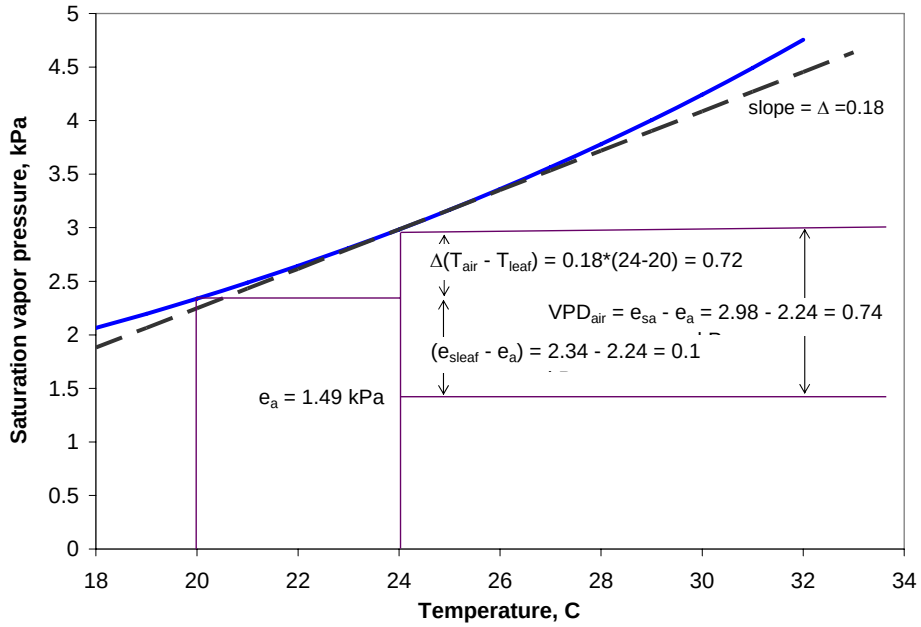

Figure 1-2. Leaf to air vapor pressure deficit approximation. To eliminate leaf surface temperature from the evapotranspiration model, Penman (1948) introduced an approximation for $VPD_{leaf\text{-}air}$. This approach assumes that the saturation vapor pressure curve can be approximated by a straight line with slope calculated at air temperature for small differences between leaf and air temperature (figure adapted from Jones, 1992).

Substituting equation 1-6 into 1-3 yields an equation for latent heat flux as a function of leaf to air temperature difference. The leaf temperature can be eliminated by combining this new equation with 1-3. Substitution into the heat balance of equation 1-1 and rearranging gives a standard from of the Penman-Monteith equation (Monteith, 1965) that does not require knowledge of leaf temperature.

$$LE = \frac{\Delta R_n + \rho_a c_{pa} VPD_{air} / r_h}{\Delta + \gamma\left(1 + r_s / r_h\right)} \quad (1\text{-}8)$$

The Penman-Monteith model requires the measurement or estimation of five variables to calculate the rate of evapotranspiration. The net radiation, R_n, and air vapor pressure deficit, VPD_{air}, are environmental parameters. The external and surface resistances to evapotranspiration are estimated via heat transfer and biological models. The external resistance, r_h, is the resistance to sensible heat transfer from the leaf and is calculated by convection heat transfer models. The surface resistance, r_s, is the resistance of water vapor transfer through the leaf cuticle layer and the stomata. Models for surface resistance account for the effects of environmental conditions (e.g PAR, VPD, CO_2) on stomatal behavior. The remaining model parameters are physical constants for particular environmental conditions.

Research Objectives

Several researchers have shown that, despite increases in transpiration rate, plants are capable of surviving in low pressures and at moderate pressures may even experience enhanced growth due to higher photosynthesis rates. However, it is important that plants be not only capable of survival, but also of thriving to produce fruit and seed. To optimize life support functions plant responses must be considered along with physical constraints in the design of a greenhouse system for Mars.

There is a significant amount of research modeling the effects of environmental factors on plant growth and development and applying these models to control systems in order to optimize the plant environment. There is also an increasing amount of research on the effects of reduced atmospheric pressure on short-term plant growth. This proposed research would extend and complement this previous research in several ways.

Extreme low atmospheric pressure (< 20 kPa) is an environmental factor that has not yet been fully explored with regard to its effect on plant response especially with regard to interactions CO_2, PAR, and VPD. Furthermore, leaf temperature has not been measured during reduced pressure experiments and should provide useful information with regard to evapotranspiration rates and plant water status. The goal of this research is to improve the current understanding of the effects of atmospheric pressure on plant evapotranspiration via the use of short-duration experiments and mathematical modeling. Using a modeling approach makes it possible to test current understanding of the effects of pressure on plant evapotranspiration including stomatal conductance, which cannot be measured during low pressure experiments using current technology.

The objectives of this research are to:

1. Quantify the effects of pressure on external and surface resistances to canopy sensible and latent heat transfer.
2. Investigate the effects of changes in evapotranspiration rate at low pressures on leaf temperature of mature radish plants.
3. Incorporate the effects of atmospheric pressure into an evapotranspiration model and apply the model to predict water loss rates of plants growing in a greenhouse on Mars.

Dissertation Organization

This dissertation is organized topically with chapters two through six each focusing on a different component of the research objectives. The development and performance of a small-scale low pressure system is described in chapter two. This system was used to measure the effects of pressure on surface resistance (chapter three), external resistance (chapter four), and leaf temperature (chapter five). Chapters three and four

include the development of mathematical models for surface and external resistances, respectively. In chapter six, these models are incorporated into a model to simulate evapotranspiration rate of radish plants as a function of pressure. Chapter seven addresses the overall conclusions and future recommendations resulting from this body of work. The references list for the entire dissertation is included following chapter 7. Appendices include supplementary information such as sensor calibrations, engineering drawings, and the control algorithm.

CHAPTER 2
DEVELOPMENT OF SMALL-SCALE PRESSURE-CONTROLLED PLANT CHAMBERS

Simulation of a Mars greenhouse environment is complex. It requires a chamber capable of maintaining low pressures for extended periods of time and a control system for many linked environmental parameters. The objective of this chapter is to describe the development of three small-scale pressure-controlled plant chambers used in this research.

Literature Review

As interest in advanced life support systems for Mars exploration missions has increased during the past several years, so has research activity regarding plant responses to low pressure environments. Researchers at Kennedy Space Center, Texas A&M University, University of Guelph, and University of Tokyo, as well as the University of Florida have each developed their own unique low pressure growth systems for studying the effects of Mars greenhouse conditions on plants.

The Mars Dome, developed by researchers at Kennedy Space Center and the University of Florida, is a polycarbonate dome joined to a stainless steel base (Fowler at al., 2002). It was originally designed to operate as a pressurized vessel inside a larger vacuum chamber, but added reinforcement made it possible to grow plants at reduced pressures (≥ 25 kPa) inside with Earth normal pressure outside. A microcontroller system monitored and controlled temperature, pressure, humidity and plant irrigation.

The main component of the Mars Dome was a central tower that contained all electronic components and temperature and humidity control devices. Nine scales surrounded the tower. Plants were weighed throughout an experiment to quantify evapotranspiration rates and activate irrigation events.

A group of engineers and plant scientists at Texas A&M University designed and built small cylindrical low-pressure plant growth chambers (Brown, 2002; Purswell, 2002). Six clear acrylic cylinders each measuring 0.31 m in diameter and 0.91 m in height were placed in a larger environment chamber to control light and temperature. A distributed control system monitored and controlled pressure and concentrations of oxygen and carbon dioxide. A cooling coil provided a condensing surface for dehumidification.

The University of Guelph developed two different types of low-pressure growth systems. They developed large vacuum chambers with hydroponics systems and some smaller steel cylindrical growth chambers. Both types of growth chambers offered control of critical environmental parameters – pressure, light, temperature, relative humidity, and carbon dioxide concentration.

Engineers at the University of Florida designed and built two new low pressure systems. One was a large vacuum chamber placed inside a large freezer. The environment inside the vacuum chamber closely resembled that of the Martian surface – virtually no atmospheric pressure and temperatures below freezing. A polycarbonate dome with steel base, similar to the Mars Dome described above, was placed inside the vacuum chamber and pressurized to simulate a greenhouse on Mars. Experiments were performed with this system to better understand heat transfer in a Martian greenhouse and

develop temperature and humidity control systems for reduced pressures. A small-scale system for detailed plant experiments was also developed at UF and KSC and is described in the remainder of this chapter.

Replication is necessary in plant experiments to perform statistical analysis, draw sound conclusions, and extrapolate conclusions to other situations. Plant experiments performed in the large low-pressure systems described above such as the Mars Dome and the UF low temperature vacuum chamber must be replicated in time. To save time and ensure identical treatments, it is desirable to perform replications simultaneously. Three bell jars were used in this research for plant experiments (see Figures 1 and 2). An aluminum base was designed and constructed to house the temperature and humidity controls and wiring. A PC based data acquisition and control system was developed to monitor and control pressure, temperature, humidity, and carbon dioxide concentration. Plant weight and leaf temperature were also measured to evaluate evapotranspiration and water stress.

Objectives

The objective of the work described in this chapter was to design and construct plant growth chambers to meet the following design criteria:

- Steadily maintain pressures as low as 10 kPa over long periods of time,
- Allow exterior lighting to reach plant canopy,
- Three simultaneous replications,
- Control pressure, air temperature, humidity, CO_2 concentration, and
- Monitor environmental parameters, leaf temperature, and plant weight.

Bell Jar System

Bell jars were selected as the primary component of the plant growth chambers because they were readily available and easy to replace. Glass bell jars, routinely used in vacuum studies, are strong and relatively easy to seal. The inside and outside diameter of each bell jar was 213 and 222 mm, respectively They were 381 mm tall.

New aluminum bases constructed by the Kennedy Space Center Design and Development Integration Branch (prototype shop) were designed to house a cooling coil, humidifier, two fans, sensors, wiring, and fittings. Preliminary plant experiments performed in bell jars with off-the-shelf plastic bases emphasized their small volume. It was difficult and awkward to accommodate all instrumentation, heating and cooling equipment, scale, and the plant. The new bases were deep enough to house these components below the plant as shown in Figures 3 and 4. Detailed engineering drawings of the base are in appendix 3.

Ports for gases, water, and wiring were made in the bottom of the bell jar bases. Fittings for water and gases were fitted with o-rings and installed tightly to minimize leakage. To minimize costs, wire feedthroughs were constructed in-house. Art clay was packed into the center of 1.905-cm bushings to hold wires in place. The thickness of the clay was 1.25 cm. Solid wires cut to length were inserted through the clay. To minimize air passing through the wire insulation, about 0.5 cm was stripped away before wires were inserted. Epoxy was poured into both sides of the bushing so that the exposed portion of each wire was completely covered. Three wire feedthroughs containing nine wires and one with two type-T and one type-K thermocouples were made for each bell jar.

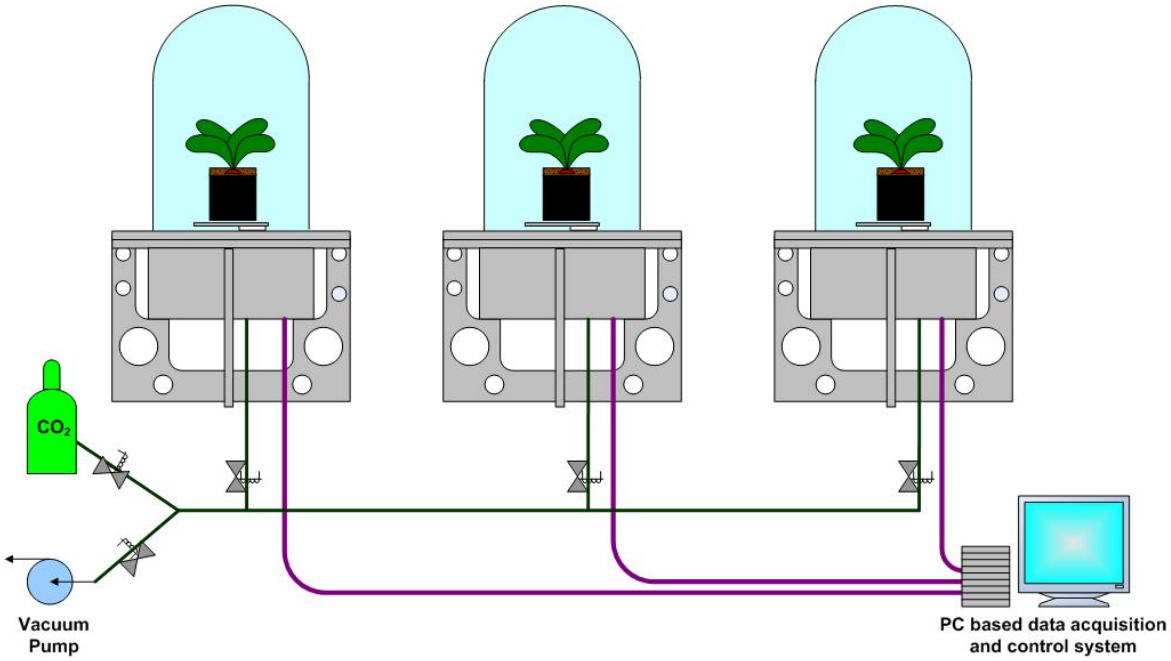

Figure 2-1. Schematic of pressure controlled plant chambers. Experimental replication was achieved using three independently controlled bell jars.

Figure 2-2. Pressure controlled plant chambers. The small chambers were placed inside a larger plant growth chamber for high-quality external lighting.

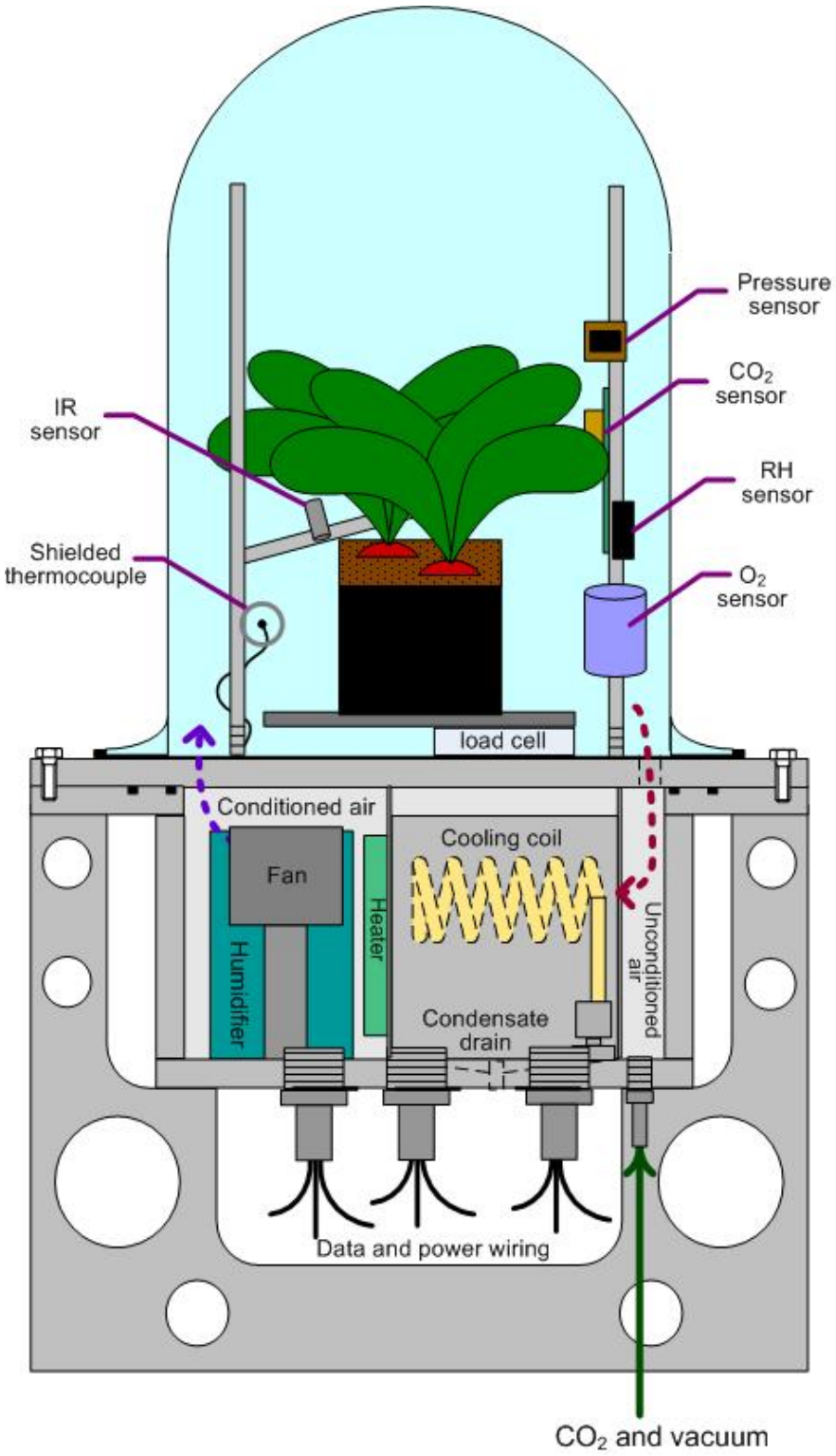

Figure 2-3. Schematic of one pressure controlled plant chamber.

Figure 2-4. Picture of one of the three pressure controlled plant chambers.

The cooling coil was designed for dehumidification. From preliminary experiments (data not shown) the average evapotranspiration rate for a single mature radish plant at 10 kPa was estimated to be approximately 0.075 g H_2O min^{-1}. Since the lowest pressure treatment applied in this research was 12 kPa, the evapotranspiration rate for 10 kPa was assumed to be a good approximation for the maximum expected in this research. Thus, the coil was designed to condense water at a rate equal to the assumed evapotranspiration rate for two mature radish plants at 10 kPa, 0.15 g H_2O min^{-1}.

The steady-state heat transfer rate required to condense water was calculated by equation 1.

$$q = (\dot{m}_{H_2O})(h_{fg}) \tag{2-1}$$

where: q = heat transfer by condensation, W

m = mass rate of water condensed, kg s^{-1}

h_{fg} = latent heat of vaporization, kJ kg^{-1}

At 10 kPa, the latent heat of vaporization is 2389 kJ kg^{-1}. The rate of heat transfer required to condense water at 0.15 gH_2O min^{-1} was 6 W.

The rate of heat transfer by water condensing on the coil was calculated by equation 2 with the average convective heat transfer coefficient taken from Incropera and DeWitt (1996) for water condensation on a horizontal tube (equation 3).

$$q = hA_{coil}(T_{air} - T_{coil}) \tag{2-2}$$

where: q = rate of heat transfer, W

h = convective heat transfer coefficient, W m^{-2} K^{-1}

A_{coil} = coil surface area, m^2

T_{air} = air temperature, K

T_{coil} = coil surface temperature, K

$$h = 0.729 \left[\frac{g\rho_l(\rho_l - \rho_v)k_l^3 h_{fg}}{N\mu_l(T_{sat} - T_s)D} \right]^{1/4} \quad (2\text{-}3)$$

where: h = convective heat transfer coefficient, W m^{-2} K^{-1}

g = acceleration due to gravity, m s^{-2}

ρ_l = density of liquid, kg m^{-3}

ρ_v = density of vapor, kg m^{-3}

k_l = thermal conductivity of liquid, W m^{-1} K^{-1}

h_{fg} = latent heat of vaporization, kJ kg^{-1}

N = number of horizontal tubes

μ_l = viscosity of liquid, kg s^{-1} m^{-1}

T_{sat} = saturation temperature, K

T_s = coil surface temperature, K

D = tubing diameter, m

The following values for properties of water vapor and saturated liquid at 10 kPa were used: ρ_v = 0.111 kg m^{-3}; ρ_l = 0.997 kg m^{-3}; k_l = 0.606 W m^{-1} K^{-1}; and μ_l = 934 x 10^{-6}. The number of horizontal tubes, N, was assumed to be two for a coil and the tube diameter, D, was 0.0635 m (0.25 in). The resulting heat transfer coefficient was 39.8 W m^{-2} K^{-1}.

Equating the two expressions for the rate of heat transfer (equations 1 and 2) and rearranging, yields an equation for calculating the coil surface area needed.

$$A_{coil} = \frac{q}{h(T_{air} - T_{coil})} \quad (2\text{-}4)$$

Assuming that the coil temperature was 3 ^{o}C and air temperature was 24 ^{o}C, the coil surface area needed to condense 0.15 g H_2O min^{-1} was calculated to be 0.0075 m^2 (11.6 in^2). Designed with a factor of safety of 2.5, the coil surface area was approximately 0.0187 m^2 (29 in^2).

Data Acquisition and Control

Environmental parameters within the bell jar were monitored and controlled by a PC-based data acquisition and control system. Pressure, air temperature, and CO_2 concentration of each bell jar were controlled independently.

Instrumentation

An Opto 22 system was used for data acquisition and control. An I/O and communications processor (SNAP ultimate brain, Opto22, Temecula, CA) managed 16 digital and analog I/O modules. Table 1 lists the modules used in this research and their application. The control program was written in *ioControl 6.*0 (Opto 22, Temecula, CA), a flowchart based software designed for the Opto system. A user interface and display program was written in *ioDisplay 6.0* software (Opto 22, Temecula, CA).

Table 2-1. Descriptions and applications of Opto 22 I/O modules used in this research.

Opto 22 module description	Quantity	Application
SNAP-OAC5, 412-250 VAC input	1	Vacuum pump, solenoid valve
SNAP-AOV-25, 0 to +10 VDC analog output	1	Mass flow controller
SNAP-ODC5SNK, 5-60 VDC output, sink	4	Solenoid valves, heaters, humidifiers, and fans
SNAP-AITM, mV or thermocouple input	2	Infrared thermocouples
SNAP-AITM2, mV or thermocouple input	5	Oxygen sensors, type-T thermocouples
SNAP-AIV-4, 0 to +10 VDC analog input	3	Pressure, CO2, and relative humidity sensors and load cells

All sensors were calibrated within one year prior to the start of experiments. Table 2 lists the calibrated accuracy of each sensor. Calibration data and error budget calculations for all sensors (excluding RH sensors which were factory calibrated) are included in appendix A. Air temperature was measured by type-T thermocouples placed just below the height of the plant canopy. They were shielded to reduce measurement error caused by the high radiation environment of the outside growth chamber. The thermocouples were calibrated using a two point calibration (10 ^{o}C and 40 ^{o}C) in a thermometer calibrator (TCAL, Sun Electronic Systems, Inc., Titusville, FL). Small integrated circuit sensors were used to monitor pressure (MPXH6115A6U, Freescale Semiconductor, Inc., Austin, TX) and relative humidity (HIH-3610-003, Honeywell, Freeport, IL). The oxygen concentration was measured using a galvanic cell type oxygen sensor (MAX-250, Maxtec, Salt Lake City, UT). A low-cost OEM ultrasonic sensor was used to measure carbon dioxide (6004 CO_2 module, Telaire, Goleta, CA). Leaf temperature was measured with infrared thermocouples (OS36SM-K-140F, Omega, Stamford, CT). Load cells were used for measuring plant weight (LPS-2kg, Celtron Technologies, Inc., Colvina, CA).

Table 2-2. Calibrated sensor accuracies. All sensors were calibrated within one year of the start of experiments.

Parameter	**Sensor description**	**Accuracy**
Air temperature	Type-T thermocouples	± 0.5 ^{o}C
Pressure	Integrated circuit pressure sensor	± 0.53 kPa
Relative humidity	Integrated circuit RH sensor	± 2.1 %
Oxygen	Galvanic cell sensor	± 1.0 %
Carbon dioxide	Ultrasonic sensor	± 100 ppm (at 2000 ppm)
Leaf temperature	Mini infrared thermocouples	± 0.8 ^{o}C
Plant weight	Load cell	± 0.1 g

Temperature and Humidity Control

The air temperature of each bell jar was determined by the outside temperature of the bell jar, the coil temperature, and a heater. At the beginning of the control loop, the current air temperature of each jar was compared to the setpoint temperature. The heater or cooling coil was activated as needed. Only one solenoid valve was available for controlling the water flow through the cooling coils. Thus, cooling coil temperature was not controlled independently and was similar in the three bell jars at all times.

Relative humidity was determined by the rate of plant evapotranspiration and the cooling coil temperature. When the relative humidity of any one of the three bell jars was higher than setpoint, the solenoid valve was opened to allow chilled water to flow through the coils. On the other hand, if relative humidity was too low in a bell jar, the humidifier for that bell jar was turned on until setpoint was achieved.

The surface temperature of the copper cooling coils was determined by the temperature and flow rate of water flowing through them. Both of these factors were controlled by a chilled water bath and were the same for all three bell jars. A solenoid valve in the chilled water line was opened to allow water to pass through the cooling coil if the air temperature or relative humidity of any one of the bell jars was too high.

A 50 W, 1 Ω power resistor was used as the heating source in each bell jar. The power output of the resistor was set by varying the voltage across it. The Opto modules used to turn the heaters on/off were rated at 4 A. The resistors were 1 Ω, so the theoretical magnitude of the current draw (A) was equal to the magnitude of the voltage drop (V). However, at 8 A the current draw was only 4 A, within the limit of the Opto module. The power output of the heater was 28 W as calculated by equation 5.

$$P = IV \tag{2-5}$$

where P = power, W

I = current, A

V = voltage, V

Each bell jar had two manually controlled fans (BM5115-04W-B50-L00, NMB Technologies, Chatsworth, CA) to maintain air circulation. The specified air flow rate at standard pressure was 1.42 L s^{-1} (3 cfm) per fan. To reduce disturbance caused by high air velocities within the plant canopy, a pulse width modulation routine was applied to reduce the fan flow rate. Power to the fans (12 V) was cycled on/off every 500 milliseconds. The volumetric flow rate of a given fan is proportional to the fan speed and diameter (Henderson et al., 1997). Therefore, although the mass flow rate of air decreased at lower pressures due to decreased air density, air velocity was not affected by pressure. Some leaf movement was observed at pressures as low as 12 kPa, leading to the conclusion that the fan output was adequate for air mixing within the range of pressures used in this research. All fans were turned on at the start and remained on throughout the duration of each experiment.

Pressure and Carbon Dioxide Concentration Control

Internal pressure and carbon dioxide concentration control for all three bell jars were carried out in the same *ioControl* chart to avoid timing conflicts. At the beginning of the control loop, the current CO_2 concentration (ppm) in each bell jar was compared to the setpoint concentration (ppm) for that bell jar. The measured and setpoint concentrations, given in units of parts per million, were converted to units of mass by equation 6 derived from the ideal gas law.

$$CO_2\_mass = 44 * \frac{\left({[CO_2]}/{10^6} \right) * p * V_{bj}}{8.3144 * T_{airK}} \qquad (2\text{-}6)$$

where CO_2_mass = mass of carbon dioxide inside, g

$[CO_2]$ = carbon dioxide concentration, ppm

p = bell jar pressure, Pa

V_{bj} = bell jar volume, m^3

T_{airK} = absolute temperature of air inside bell jar, K

The current mass of CO_2 in each bell jar was compared to the setpoint mass for that particular jar. If the current level was more than 120 ppm below setpoint, the mass of CO_2 required to reach the setpoint was calculated and CO_2 was added by the mass flow controller (FMA3202-CO_2, Omega, Stamford, CT). To avoid overshoot that sometimes occurs when the mass flow controller (MFC)was first turned on, the MFC is turned on and vented for 12 seconds before the three-way solenoid valve was switched to permit CO_2 flow into one of the three bell jars. One of three solenoids was opened to allow CO_2 into the desired bell jar. The MFC flow rate was always set at 40 ml/min. After time elapsed to add 70% of the calculated mass of CO_2 needed to the bell jar the MFC was turned off. The bell jar solenoid valve remained open for 30 seconds to allow CO_2 in the tubing to diffuse into the bell jar. With plants present, mixing within the bell jar was allowed for 60 seconds before the next CO_2 addition. Without plants, mixing was allowed for ten minutes.

Pressure control logic occurred immediately following the carbon dioxide control. As in the CO_2 control logic, pressures of the three bell jars were independently controlled one at a time. The pressure of each bell jar was compared to the setpoint pressure of that

jar. If pressure exceeded the setpoint by 1 kPa, the solenoid valve for that bell jar opened and the vacuum pump was turned on. The vacuum pump remained on until the current pressure was equal to the setpoint. After pressure control of the bell jar, the entire CO_2/pressure control loop began again.

Light Control

The light within the bell jars was controlled externally to the system. The light level on the bases without the bell jars was 349.9, 372.8, 353.2 μmol m^{-2} s^{-1} for chambers 1, 2, and 3 respectively. With the bell jars in place the light level were 338.4, 351.4, and 333.3 μmol m^{-2} s^{-1}. Thus, the average transmissivity of the bell jars was 95%. It is believed that the highly reflective surfaces of the external growth chamber contributed to such a large amount of light transmitted through the bell jar.

A "sock" made of a lightweight screening material was configured for each bell jar to reduce the internal light level for low light treatments (see Figure 5). With the socks in place, the light levels inside the three bell jars were 158.5, 166.5, and 156.5 μmol m^{-2} s^{-1}.

Figure 2-5. Light level control. Fine mesh screening material was used to reduce the PAR level inside the bell jars from an average of 341 μmol m^{-2} s^{-1} to 161 μmol m^{-2} s^{-1}.

Performance Testing

Data from several experiments were used to quantify the performance of the small-scale chambers. When applicable, environmental data are reported as described in ANSI/ASAE Standard EP411.1 "Guidelines for Measuring and Reporting Environmental Parameters for Plant Experiments in Growth Chambers".

Pressure

The system was operated for one hour at a pressure setpoint of 12 kPa for all three bell jars. Pressure was recorded every minute during this time. The maximum, minimum, average, and standard deviation of the pressure data for each bell jar are given in Table 2-3. Since leakage increases at low pressure, data for a setpoint of 12 kPa are given as a worst case situation.

Table 2-3. Performance of pressure control algorithm. Descriptive statistics are given for data recorded at one-minute intervals for a one hour period. All values are in kPa.

	Bell Jar 1	**Bell Jar 2**	**Bell Jar 3**
Average	12.61	12.49	12.55
Maximum	13.05	13.06	13.07
Minimum	12.12	12.04	12.09
Standard deviation	0.26	0.03	0.30

To quantify the leakage rate of each bell jar, the pressure was reduced to 12, 33, or 66 kPa and the pressure control algorithm was turned off. Pressure data were again recorded every minute for a one-hour period. The leakage rate was taken as the pressure increase per minute as determined by slope of a linear regression line. Table 4 shows the rate of pressure increase for each bell jar at 12, 33, and 66 kPa.

Table 2-4. Bell jar leakage rates. The rate of pressure increase is given for each bell jar in kPa min^{-1}.

Initial pressure, kPa	Bell Jar 1	Bell Jar 2	Bell Jar 3
12	0.07	0.15	0.12
33	0.03	0.14	0.08
66	0.02	0.08	0.06

Carbon dioxide

The CO_2 control algorithm was tested with and without plants. Figure 2-6 shows the CO_2 concentration as a function of time without plants at standard pressure with the setpoint equal to 1000 ppm. CO_2 was added incrementally until the concentration was within 120 ppm of the setpoint. Within 45 minutes, the CO_2 concentration was within 60 ppm of the 1000 ppm setpoint. Achieving setpoint took much longer without plants because ten minutes was allowed for mixing versus the one minute allowed when plants were present. This longer mixing time was required to avoid overshoot that often occurred when no plants were inside the bell jar to take up CO_2.

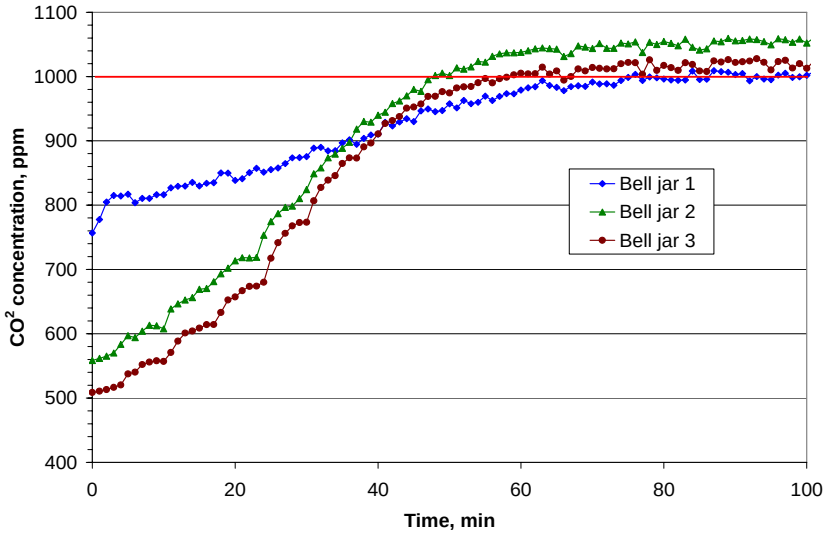

Figure 2-6. CO_2 control without plants at standard pressure. The CO_2 concentration within all three bell jars was within 60 ppm of the 1000 ppm setpoint approximately 45 minutes from the activation of the CO_2 algorithm.

The CO_2 control algorithm was also tested at a reduced pressure. Figure 2-7 shows the CO_2 concentration and pressure for a one-hour period. Data were recorded at one-minute intervals. The pressure setpoint was 12 kPa with a hysteresis of 1 kPa and the CO_2 setpoint was 9000 ppm. The CO_2 concentration dropped by approximately 800 ppm each time the pump was activated, a reduction of only about 8.2%. This corresponded well to a 8.3% decrease in pressure in reducing it from 13 to 12 kPa, indicating that the air within the bell jar was well mixed. At higher pressures, the vacuum pump activity had less effect on CO_2 concentration. For example, if the total pressure was 67 kPa and the vacuum pump was turned on to reduce the pressure by 1 kPa, assuming the air inside the bell jar is well mixed, the decrease in CO_2 would be only 1.5%.

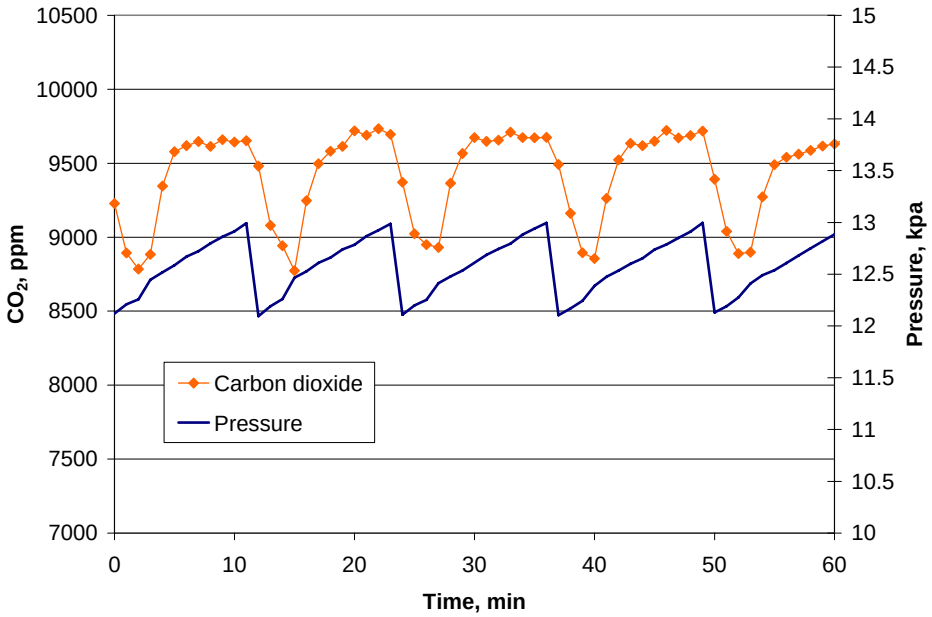

Figure 2-7. Effect of vacuum pump on CO_2 control at low pressures. At 12 kPa, with no plants, the activity of the vacuum pump to maintain the pressure setpoint had a considerable effect on the CO_2 concentration.

Another test of the CO_2 algorithm was performed with plants inside the bell jar. With a total pressure setpoint of 12 kPa, the CO_2 setpoint was 3367 ppm (0.04 kPa partial

pressure). Figure 2-8 shows the CO_2 concentration over time for each of the three bell jars with two mature radish plants inside. Summary statistics for the same data as in Figure 2-7 are given in Table 2-5. The control system was successful in responding to plant CO_2 uptake and reductions caused by vacuum pump activity and maintained the CO_2 setpoint with a maximum standard deviation of 267 ppm.

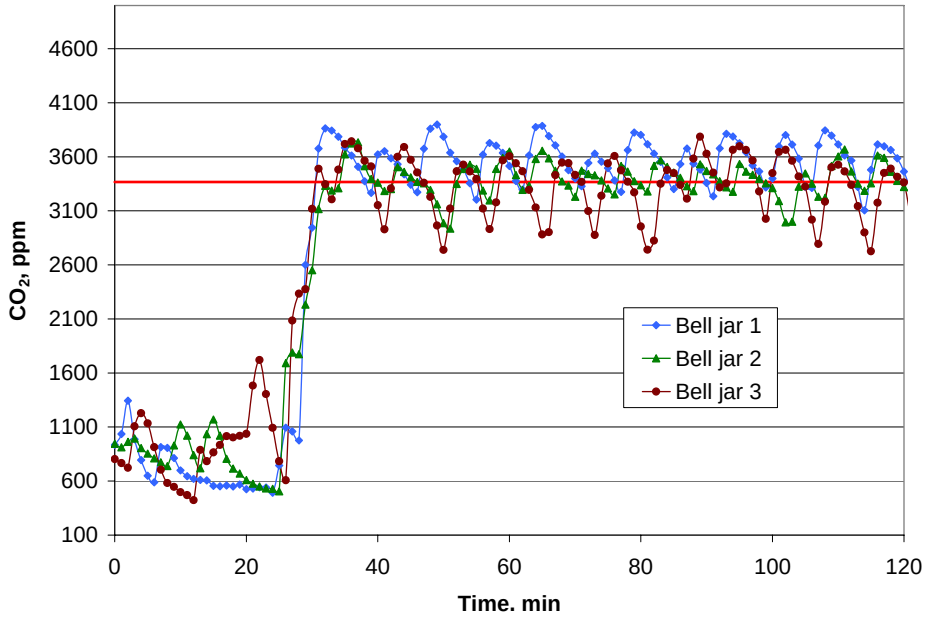

Figure 2-8. CO_2 control with plants at 12 kPa. The CO_2 control algorithm reached the 3367 ppm setpoint in less than 40 minutes from the start of the experiment.

Table 2-5. Performance of CO_2 control algorithm at 12 kPa with plants. Descriptive statistics are given for data recorded at one-minute intervals for a one hour period. The CO_2 setpoint was 3367 ppm. All values are in ppm.

	Bell Jar 1	**Bell Jar 2**	**Bell Jar 3**
Average	3574	3383	3335
Maximum	3885	3656	3786
Minimum	3204	2935	2738
Standard deviation	181	157	267

Air Temperature and Relative Humidity

The air temperature and relative humidity control algorithm was also tested at 12 kPa. The setpoints, 24 ^{o}C and 70%, were chosen to achieve a VPD_{air} of 0.9 kPa. Figure

2-9 shows the air temperature and relative humidity for the 50-minute period beginning one hour after the start of the experiment. The air temperature of bell jar 3 was the last to reach its setpoint. As previously mentioned, the power resistors that served as the bell jar heating elements could not be operated simultaneously to avoid exceeding the current rating of the Opto output modules. The control algorithm placed priority numerically. In other words, power was given to the resistor in bell jar 3 only if the air temperatures in bell jars 1 and 2 were at or above setpoint. Furthermore, heating occurred slowly because current was limited to only 4 A. From equation 5, the power output of the resistor was calculated to be 28 W. Although it took some time to achieve the setpoint in bell jar 3, once the air temperature reached 24 ^{o}C, the heater was sufficient to maintain temperature as demonstrated by a maximum air temperature standard deviation of 0.3 ^{o}C (see Table 2-6).

Relative humidity was maintained fairly constant throughout the duration of the setpoint. From Table 2-6, which gives descriptive statistics for air temperature and relative humidity, the maximum standard deviation over the 50-minute period was only 1.1%. The mean values for bell jars 1 and 2 were slightly below the 70% setpoint. This occurred because chilled water flow to the three cooling coils was controlled together. The coil remained on as long as the humidity in any one of the bell jars was above the setpoint. However, it should be pointed out that humidity in all three bell jars was within the 5% deviation from setpoint recommended by ASAE standard ANSI/ASAE Standard EP411.1 during the entire experiment.

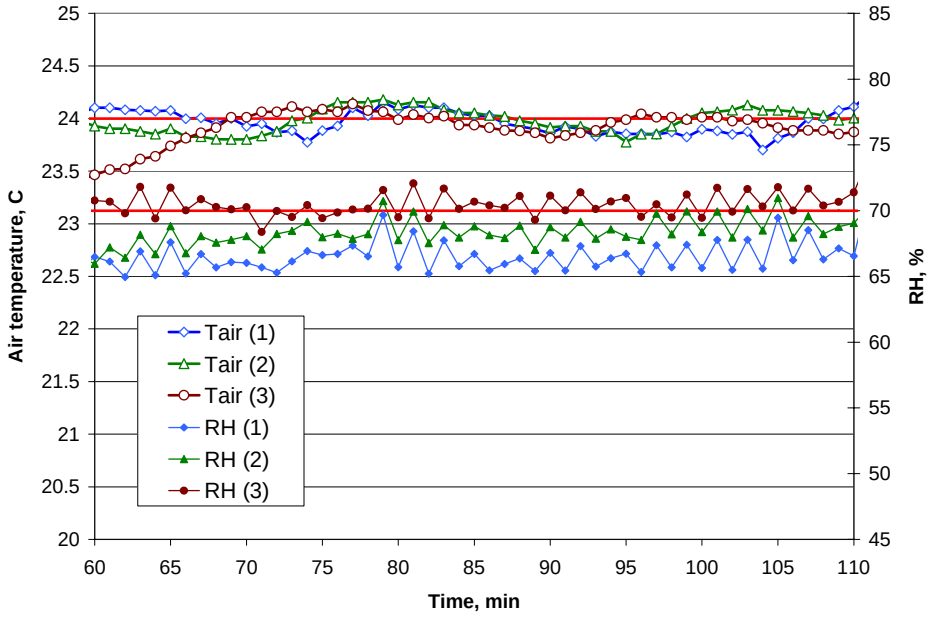

Figure 2-9. Air temperature and relative humidity control at 12 kPa with plants. The control algorithm successfully achieved and maintained the 24 °C and 70% setpoints one hour after the start of the experiment.

Table 2-6. Performance of the air temperature and relative humidity control algorithm at 12 kPa with plants. Descriptive statistics are given for data recorded at one-minute intervals for a 50-minute period. The air temperature and relative humidity setpoints were 24 °C and 70% to achieve a VPD_{air} of 0.9 kPa.

	Bell Jar 1	**Bell Jar 2**	**Bell Jar 3**
	Air temperature, °C		
Average	24.0	24.0	23.8
Maximum	24.2	24.2	24.1
Minimum	23.7	23.8	23.0
Standard deviation	0.1	0.1	0.3
	RH, %		
Average	66.4	68.2	70.6
Maximum	69.7	71.0	72.4
Minimum	65.0	66.0	68.4
Standard deviation	1.1	1.1	0.9

Conclusions and Future Development

The bell jar based small-scale controlled environment chambers described in this chapter worked well for the purposes of this research to study short term effects of pressure, CO_2, and light on plant evapotranspiration. The control algorithm successfully

maintained pressure, CO_2 concentration, air temperature, and relative humidity while measuring plant weight and leaf temperature.

There were a few limitations of the system. Leakage rates were higher than desired. The wire feedthrough and water fittings built in the lab were adequate, but did not perform as well as commercial vacuum fittings. For this research, maintaining pressure and CO_2 setpoints was a primary objective. The vacuum pump and CO_2 algorithm were capable of overcoming leakage to sufficiently maintain the pressure and CO_2 setpoints. In other applications of this system, such as monitoring CO_2 drawdown to measure photosynthesis, high leakage rates may be of more concern.

Another limitation of this system was the heating power limitations. The current rating of the output modules limited the power for heating to 28 W for a single bell jar at a time. If more current could be applied to the 50-W resistors for heating, the air temperature setpoints could be achieved more quickly. For the purposes of this research the ambient environment was buffered by the external growth chamber and the heat output of the power resistor was capable of overcoming the temperature decrease that occurred when the cooling coil was turned on. However, in settings with a higher heating load, more power may be needed to maintain the temperature setpoint.

CHAPTER 3
EFFECTS OF PRESSURE ON LEAF CONVECTIVE HEAT TRANSFER

The rate of water loss from leaves is governed by the leaf energy balance that includes the effects of radiation, water evaporation, and convection. Heat transfer by convection occurs when air passes over the leaf surface and is significantly affected by the density of air, which is determined by total pressure. This chapter presents convective heat transfer analysis for a leaf represented by a horizontal flat sheet as affected by pressure and air velocity.

Literature Review

The rate of sensible heat transfer by convection (equation 1-2) has a significant impact on the leaf energy balance. Convection determines the degree to which the leaf is affected by the ambient aerial environment. When convective heat transfer is high, as for a plant outdoors in windy conditions, leaf temperature approaches air temperature regardless of the radiative load (Jarvis and McNaughton, 1986; Jones, 1992). On the other hand, if the rate of convective heat transfer is low, radiation heat transfer dominates the leaf energy balance.

Convective heat transfer analysis is also significant because it provides a way to estimate the thickness of boundary layers. Knowledge of the thickness of the velocity and thermal boundary layers that form over the surface of a leaf are important in order to accurately quantify the ambient environment. Within the boundary layer there are gradients of air velocity, gas concentration, and temperature. Sensors must be located outside the boundary layer in the free stream to best measure the surrounding

environment. On the other hand, locating sensors within the boundary layer provides information about the leaf microclimate.

Convection Heat Transfer

Resistance to convective heat transfer is caused by the boundary layer that forms above the leaf as air passes over. Figure 3-1 shows a theoretical diagram of the velocity boundary layer over a horizontal thin plate. The air above the plate surface can be thought of as a series of infinitely thin horizontal layers of particles. The air particles that come in contact with the surface of the plate have zero velocity and exert a shear stress on the layer just above it, slowing it down. This second layer slows down the third by exerting a shear force and so on until the effect is negligible and the local velocity reaches the free stream velocity, u_∞. A horizontal velocity gradient exists between the plate surface ($u = 0$) and the free stream ($u = u_\infty$). The boundary layer thickness,δ, is defined as the vertical distance, y, at which $u = 0.99\ u_\infty$ (Incropera and DeWitt, 1996).

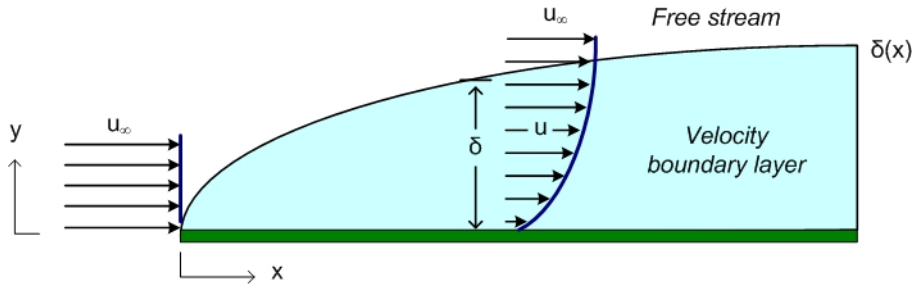

Figure 3-1. Velocity boundary layer over a horizontal flat plate (adapted from Incropera and DeWitt, 1996).

A thermal boundary layer similar to the velocity boundary layer also develops over the surface of a flat plate. Figures 3-2 and 3-3 show the thermal boundary layer over a horizontal flat plate with a surface temperature warmer (Figure 3-2) and cooler (Figure 3-3) than the free stream air temperature. A horizontal temperature gradient develops

between the surface temperature, T_s, and the free stream temperature, T_∞. The thickness of the thermal boundary layer, δ_t, is defined as the vertical distance at which the air temperature, T, is equal to $0.99T_\infty$ (Incropera and DeWitt, 1996).

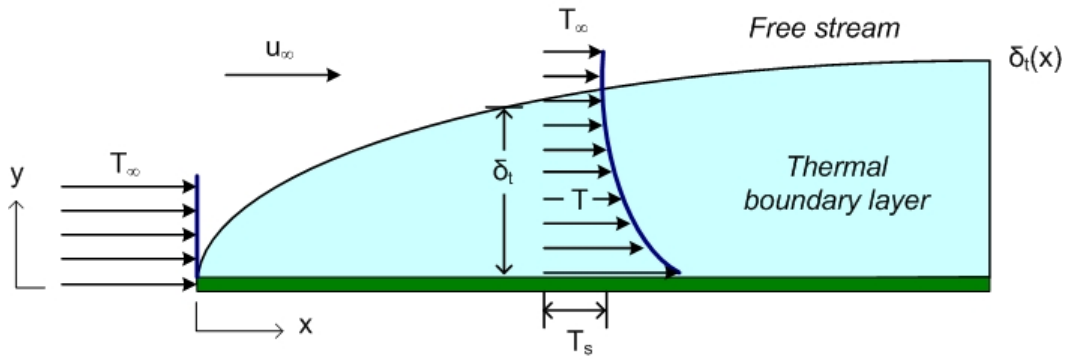

Figure 3-2. Thermal boundary layer over a horizontal flat plate that is warmer than the surrounding air (adapted from Incropera and DeWitt, 1996).

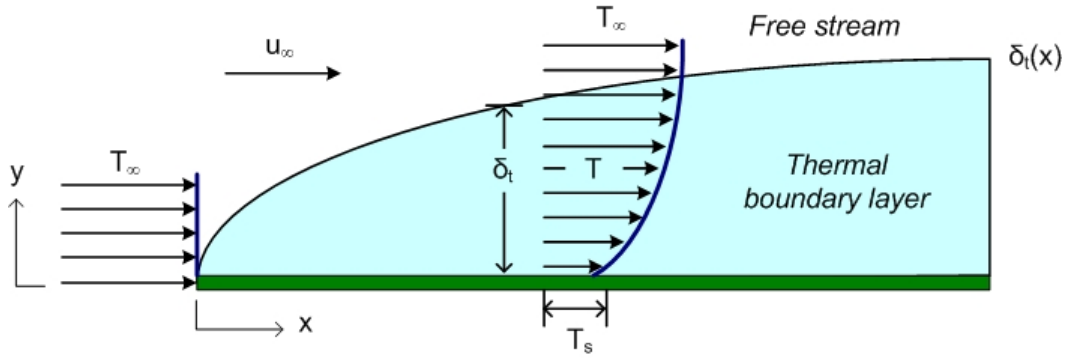

Figure 3-3. Thermal boundary layer over a horizontal flat plate that is cooler than the surrounding air (adapted from Incropera and DeWitt, 1996).

The mathematical derivations involved in boundary layer analysis are beyond the scope of this review and are not included. To simplify analysis, the following non-dimensional groups – Reynolds, Prandtl, Grashof, and Nusselt numbers – are employed in the solutions. The Reynolds and Grashof numbers are used to determine if forced, free, or mixed convection is dominant. Then, based on the dominant mode of convection, non-dimensional groups are used to calculate resistances and boundary layer thicknesses.

Forced convection occurs when the fluid movement across the surface is driven externally by a pump, fan, or wind. Free convection is driven by buoyancy forces created by temperature gradients in the fluid. Mixed convection occurs when the effects of forced and free convection are similar in magnitude and neither can be neglected.

The Reynolds number, Re, is the ratio of inertia to viscous forces and is calculated as:

$$Re = \frac{u_\infty L}{\nu} \tag{3-1}$$

where: u_∞ = free stream air velocity, m s^{-1}

L = characteristic length, m

ν = kinematic viscosity, m^2 s^{-1}

Kinematic viscosity, a function of fluid density, is highly pressure dependent. As a result, assuming all other parameters are held constant, Reynolds number will decrease as pressure is dropped.

Prandtl number, ratio of viscosity to thermal conductivity, is calculated as follows in equation 3-2.

$$Pr = \frac{\nu}{\alpha} \tag{3-2}$$

where: α = thermal diffusivity, m^2 s^{-1}

Grashof number, ratio of buoyancy to viscous forces, is calculated by equation 3-3.

$$Gr = \frac{g\beta(T_s - T_a)L^3}{\nu^2} \tag{3-3}$$

where: g = gravitational constant, m s^{-2}

$\beta = 1/T_a$ =coefficient of thermal expansion, K^{-1}

T_S = surface temperature, K

T_a = air temperature, K

External resistance

The method of calculation of the rate of sensible heat transfer from the crop canopy is determined by the dominant mode of convective heat transfer – forced, free, or mixed. In typical field conditions wind velocities are in the range of 1 to 5 m s^{-1} and forced convection is the primary mode of sensible heat transfer (Hanan, 1998). In Earth greenhouse applications typical air velocities of 0.5 to 0.7 m s^{-1} are considered acceptable (ASHRAE, 2001). In these lower air velocities, free convection plays a larger role and a mixed convection model is most accurate (Bailey and Meneses, 1995; Stanghellini, 1987; Zhang and Lemeur, 1992).

The magnitude of the ratio Gr/Re^2 determines the principal mode of convection. If $Gr/Re^2 \approx 1$, both free and forced convection must be considered (mixed convection). If $Gr/Re^2 << 1$, forced convection dominates and free convection may be neglected. Likewise, if $Gr/Re^2 >> 1$, forced convection may be neglected

The Nusselt number is a measure of the magnitude of convection heat transfer occurring at a surface. Calculation of the Nusselt number depends on the dominant mode of convection heat transfer. In the case of forced convection, the Nusselt number for a horizontal thin plate is (Incropera and DeWitt, 1996):

$$Nu = 0.664\, Re^{1/2}\, Pr^{1/3} \tag{3-4}$$

For free convection of the upper surface of a horizontal, heated plate, the Nusselt number is (Incropera and DeWitt, 1996):

$$Nu = 0.54 (Gr\, Pr)^{1/4} \tag{3-5}$$

Equation 3-5 for a heated upper surface was applied in this analysis because it is most appropriate for the convection experiments performed in this research. In the case of an actual leaf at reduced pressures equation 3-6 for a cooler than air surface may be more appropriate considering evaporative cooling caused by high transpiration rates.

$$Nu = 0.27(Gr\,Pr)^{1/4} \tag{3-6}$$

In free convection conditions equation 3-7 for characteristic length, L, suggested by Incropera and DeWitt (1996) was applied to improve model accuracy.

$$L \equiv \frac{A}{P} \tag{3-7}$$

Stanghellini (1987) developed equation 3-8 for the Nusselt number in mixed convection conditions that worked well for horizontal leaves in a greenhouse.

$$Nu = 0.37(Gr + 6.92\,Re^2)^{1/4} \tag{3-8}$$

From the Nusselt number, the external resistance to sensible heat transfer for a single leaf can be calculated by equation 3-9.

$$r_e = \frac{L}{\alpha Nu} \tag{3-9}$$

The external resistance of a crop canopy, r_h, was estimated by Zhang and Lemeur (1992) from the r_e of a horizontal flat plate by equation 3-10. This equation assumes that all leaves contribute equally to sensible heat transfer.

$$r_h = \frac{r_e}{2LAI} \tag{3-10}$$

Boundary layer thickness

The average thickness of the velocity boundary layer for forced flow over a horizontal, thin flat plate is given by equation 3-11 (Incropera and DeWitt, 1996).

$$\delta = \frac{5L}{Re^{1/2}} \tag{3-11}$$

The Prandtl number, a measure of the ratio of the viscosity forces to diffusion, can be used to estimate the thickness of the thermal boundary layer, δ_t, based on δ.

$$\frac{\delta}{\delta_t} = Pr^{1/3} \tag{3-12}$$

Objectives

The objective of this chapter was to use classical convection heat transfer analysis to determine the effects of pressure and air velocity on the external resistance and boundary layer thickness of radish plants growing at atmospheric pressures as low as 12 kPa. The theoretical heat transfer model described above was compared with data from a series of controlled lab experiments.

Materials and Methods

The sensible heat transfer from a leaf replica was measured to evaluate the effects of pressure and air velocity on external resistance. The rectangular-shaped replica (Figure 3-4) was made by wrapping a 12.7 cm x 2.54 cm (5 in x 1 in) flexible 10-W Kapton heater (model BKL3005, Birk Manufacturing, Inc., East Lyme, CT) with standard grade aluminum foil (thickness = 0.16 mm). A small type-T thermocouple was sandwiched between the heater upper surface and the foil. It was assumed that there was no temperature gradient along the thickness of the foil so that the temperature measured by the thermocouple was equal to the upper surface temperature of the leaf replica. Power to the heater was supplied by a DC power supply. The voltage input was 13.2 V and the current draw was 0.82 A.

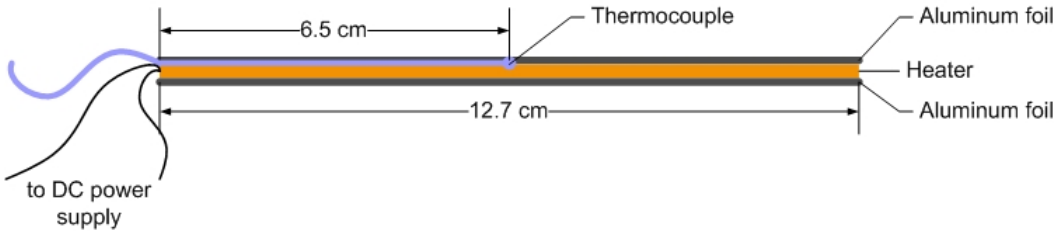

Figure 3-4. Leaf replica. A leaf replica made by wrapping a thin, flexible heater with aluminum foil was used to measure the effects of pressure and air velocity on convective heat transfer.

A fan (BM5115-04W-B50-L00, NMB Technologies, Chatsworth, CA) was positioned about 2.5 cm in front of the leading edge of the heated sheet as shown in Figure 3-5. The fan output was varied by cycling power to the fan (1 second delay) and positioning layers of screening material over the fan outlet. The volumetric flow rate of a given fan is proportional to the fan speed and diameter (Henderson et al., 1997). Therefore, although the mass flow rate of air decreased at lower pressures due to decreased air density, air velocity was not affected by pressure. At standard pressure, air velocity was measured about 5 cm above the sheet with a hot wire anemometer (model 407123, Extech Instruments, Waltham, MA). One of the bell jar chambers and the data acquisition system described in chapter 2 was modified for these experiments to control pressure.

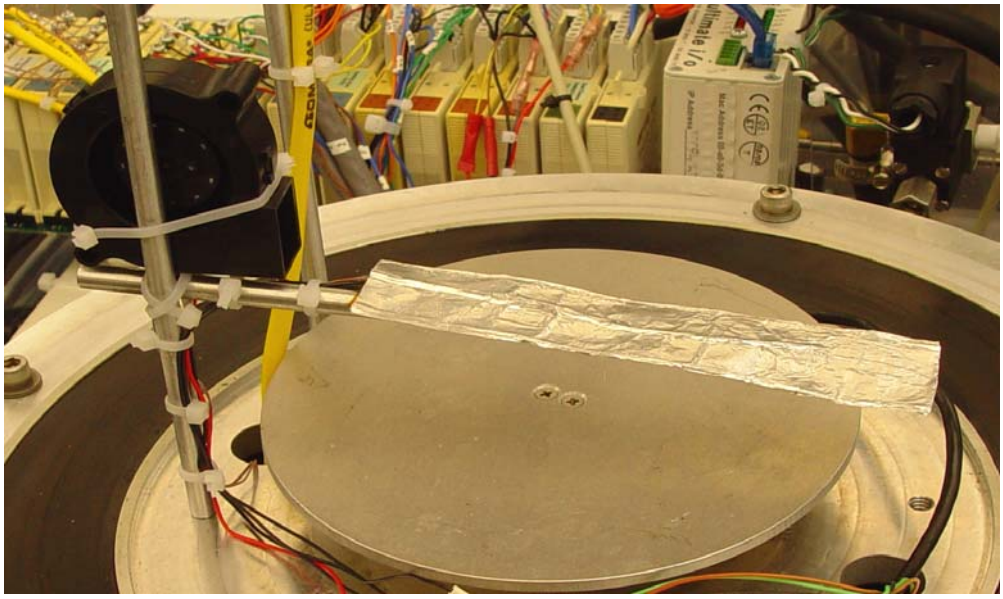

Figure 3-5. Convection heat transfer experimental setup. A fan was positioned in front of a thin heated sheet inside one of the bell jar chambers.

External resistance was determined from cooling curves generated for the heated foil sheet at four levels of pressure (12, 33, 66, and 101 kPa) and air velocity (0, 1.8, 2.9, and 5.8 m s^{-1}). Power was turned on to the heating element of the sheet until the surface temperature approached 80 ^{o}C. The power supply was then turned off and the sheet was allowed to cool until the surface temperature approached the ambient air temperature measured by a type-K thermocouple located about 5 cm above the sheet. Figure 3-6 is an example of a cooling curve at 5.8 m s^{-1} and 101 kPa.

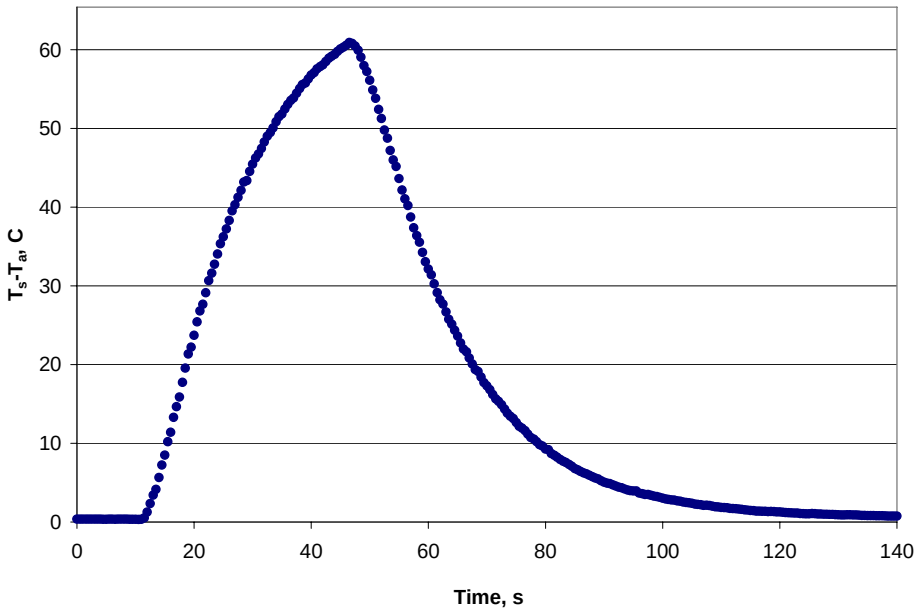

Figure 3-6. Temperature profile for leaf replica during heating and subsequent cooling phase at 101 kPa and an air velocity of 5.8 m s^{-1}.

The slope of the cooling curve was related to the rate of sensible heat loss as determined by a mass balance of the foil sheet given by equation 3-13.

$$C = H + R_n \tag{3-13}$$

where: C = rate of change of heat content of foil sheet, W m^{-2}

H = rate of sensible heat transfer, W m^{-2}

R = rate of radiation heat transfer, W m^{-2}

The rate of change in the heat content of the foil sheet is given by equation 3-14.

$$C = \rho_s c_{ps} L \frac{dT_s}{dt} = \rho_s c_{ps} L \frac{d(T_s - T_a)}{dt} \tag{3-14}$$

where: ρ_s = density of leaf replica sheet, kg m^{-3}

c_{ps} = specific heat of leaf replica sheet, kJ kg^{-1} K^{-1}

L = length of sheet, m

T_s = sheet surface temperature, ^oC

T_a = air temperature, ^oC

The rate of sensible heat transfer, H, is given by equation 1-2. Note that the canopy resistance term, r_h, was replaced by the resistance for a single flat plate, r_e, for this analysis. Net radiation was calculated by the following equation 3-15. Variables in bold denote absolute temperature.

$$R_n = \sigma\varepsilon(\mathbf{T}_s^4 - \mathbf{T}_{sur}^4) \tag{3-15}$$

where: σ = Stefan-Boltzmann constant = 5.670 x 10^{-8} W m^{-2} K^{-4}

ε = emissivity of sheet surface

$\mathbf{T}_{sur}$ = average temperature of surrounding surfaces, K

It was assumed that the system was in equilibrium and the temperature of the surroundings could be well approximated by air temperature.

An approximation was employed to eliminate the fourth order terms of the radiation equation 3-14 and simply the solution of the heat balance. A coefficient, h_r, was introduced to cast the net radiation equation in a form similar to the convection equation.

$$R_n = \sigma\varepsilon(\mathbf{T}_s^4 - \mathbf{T}_a^4) = h_r(T_s - T_a) \tag{3-16}$$

where: h_r = radiation heat transfer coefficient, W m^{-2} K

Rearranging to solve for h_r and expanding the fourth order polynomial

$$h_r = \sigma\varepsilon\frac{(\mathbf{T}_s^4 - \mathbf{T}_a^4)}{(\mathbf{T}_s - \mathbf{T}_a)} = \sigma\varepsilon\frac{(\mathbf{T}_s^2 - \mathbf{T}_a^2)(\mathbf{T}_s^2 + \mathbf{T}_a^2)}{(\mathbf{T}_s - \mathbf{T}_a)} = \sigma\varepsilon\frac{(\mathbf{T}_s - \mathbf{T}_a)(\mathbf{T}_s + \mathbf{T}_a)(\mathbf{T}_s^2 + \mathbf{T}_a^2)}{(\mathbf{T}_s - \mathbf{T}_a)} \tag{3-17}$$

and simplifying

$$h_r = \sigma\varepsilon(\mathbf{T}_s + \mathbf{T}_a)(\mathbf{T}_s^2 + \mathbf{T}_a^2) \tag{3-18}$$

To further simplify the equation two more variables, $\mathbf{T}_m$ and e, were introduced. $\mathbf{T}_m$ was the mean of the sheet surface temperature, $\mathbf{T}_s$, and the air temperature, $\mathbf{T}_a$. The difference between $\mathbf{T}_s$ and $\mathbf{T}_a$ was 2e so that:

$$\mathbf{T}_a + e = \mathbf{T}_m \tag{3-19}$$

and

$$\mathbf{T}_s - e = \mathbf{T}_m \tag{3-20}$$

Combining equations 3-18, 3-19, and 3-20 and simplifying,

$$h_r = \sigma\varepsilon 2\mathbf{T}_m\left[2\mathbf{T}_m^2 + \frac{(\mathbf{T}_s - \mathbf{T}_a)^2}{2}\right] \tag{3-21}$$

Assuming that the difference between the surface and air temperatures, $\mathbf{T}_s$-$\mathbf{T}_a$, was significantly less than the absolute temperature of either the surface or air, the last term could be neglected. Therefore, the radiation heat transfer coefficient was given by equation 3-22.

$$h_r = \sigma\varepsilon 4\mathbf{T}_m^3 \tag{3-22}$$

Substituting equations 1-2, 3-14, 3-16, and 3-22 into the heat balance of equation 3-13 gave the following differential equation.

$$\rho_s c_{ps} L\frac{d(T_s - T_a)}{dt} = \frac{-\rho_a c_{pa}(T_s - T_a)}{r_e} - h_r(T_s - T_a) \tag{3-23}$$

Dividing both sides by $\rho_s c_{ps} L$

$$\frac{d(T_s - T_a)}{dt} = \frac{-\rho_a c_{pa}(T_s - T_a)}{r_e \rho_s c_{ps} L} - \frac{h_r}{\rho_s c_{ps} L}(T_s - T_a) \tag{3-24}$$

and rearranging to simplify yielded equation 3-25.

$$\frac{d(T_s - T_a)}{dt} = -\left[\frac{\rho_a c_{pa}}{r_e \rho_s c_{ps} L} + \frac{h_r}{\rho_s c_{ps} L}\right](T_s - T_a) \tag{3-25}$$

The solution to the differential equation 3-25 was 3-26.

$$ln(T_s - T_a)_2 - ln(T_s - T_a)_1 = -\left[\frac{\rho_a c_{pa}}{r_e \rho_s c_{ps} L} + \frac{h_r}{\rho_s c_{ps} L}\right](t_2 - t_1) \qquad (3\text{-}26)$$

Equation 3-26 was related to the cooling curves (as in Figure 3-6) to solve for the external resistance. Figure 3-7 shows a plot of the natural logarithm of T_s-T_a of the same data as Figure 3-6 for time equal 50 to 110 seconds. Equating the slope, m, of a linear regression line through this data with equation 3-26 and rearranging gave equation 3-27 for external resistance, r_e.

$$r_e = -\frac{\rho_a c_{pa}}{m(\rho_s c_{ps} L) + h_r} \qquad (3\text{-}27)$$

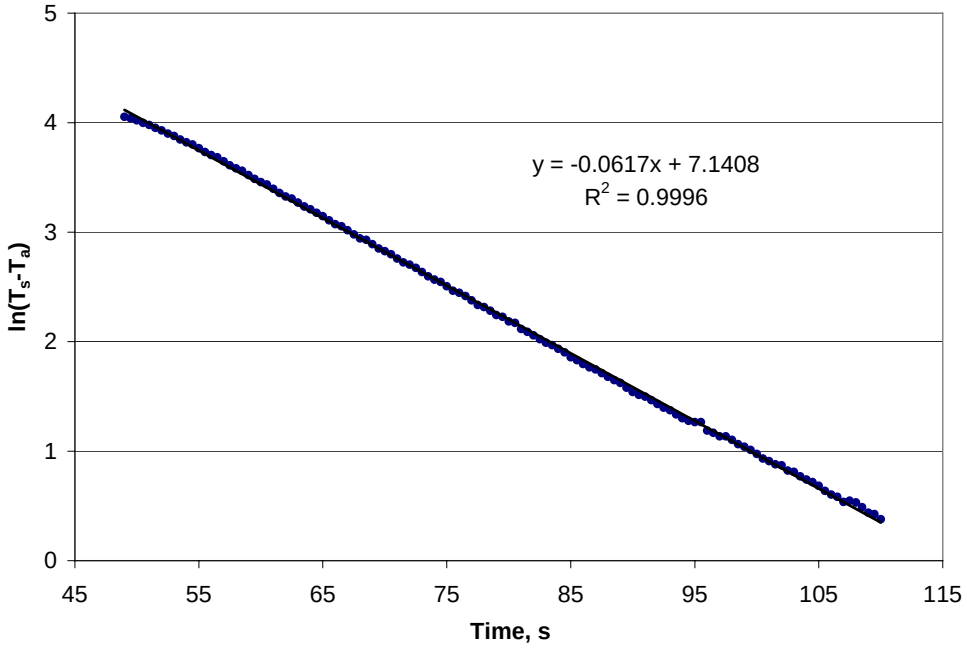

Figure 3-7. Transformed cooling data for the leaf replica at 101 kPa and an air velocity of 5.8 m s^{-1}. The slope of a linear regression line was related to Equation 3-26 to determine the external resistance to sensible heat transfer.

The slope of the linear regression line for the transformed data of Figures 3-6 and 3-7 was -0.0617. This value and the following properties for air and the sheet were

applied to Equation 3-27 to calculate the external resistance: ρ_a=1.16 kJ kg^{-1} K^{-1}; c_{pa}=1.007 kJ kg^{-1} K^{-1}; ρ_s=1800 kJ kg^{-1} K^{-1}; c_{ps}=0.98 kJ kg^{-1} K^{-1}; and L=0.22 mm. The average air temperature during all testing was 25 ^{o}C. Assuming an emissivity of bright aluminum foil of 0.05 (McQuistan and Parker, 1994) and a maximum sheet surface temperature of 80 ^{o}C, the radiation heat transfer coefficient calculated by equation 3-22 was 0.393 W m^{-2} K. This gave an external resistance of 50.1 m s^{-1}.

Results and Discussion

The external resistance of a thin, heated sheet was empirically determined at four levels of pressure and air velocity using temperature profiles during a cooling phase. Figures 3-8, 3-10, 3-12, and 3-14 show the difference between surface temperature of the sheet and air temperature during heating and subsequent cooling at 12, 33, 66, and 101 kPa, respectively. Figures 3-9, 3-11, 3-13, and 3-15 show the natural logarithm of T_s-T_a during cooling. The slopes from linear regression analysis for each curve were used to determine the external resistance, r_e, in equation 3-27. At each pressure, cooling occurred at a faster rate with increasing air velocity. Decreasing pressure also decreased the rate of cooling. As previously mentioned, volumetric flow rate and, therefore, air velocity was not affected by pressure. However, air density and mass flow rate decrease with pressure. Decreasing the air density reduced the cooling capacity of the air passing over the sheet. Note that differences in maximum temperature were due to the time period that the heating element was turned on, which was controlled manually.

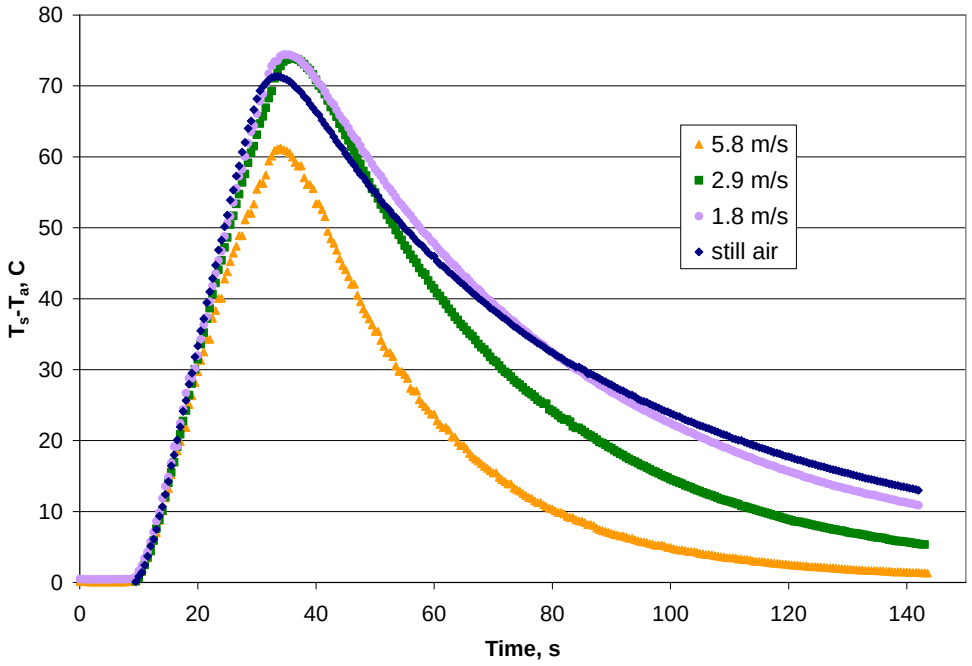

Figure 3-8. Surface temperature of leaf replica during heating and subsequent cooling phase for four air velocity treatments at 12 kPa.

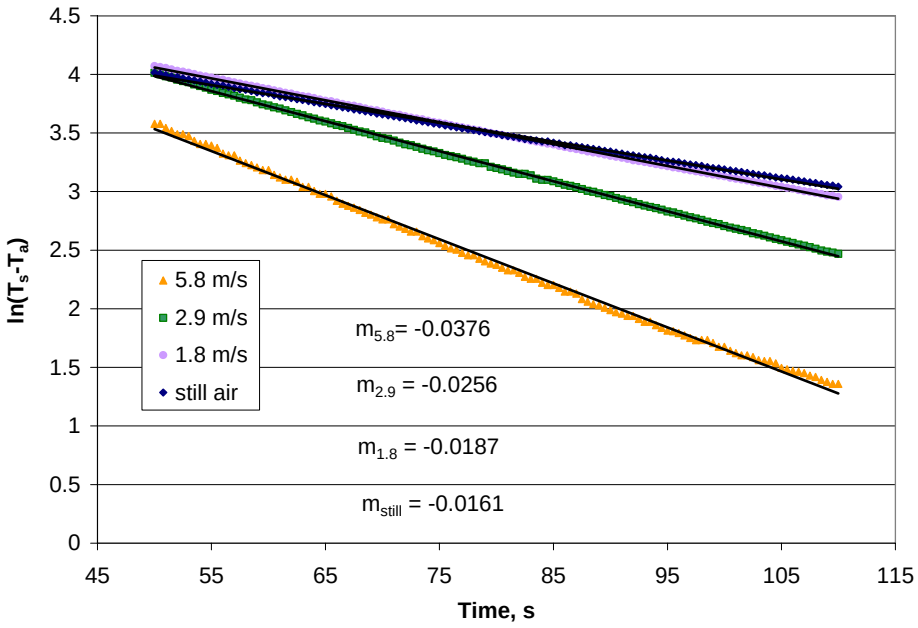

Figure 3-9. Transformed surface temperature data for leaf replica at 12 kPa.

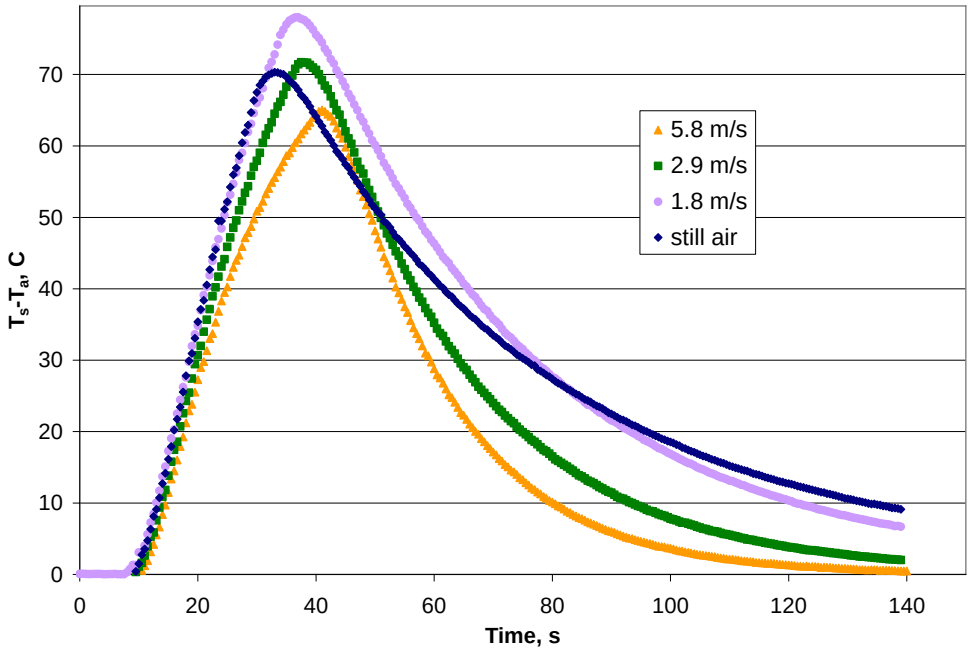

Figure 3-10. Surface temperature of leaf replica during heating and subsequent cooling phase at 33 kPa.

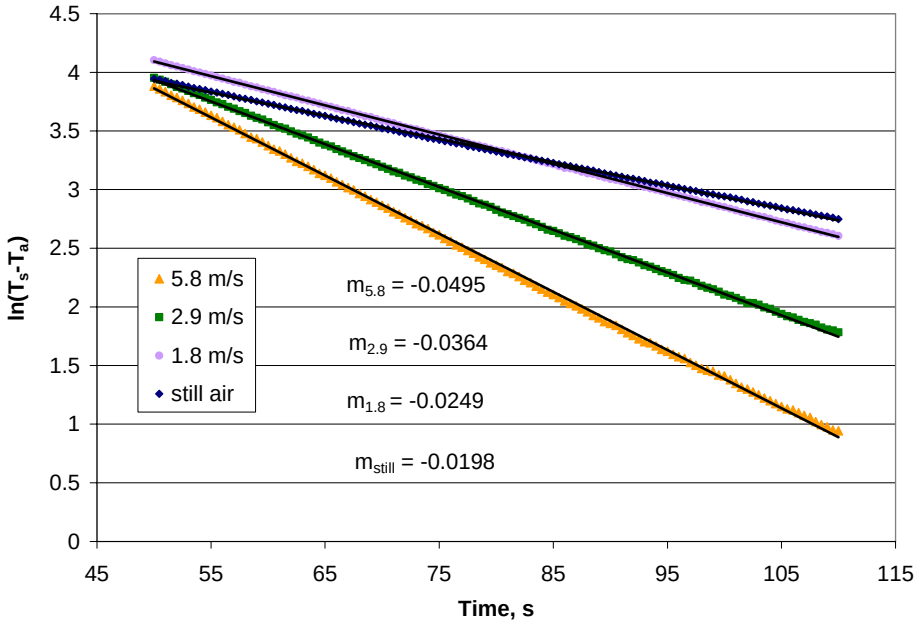

Figure 3-11. Transformed surface temperature data for leaf replica at 33 kPa.

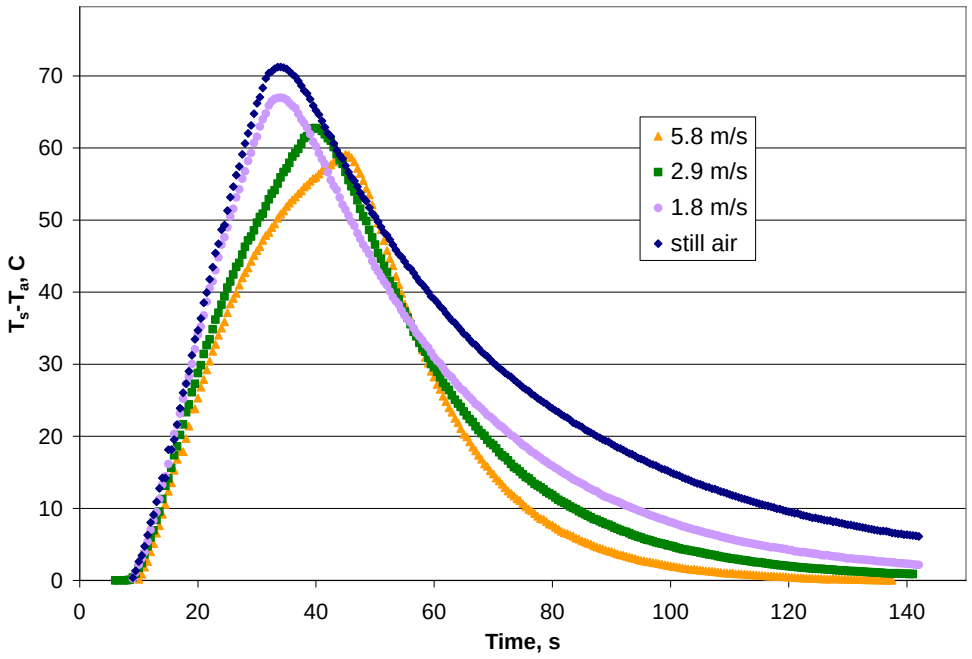

Figure 3-12. Surface temperature of leaf replica during heating and subsequent cooling phase at 66 kPa.

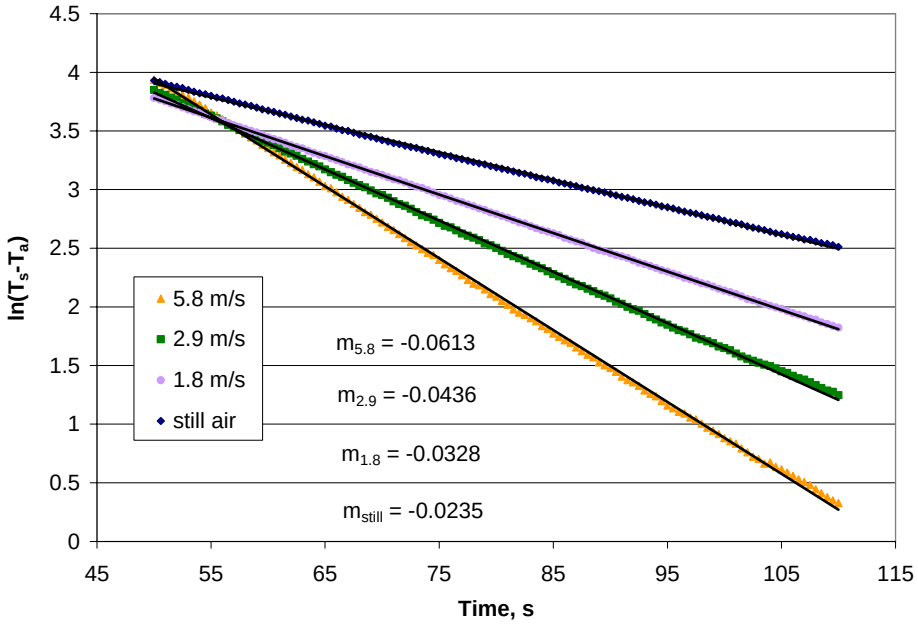

Figure 3-13. Transformed surface temperature data for leaf replica at 66 kPa.

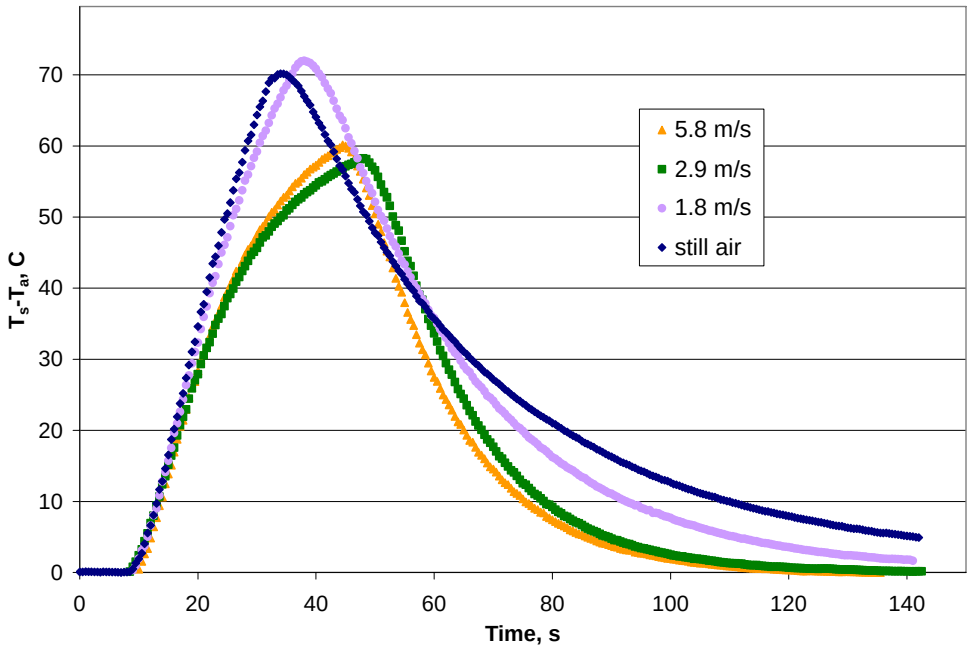

Figure 3-14. Surface temperature of leaf replica during heating and subsequent cooling phase at 101 kPa.

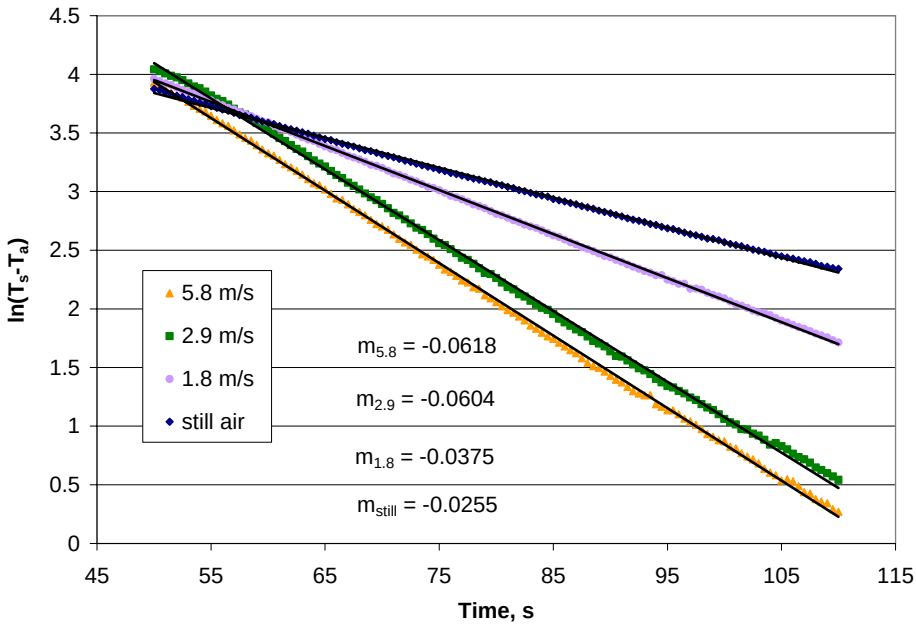

Figure 3-15. Transformed surface temperature data for leaf replica at 101 kPa.

Model Performance

The empirically determined values for external resistance were compared with the classical heat transfer model of equation 3-9. Figure 3-16 shows the empirical values and model predictions at each level of air velocity as a function of pressure. The model accurately predicted the proportional effects of both pressure and air velocity on external resistance. Resistance to heat transfer increased with increasing pressure and air velocity. Equation 1-2 predicted that the rate of convective heat transfer was inversely proportional to external resistance. That is, if air density, specific heat, and temperature difference remained the same, convective heat transfer should increase as resistance decreases. However, as previously mentioned, the significant decrease in air density at lower pressures reduced the heat transfer capacity of air passing over the surface. This was demonstrated by calculating the rate of sensible heat transfer, H, from the heated sheet for the external resistance values determined experimentally. Figure 3-17 shows the rate of heat transfer for the sheet with a surface area of 0.0032 m^2 as a function of pressure and air velocity. The rate of heat transfer was an average of 50% higher at standard pressure than at 12 kPa. This increase was much less than the 88% decrease in air density from 101 to 12 kPa demonstrating the effect of external resistance. Higher values of r_e at standard higher pressures reduced the magnitude of the effect on convection.

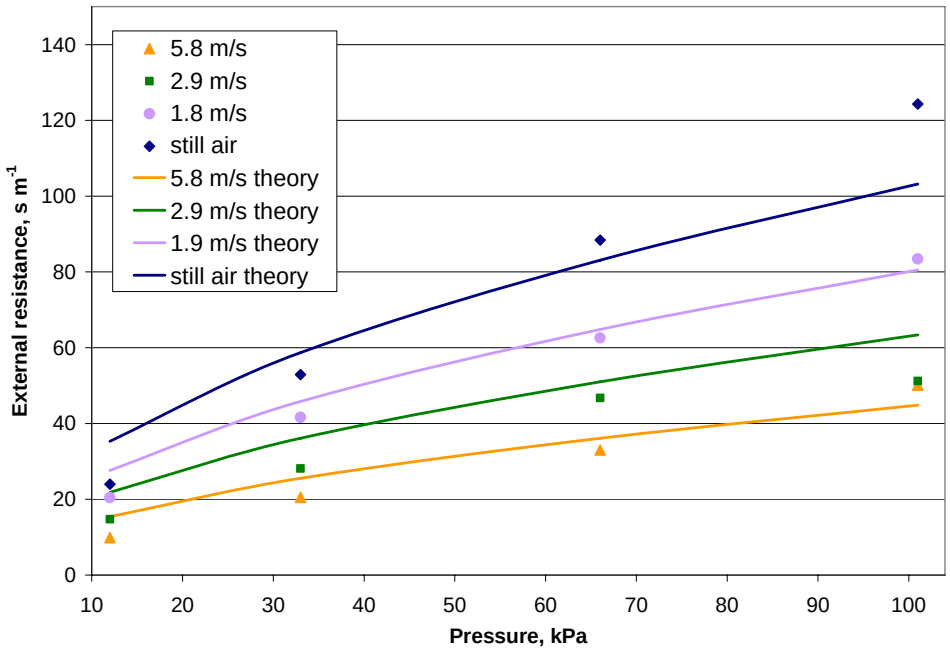

Figure 3-16. Measured and predicted values for external resistance of leaf replica as a function of pressure and four levels of air velocity.

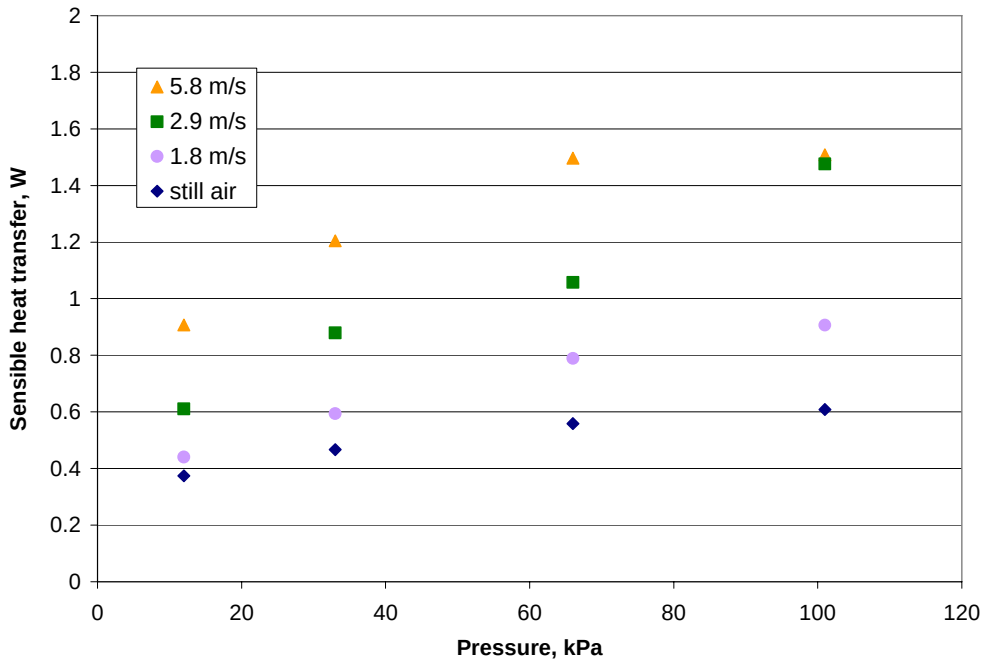

Figure 3-17. Rate of heat transfer from leaf replica as a function of pressure and air velocity.

The ability of the theoretical model to predict external resistance was evaluated by comparison to the experimentally determined values. Figure 3-18 and 3-19 show two tests for model performance. In Figure 3-18 the predicted values were plotted against empirical values. The 1:1 line represents perfect model fit. The points lined up nicely along the 1:1 line which indicated that the predicted values closely matched the experimental values for both free and forced convection conditions. Forced convection dominated at air velocities above 1.8 m s^{-1} and free convection was dominant in still air. None of the combinations of pressure and air velocity tested resulted in mixed convection. The actual model error as given by the difference between predicted and experimentally determined values was plotted as a function of pressure in Figure 3-19. The maximum error was 21.1 s m^{-1} and the average error was only 2.6 s m^{-1} for all conditions tested.

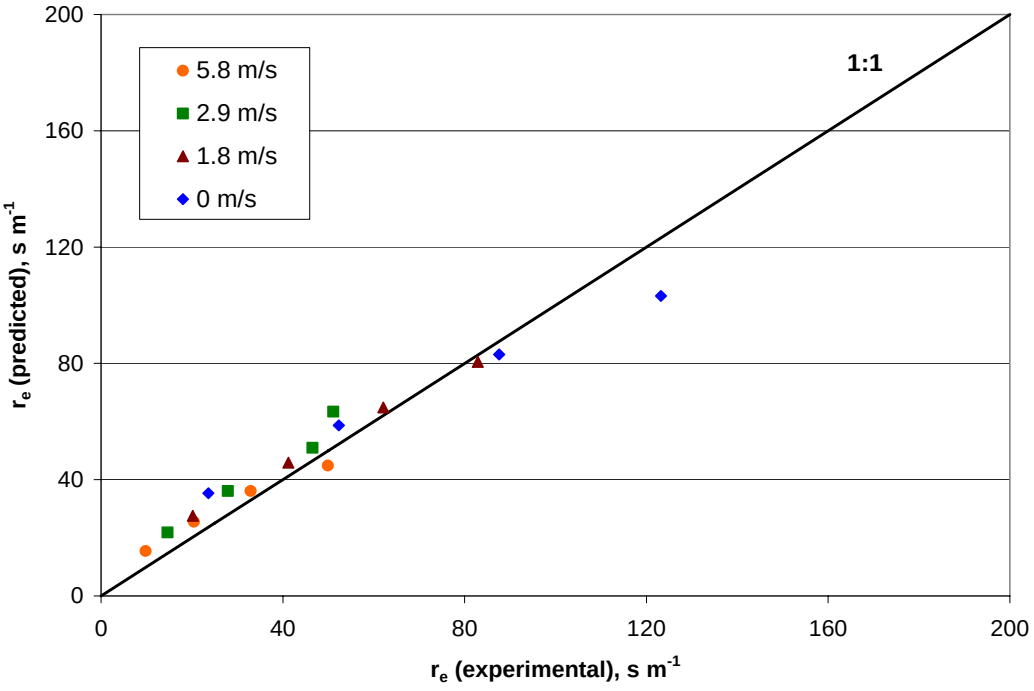

Figure 3-18. External resistance model performance. Predicted values of re are shown plotted against empirically determined values.

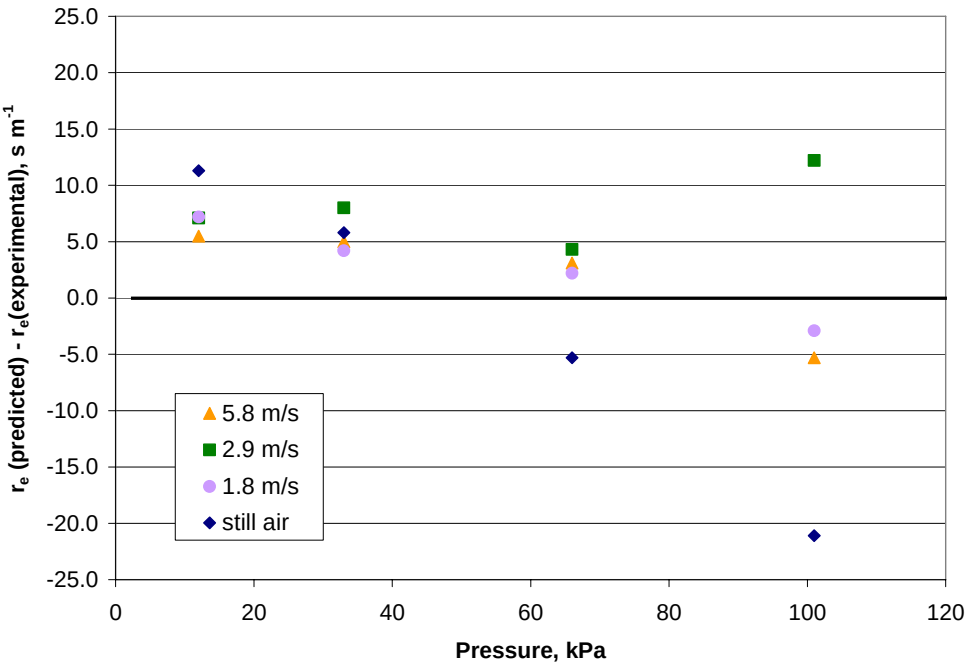

Figure 3-19. External resistance model error. The difference between predicted and experimental external resistance is plotted as a function of pressure.

Boundary Layer Thickness

Pressure and air velocity also play significant roles in the thickness of the boundary layer, δ, that forms over the horizontal surface. Figure 3-20 and 3-21 show the effects of pressure and air velocity, respectively, on boundary layer thickness (equation 3-11). In Figure 3-20 the velocity boundary layer thickness was plotted as a function of pressure for an air velocity of 1.0 m s^{-1}. The thickness of the boundary layer increased exponentially as pressure decreased so that it was greater than 2 cm as pressure approached zero.

Boundary layer thickness at standard pressure was plotted as a function of air velocity in Figure 3-21. At air velocities of 1.0 m s^{-1} and above, there was little change in δ. However, when the air velocity was low the boundary layer increased significantly.

Note that this predicted trend held true for all pressures. Changes in pressure only shift the magnitude of these curves.

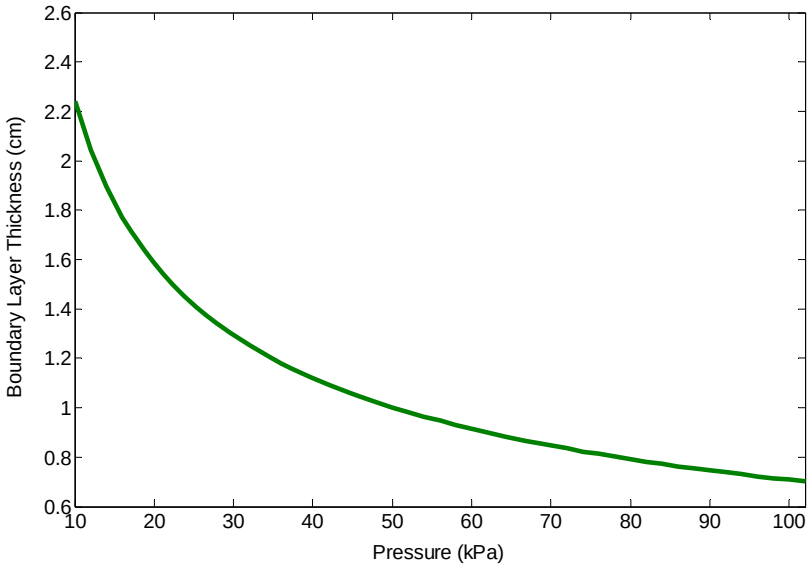

Figure 3-20. Effect of atmospheric pressure on boundary layer thickness of a horizontal flat plate. Air velocity was held constant at 1.0 m s^{-1}.

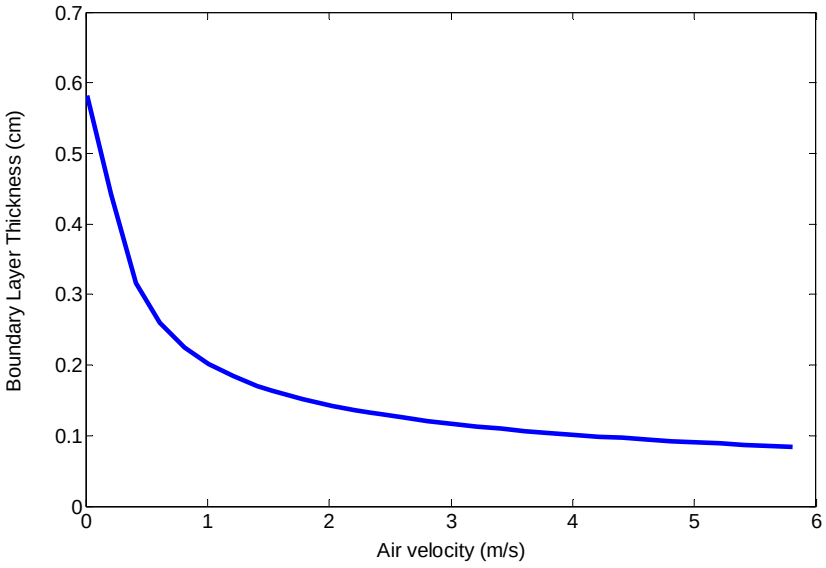

Figure 3-21. Effect of air velocity on boundary layer thickness of a horizontal flat plate. Pressure was held constant at 101 kPa.

Conclusions

To predict the external resistance and boundary layer thickness for a mature radish leaf, convection heat transfer analysis was performed both theoretically and experimentally for a horizontal flat plate. A classical heat transfer model for both free and forced convection regimes was compared with data from controlled experiments. The model fit well for all levels of pressure (12, 33, 66, and 101 kPa) and air velocities (still air, 1.9, 2.8, and 5.8 m s^{-1}) tested. The average error between the predicted and empirical resistances was 2.6 s m^{-1}. As predicted by the model and observed in experiments, external resistance was proportional to both pressure and air velocity. Boundary layer thickness, however, increased significantly at low pressures and air velocities less than 1 m s^{-1}. The external resistance model developed here was a necessary component of the evapotranspiration model that was the overall goal of this research. This analysis also served as a mechanism for testing conventional convection heat transfer equation in low pressure conditions. Predictions of boundary layer thickness, although not tested experimentally, provided some guidance for choosing appropriate locations to measure environmental conditions. Large boundary layers that occurred at low pressures and low air velocities should be considered in the design of low pressure systems.

CHAPTER 4

SURFACE RESISTANCE TO EVAPOTRANSPIRATION IN REDUCED PRESSURE ENVIRONMENTS

Evapotranspiration, the total water lost by plant transpiration and evaporation from the plant and surrounding ground surfaces, can be predicted by the Penman-Monteith model (equation 1-8). Monteith (1965) modified an evaporation model developed by Penman (1948) to account for resistances of the crop canopy to water vapor loss. In this research, surface resistance is defined as the resistance to water vapor transfer through the leaf cuticle layer and stomata. Changes in surface resistance are caused by the opening and closing of stomata while the cuticle resistance remains relatively constant. This chapter examines the effect of atmospheric pressure and other environmental variables on the surface resistance to evapotranspiration.

Literature Review

The rate of water loss by evapotranspiration is determined by both physical and biological parameters. Water vapor diffuses mostly through stomata, and to a lesser extent through the leaf cuticle, from saturated air inside the leaf to the surrounding environment. The rate of water diffusion through the leaf surface is limited by stomatal aperture allowing the plant some control of transpiration rate.

Effects of Environmental Variables on Stomatal Control

Stomata reduce plant water loss while allowing CO_2 diffusion into the leaf for photosynthesis. Therefore, it is no surprise that stomatal control is significantly affected

by the ambient environment. Photosynthetically active radiation (PAR), CO_2 concentration, vapor pressure deficit (VPD), and plant water status are all known to have an effect on stomatal action.

Vapor pressure deficit

During the past two decades a considerable amount of research has been done to investigate stomatal control with regard to ambient humidity. In question is whether guard cells "sense" humidity or the rate of evapotranspiration. Most researchers have concluded that plants use a "feedback" method of control in which they detect and respond to changes in the rate of evapotranspiration and/or water status and not humidity (Comstock, 2002; Lhomme, 2001; Monteith, 1995; Mott and Parkhurst, 1991; and Outlaw, 2003). If the rate of water loss is greater than the rate of water uptake, the water potential of the tissue surrounding the guard cells decreases. Although the exact mechanism is not known, these desiccating cells are believed to send a signal to nearby guard cells causing them to close and the rate of evapotranspiration to decrease (Comstock, 2002). High rates of evapotranspiration may also have a direct affect on guard cell action. According to Outlaw (2003), solutes accumulate in the guard cell apoplast (dead tissue including cell walls, intracellular spaces, and xylem elements through which water flows) as the transpiration stream evaporates. The solute concentration increases at high rates of transpiration and, by osmosis, water flows into the apoplast leaving the guard cells less turgid and causing them to close.

The relationship between stomatal resistance, evapotranspiration rate, VPD, and mass diffusivity was cleverly demonstrated in experiments by Mott and Parkhurst (1991). They compared stomatal resistance of several plant species in air and in helox (79% helium and 21% oxygen). Water evaporates 2.33 times faster in helox than in air due to

the higher mass diffusivity of water in helox. Therefore, in cases of equal stomatal aperture and VPD, evapotranspiration occurred faster for plants in the helox mixture.

Carbon dioxide

In normal and slightly above Earth ambient CO_2 concentrations in the range of 400 to 1000 ppm (P_{co2} = 40.4 to 101 Pa) decreases in concentration cause stomatal opening (Assmann, 1999; Wheeler et al., 1999) and thus, an increase in surface resistance. At CO_2 concentrations above approximately 1000 ppm there is little to no change in stomatal resistance (Jarvis, 1976; Stanghellini and Bunce, 1993). However, in plants exposed to super-elevated CO_2 concentrations greater than 10,000 ppm (P_{CO2} = 1.01 kPa) stomatal resistance was shown to decrease in potato and wheat plants leading to decreased water use efficiency (Wheeler et al., 1999).

Some plants may acclimate to higher CO_2 concentrations as shown by Stanghellini and Bunce (1993). Stomatal resistance increased less as CO_2 concentration was increased from 500 to 2000 ppm for tomato plants grown at 700 ppm versus plants grown at 350 ppm. The decreased sensitivity to changes in CO_2 may mean that plants grown at higher concentrations have increased water use. Soybeans grown at 800 ppm of CO_2 had similar values of canopy surface resistance during short-term exposure to 330 ppm as plants grown at 330 ppm (Jones et al., 1985). Likewise, the surface resistance of plants grown at 330 ppm was similar during short-term exposure to 800 ppm as the plants grown at the higher CO_2 concentration. A more significant effect of long-term exposure to higher CO_2 concentrations was the increase in leaf area. The leaf area of soybeans grown at 800 ppm was 1.8 times greater than those grown at 330 ppm. Increased leaf area led to higher transpiration rates for plants grown at 800 ppm when the surface resistance decreased during exposure to an ambient CO_2 concentration.

Photosynthetically active radiation

Stomata respond to light both directly and indirectly. As the intracellular CO_2 concentration decreases due to photosynthesis, stomata open to take in more CO_2 (Outlaw, 2003). Stomatal resistance of poinsettia cuttings decreased significantly when incident radiation was increased from 50 to 300 W m^{-2} (400-700 nm) in work by Zolnier et al. (2001). There is less of an effect of the magnitude of PAR on stomatal resistance at levels above 500 μmol m^{-2} s^{-1} (Jarvis, 1976).

Mass Diffusivity and Stomatal Resistance

Because mass diffusivity is pressure dependent, growing plants in reduced pressure environments can be expected to yield results similar to those of Mott and Parkhurst's (1991) helox experiments. Equation 4-1 gives the relationship derived from the ideal gas law to quantify the effect of pressure on mass diffusivity (Incropera and DeWitt, 1996). It is assumed that the ideal gas law is valid for the range of pressures used in this research (≥ 10 kPa).

$$D_w = D_w^0 \left(\frac{P^0}{P} \right) \tag{4-1}$$

where D_w = mass diffusivity of water at pressure P, m^2 s^{-1}

P^0 = standard pressure= 101.3 kPa

D_w^0 = mass diffusivity of water at standard pressure = 2.50 x 10^{-5} m^2 s^{-1}

A plot of mass diffusivity as a function of pressure, calculated by equation 4-1, is shown in Figure 4-1. Note that the rate of water diffusion increases significantly at pressures less than 25 kPa. A sharp increase in mass diffusivity at pressures below 25 kPa was verified in experiments by Rygalov et al. (2002).

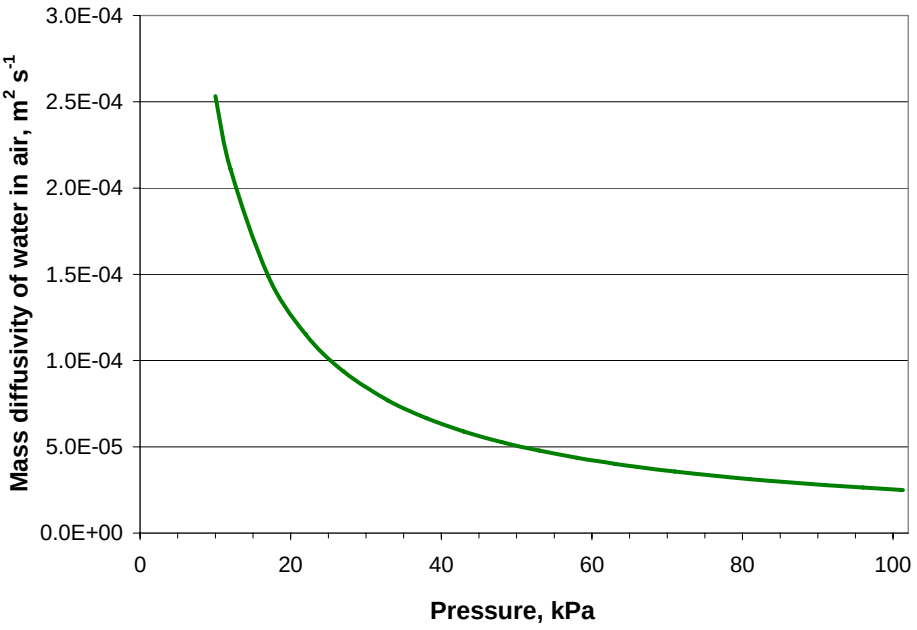

Figure 4-1. The effect of pressure on mass diffusivity of water in air. At pressures lower than 30 kPa, such as those being considered for a greenhouse on Mars, water diffusion occurs much faster than at standard pressure.

Nobel (1999) gives equation 4-2 to calculate stomatal conductance, the inverse of stomatal resistance.

$$g_s = \frac{D}{\ell} = \frac{1}{r_s} \tag{4-2}$$

where g_s = surface conductance, mm s^{-1}

D = mass diffusivity, mm^2 s^{-1}

ℓ = effective path length for diffusion through stomatal pore, mm

r_s = surface resistance, s mm^{-1}

If stomatal density and pore depth does not change the effect path length, ℓ, is a function of stomatal aperture only (Mott and Parkhurst, 1991).

Note from equation 4-2 that surface resistance is negatively proportional to mass diffusivity. As an example, consider a plant at 10 kPa and one at standard earth pressure

(101.3 kPa). If all other conditions remain the same and stomatal opening does not change, stomatal conductance will increase by the ratio of the mass diffusivity at 10 kPa to the mass diffusivity at 101.3 kPa. The result is an increase in stomatal conductance by approximately a factor of 10 (see equation 4-3). The corresponding change in stomatal resistance would be a decrease by a factor of 10.

$$g_{s10} = g_{s101.3}\left(\frac{D_{10}}{D_{101.3}}\right) = g_{s101.3}\left(\frac{2.53x10^{-4}}{2.5x10^{-5}}\right) \quad (4\text{-}3)$$

where: g_{s10} = stomatal conductance at 10 kPa, m s^{-1}

$g_{s101.3}$ = stomatal conductance at 101 kPa, m s^{-1}

D_{10} = mass diffusivity of water at 10 kPa, m^2 s^{-1}

$D_{101.3}$ = mass diffusivity of water at 101.3 kPa, m^2 s^{-1}

Plant Adaptation and Surface Resistance

This research focused on short term response of surface resistance to changing environmental conditions and did not consider effects of adaptations of plants grown at high CO_2 concentrations or low pressures. Adaptation of plants to Mars greenhouse conditions may affect surface resistance. For example, stomatal density has been shown to be significantly affected by environmental conditions during development.

In a study by Schoch et al. (1980), a decrease in the stomatal index (ratio of stomatal cells to total number of cells) of new, developing leaves of *Vigna sinensis* plants growing in high light conditions was observed following exposure to only one day of shade. Gay and Hurd (1975) found that tomatoes grown under high light conditions (100 W m^{-2}) had 30 stomata mm^{-1} on the upper surface of the leaf compared to less than one stomata mm^{-1} for those grown in low light (20 W m^{-2}).

Humidity and carbon dioxide concentrations have also been shown to impact stomatal frequency. A study by Bakker (1991) compared the stomatal density and average size of stomata for cucumber, tomato, and sweet pepper grown in a range of air vapor pressure deficit (VPD_{air}) treatments from 0.2-1.6 kPa. Their results showed that both stomatal density and size, and, consequently, total pore area, increased with lower VPD_{air} (high humidity). Woodward (1987) found that stomatal frequencies have decreased by about 40% since before the industrial revolution when atmospheric CO_2 concentration was about 60 ppm lower than current levels. Similarly, during exposure to the same VPD_{air} and PAR levels tomato plants grown at 700 ppm experienced higher rates of water loss than plants grown at 350 ppm (Stanghellini and Bunce, 1993). It should be noted that there is significant variation between species with regard to the effect of carbon dioxide concentration on stomatal density.

Environmental conditions may also affect the leaf area and/or size of stomata so that changes in stomatal density do not necessarily denote changes in total pore area. Bakker (1991) showed that statistical changes in stomatal pore area may not necessarily result in significant changes in stomatal conductance. In a study by Jones et al. (1985) leaf area was a factor of 1.8 greater for soybeans grown at 800 ppm than plants grown at 330 ppm. Surface resistance was similar for both sets of plants at the same CO_2 concentration leading the authors to conclude that increased water loss rates of plants acclimated to higher CO_2 conditions was caused by enhanced leaf area and not surface resistance adaptations.

Objectives

The objective of this chapter is to quantify the effects of atmospheric pressure, CO_2, and PAR on evapotranspiration and surface resistance. These effects will be

incorporated into an empirical model of surface resistance for mature radish plants acclimated to standard pressure.

Materials and Methods

Experiments to collect data for calculation of surface resistance were performed in controlled environment conditions as suggested by Jarvis (1976). Evapotranspiration rates of radish plants were measured during short-term exposure to different levels of pressure, CO_2 concentration, and PAR inside the small-scale pressure controlled chambers described in chapter 2. Each of the three bell jar-based chambers was considered a replication as it offered independent control of pressure, CO_2 concentration, air temperature, and relative humidity. Maximum PAR was determined by the external growth chamber and screens were added to reduce the light level.

Plant Material

A group of twelve pots each containing two 18-to-24-day-old radish plants (Raphanus sativa L. 'Cherry Bomb II') were available for each three-hour measurement period. Seeds were pretreated for 15-20 minutes in a 10% trisodium phosphate solution prior to planting. Three or four pretreated seeds were planted per pot containing in metro mix media. All plants were grown in the same controlled environment chamber as the small-scale pressure controlled chambers. The chamber environmental conditions are given in Table 4-1. Plants were culled after one week to leave two similar sized seedlings per pot. Plants were watered daily with a 1 X Hoagland's solution. Planting dates were staggered so that 12 pots of 18-to-24-day-old radish plants were available for each week of experimentation. One pot per chamber was randomly selected for each measurement period. Each pot was never used more than once per day to allow for complete recovery following stress event.

Table 4-1. Controlled environment chamber conditions. The radish plants used in this research were grown in the following conditions for 24 days.

Parameter	Setpoint
Air temperature	24 ^{o}C
Relative humidity	70%
PAR	360 μmol m-2 s-1
Photoperiod	16/8

Evapotranspiration Measurement

To measure evapotranspiration, a randomly selected pot of radish plants was centered on the load cell of the bell jar chamber. Before the start of each run, 20 mL of nutrient solution was added to a small tray placed underneath the pot of radishes to make certain that plants were well-watered throughout the measurement period. The bell jar was then placed on top of the base and, if necessary, the shading material was slipped over the bell jar to reduce the light level. Environment setpoints were added to the control program and data logging was activated. One hour was allowed for the system and plants to stabilize. The rate of evapotranspiration was taken as the slope of a linear regression line fit to the weight data for the subsequent two-hour period. Each run of three replications lasted a total of three hours.

A preliminary experiment was performed to determine the amount of time needed for plants to reach steady-state. Leaf temperature was measured with an infrared thermocouple while plants were subjected to 12 kPa for three hours (see Figure 4-2). Plants reached steady-state, as indicated by stabilization of leaf temperature, approximately 45 minutes after the pressure was reduced to 12 kPa.

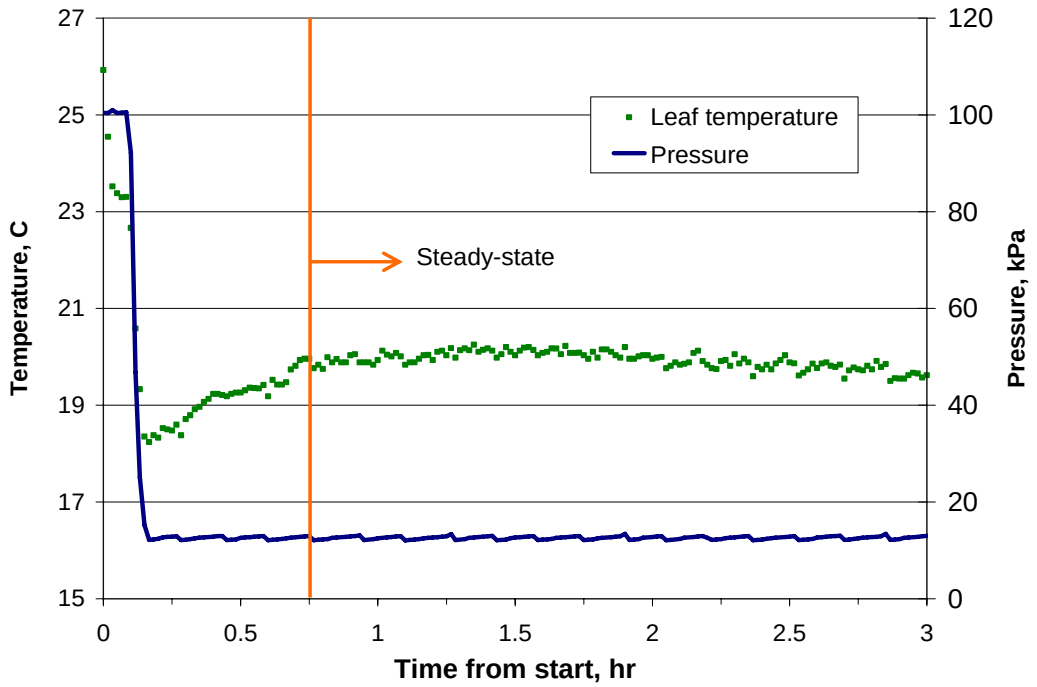

Figure 4-2. Leaf temperature transient response to changes in total pressure. Radish plants subjected to 12 kPa reached steady-state within one hour of initial pressure drop.

Experimental Design

Experiments were completely randomized with a 4x2x2 factorial treatment structure. Table 4-2 gives the levels of pressure, CO_2, and PAR treatments applied. Data not used in the development of the surface resistance model were used for validation of the evapotranspiration model (chapter 6). As previously mentioned, a pot containing two radish plants inside each of the bell jars for the three-hour measurement period was considered a replication.

Table 4-2. Evapotranspiration treatment structure. A 4x2x2 factorial treatment structure was used in this research to determine the effects of pressure, CO_2, and PAR on evapotranspiration and surface resistance of radish plants.

Treatment	Levels
Pressure	12, 33, 66, and 101 kPa
CO2	40 and 150 Pa
PAR	340 and 160 μmol m^{-2} s^{-1}

Model Development

Empirical models for surface resistance based on the work of Jarvis (1976) have been widely used in greenhouse applications (Baille et al., 1994; Stanghellini, 1987; Zolnier et al., 2001) to predict the effects of environmental conditions on surface resistance, r_s. These models predict surface resistance as a reference value multiplied by a dimensionless function that accounts for the change in surface resistance caused by changes in environmental conditions. Equation 4-4 gives an example of a Jarvis-type model for surface resistance that accounts for the effects of solar radiation (PAR), air vapor pressure deficit (VPD_{air}), and carbon dioxide concentration (CO_2). Note that the functions for environmental factors are not necessarily of the same mathematical form.

$$r_s = r_{s\,ref}\, f_1(PAR)\, f_2(VPD)\, f_3(CO_2) \tag{4-4}$$

The reference resistance, r_{sref}, is a physiological value and can be determined from experimentation or from literature (Stanghellini, 1987). This model assumes that there are no interactions among environmental variables. The nature of the functions for environmental factors is best determined by regression analysis from controlled environment data (Jarvis, 1976).

The simple, empirical model of equation 4-4 is often chosen over more complex, mechanistic models for predicting surface resistance. Stomatal control is complicated and likely involves signals from a number of sources throughout the plant. The level of

detail required for development and application of a mechanistic model of stomatal action is often not feasible or necessary. Aubinet et al. (1991) found that when considering a crop grown in protected culture, external resistances caused by leaf boundary layers were typically much larger than the surface resistances. Their data suggest that stomatal opening and closing has little effect on evapotranspiration rate compared to the external resistance on a canopy scale.

Surface resistance, equations 4-5 and 4-6, was calculated from evapotranspiration rates measured in the previously described experiments by inversion of a) the latent heat loss equation (1-3) and b) the Penman-Monteith evapotranspiration model (equation 1-8). Values of surface resistance estimated by these two equations were compared to determine the applicability of the Penman-Monteith model for low-pressure conditions. Inversion of equation 1-3 yielded the following equation for surface resistance.

$$r_s = \frac{\frac{\rho_{air} c_a}{\gamma} VPD_{leaf-air}}{LE} - r_h \tag{4-5}$$

where: ρ_a = density of air, kg m^{-3}

c_p = specific heat of air at constant pressure, J kg^{-1} $^oC^{-1}$

$VPD_{leaf-air}$ = leaf-to-air vapor pressure deficit, kPa

γ = psychrometric constant, Pa $^oC^{-1}$

LE = latent heat flux, W m^{-2}

r_h = canopy external resistance for sensible heat transfer, s m^{-1}

Equation 4-6 was obtained by inversion of the Penman-Monteith model.

$$r_s = \frac{\rho_{air} c_a VPD_{air}}{\gamma LE} - r_h \left(1 + \frac{\Delta (LE - R_n)}{\gamma LE} \right) \tag{4-6}$$

where: VPD_{air} = air vapor pressure deficit, kPa

Δ = slope of saturation vapor pressure curve, Pa $^{o}C^{-1}$

R_n = net radiation, W m^{-2}

Equations 4-5and 4-6 required estimation of several heat fluxes and air properties. Latent heat flux, LE, was estimated by equation 4-7. The latent heat of vaporization, λ, was assumed to be 2442 kJ kg^{-1} for an air temperature of 24 ^{o}C. ET (g m^{-2} s^{-1}) was the measured evapotranspiration from the experiments described above.

$$LE = \lambda * ET \tag{4-7}$$

The procedure for estimating net radiation, R_n, was the same as used in Zolnier et al. (2004). Net radiation, equation 4-8, was the sum of the effects of long- and short-wave radiation. Incoming shortwave radiation, R_{sw}, was measured at canopy height beneath the bell jar with and without shading material by an Eppley pyranometer (Model PSP, The Eppley Laboratory, Inc, Newport, RI). The average incoming short-wave radiation was 95 W m^{-2} without shading and 48 W m^{-2} with shading in place. Long wave radiation was calculated by the Stefan-Boltzmann equation. The reflectance and emissivity of the canopy was assumed to be 0.27 and 0.90 respectively (Zolnier et al., 2004).

$$R_n = (1-\rho)R_{sw} + \sigma\varepsilon(\mathbf{T}_{sur}^4 - \mathbf{T}_s^4) \tag{4-8}$$

where: ρ = reflectivity, dimensionless

σ = Stefan-Boltzmann constant, W m^{-2} K^{-4}

ε = emissivity, dimensionless

$\mathbf{T}_{sur}$ = average absolute temperature of surroundings, K

$\mathbf{T}_s$ = average absolute temperature of canopy, K

It was assumed that the bell jar was in equilibrium with the external chamber and that $\mathbf{T}_{sur}$ could be well estimated by the chamber temperature of 24 ^{o}C.

The canopy external resistance, r_h, was calculated by equation 3-10 from values of r_e predicted by the model described in chapter 3 for air velocity equal to 1.3 m s^{-1}. Leaf area of each plant was measured on day 24 by a leaf area meter (LI-3000A, Licor Biosciences, Lincoln, NE). A preliminary experiment was performed to determine the change in leaf area from day 18 to day 24. There were no statistical differences between total leaf area of radish plants on days 18, 20, 22, and 24 ($\alpha = 0.05$). From this, it was concluded that measuring leaf area each day during experimentation was not necessary.

Functional relationships for the effects of many environmental factors including PAR, CO_2, VPD, and leaf temperature have been developed for a variety of crops. In this research, data from short duration controlled environment experiments with mature radish plants were used to determine the effect of pressure on r_s. Effects of CO_2 and PAR were incorporated in r_{sref}. Although it is recognized that there may be adaptations, such as changes in stomatal density, that occur during long term exposure to different environmental conditions, only the short term responses were considered in the scope of this research.

Results and Discussion

Mean values of evapotranspiration, canopy external resistance (r_h), and surface resistance (r_s) calculated by equation 4-5 are shown in Table 4-3. Values of surface resistance estimations made by the Penman-Monteith model at the lowest pressures were negative. Negative values of surface resistance are not physically possible and this estimation error was attributed to the lower leaf temperatures that occurred at 12 kPa (see chapter 6). Thus, the remaining results and conclusions are based on surface resistance

calculated by the latent heat equation. Reference conditions were at 101 kPa. The effects CO_2 and PAR on evapotranspiration and surface resistance were evaluated by comparison to these reference conditions.

Evapotranspiration (ET) was negatively proportional to pressure (Figures 4-3 and 4-3). At reference levels of CO_2 and PAR (40 Pa and 341 μmol m^{-2} s^{-1}) average ET increased from 2.3 g m^{-2} min^{-1} at 101 kPa to 3.3 g m^{-2} min^{-1} at 12 kPa. The same trend in ET as a function of pressure was observed in different levels of CO_2 and PAR. In elevated CO_2 conditions (150 Pa) ET increased from 2.0 to 2.7 g m^{-2} min^{-1} between 101 and 12 kPa. Likewise, ET increased from 1.4 to 3.1 g m^{-2} min^{-1} in a low PAR environment (161 μmol m^{-2} s^{-1}). Because the observed trend in evapotranspiration as a function of pressure was similar to that of mass diffusivity (Figure 4-1), it is hypothesized that increases in ET were direct results of increases in stomatal conductance at reduced pressures. This agreed with the relationship given by Mott and Parkhurst (1991) for stomatal conductance. Surface resistance (Table 4-3), calculated by equation 4-5, decreased with pressure as predicted by equation 4-4. The lowest resistances were observed at 12 and 33 kPa (Figure 4-5). ET was also influenced by decreases in external resistance at low pressures (Chapter 3).

Elevated CO_2 concentrations decreased ET (data shown in Table 4-3). When the concentration of CO_2 was increased from 40 to 150 Pa, ET decreased some, although not significantly, at 33, 66, and 101 kPa (Figure 4-4). At 12 kPa, however, ET decreased from 3.3 to 2.7 g m^{-2} min^{-1} which was statistically significant (α=0.05). This decrease in ET at elevated CO_2 corresponded to an increase in r_s from at 12 kPa from 178.6 s m^{-1} to 228.3 m^{-1} (Figure 4-6). The mass diffusivity of water vapor, a function of pressure, was

the same for these two treatments. Therefore, the increase in r_s in elevated CO_2 conditions could only have been a physiological response. As in research by Assmann (1999) and Wheeler et al. (1999), stomata closed when CO_2 levels rose from 40 to 150 Pa causing an increase in r_s. The increase in r_s was enough to protect the plants from the severe water stress observed at 12 kPa and 40 Pa of CO_2 (see photo in Figure 4-3). In fact, there were no statistical differences between ET at 12 kPa and elevated CO_2 (ET = 2.7 g m^{-2} min^{-1}) and 101 kPa and 40 Pa of CO_2 (ET = 2.3 g m^{-2} min^{-1}). There was a slight decrease in ET, although not significant at all pressures, when PAR was reduced from 341 to 161 μmol m^{-2} s^{-1} (Table 4-3 and Figure 4-6). The decrease in incident radiant energy reduced the energy available for water evaporation.

An empirical equation for surface resistance as a function of pressure was determined by linear regression in Figure 4-7. This equation was developed for incorporation in the surface resistance model of equation 4-4. This additional function (equation 4-7) accounted for the effect of pressure on r_s in the multiplicative model.

$$r_s = r_{s101}(0.0066 * P + 0.36) \qquad (4\text{-}7)$$

To estimate surface resistance, a reference value was multiplied by an empirical linear function as in equation 4-7. The reference value, r_{s101}, was the surface resistance determined at a particular set of environmental conditions. In this research, reference values were taken as the average surface resistance at 101 kPa for a particular $CO_2$and PAR setpoint. No functions were developed to account for changes in CO_2 and PAR. 463.9 (CO_2 = 40 Pa; PAR = 341 μmol m^{-2} s^{-1}), 518.7 (CO_2 = 150 Pa; PAR = 341 μmol m^{-2} s^{-1}), and 446.4 s m^{-1} (CO_2 = 40 Pa; PAR = 161 μmol m^{-2} s^{-1}).

Table 4-3. Evapotranspiration and resistance results. Shown below are mean values (± standard deviation) of evapotranspiration, canopy external resistance (r_h), and surface resistance (r_s) for three replications. Letter superscripts indicate statistical differences among values in a column per pressure treatment and symbolic superscripts indicate differences between pressures for each treatment ($\alpha = 0.05$).

Treatment	Evapotranspiration ($g\ m^{-2}\ min^{-1}$)	r_h ($s\ m^{-1}$)	r_s ($s\ m^{-1}$)
12 kPa			
CO_2 = 40 Pa PAR = 341 μmol $m^{-2}\ s^{-1}$	3.3 (±0.1)^{A*}	15.0 (±0.68)	178.6 (±5.9)^{A*}
CO_2 = 150 Pa PAR = 341 μmol $m^{-2}\ s^{-1}$	2.7 (±0.06)^{B*}	19.5 (±3.1)	228.3 (±7.8)^{B*}
CO_2 = 40 Pa PAR = 161 μmol $m^{-2}\ s^{-1}$	3.1 (±0.1)^{A*}	16.3 (±5.5)	210.3 (±24.5)^{B*}
33 kPa			
CO_2 = 40 Pa PAR = 341 μmol $m^{-2}\ s^{-1}$	2.9 (±0.2)^{A*}	23.0 (±2.6)	293.9 (±23.5)^{A**}
CO_2 = 150 Pa PAR = 341 μmol $m^{-2}\ s^{-1}$	2.8 (±0.1)^{A*}	24.7 (±0.9)	296.2 (±16.0)^{A*}
CO_2 = 40 Pa PAR = 161 μmol $m^{-2}\ s^{-1}$	2.3 (±0.2)^{B**}	31.0 (±8.8)	378.8 (±40.0)^{B*}
66 kPa			
CO_2 = 40 Pa PAR = 341 μmol $m^{-2}\ s^{-1}$	2.4 (±0.2)**	34.0 (±6.6)	369.8 (±27.1)^{A***}
CO_2 = 150 Pa PAR = 341 μmol $m^{-2}\ s^{-1}$	2.0 (±0.3)**	35.6 (±0.9)	477.6 (±82.3)^{A**}
CO_2 = 40 Pa PAR = 161 μmol $m^{-2}\ s^{-1}$	2.0 (±0.2)***	40.6 (±14.4)	436.8 (±66.9)^{B**}
101 kPa			
CO_2 = 40 Pa PAR = 341 μmol $m^{-2}\ s^{-1}$	2.3 (±0.3)^{A**}	46.1 (±10.6)^{A}	463.9 (±52.2)^{A****}
CO_2 = 150 Pa PAR = 341 μmol $m^{-2}\ s^{-1}$	2.0 (±0.2)^{A**}	49.4 (±9.5)^{B}	518.7 (±68.3)^{A**}
CO_2 = 40 Pa PAR = 161 μmol $m^{-2}\ s^{-1}$	1.4 (±0.4)^{B***}	62.6 (±11.2)^{B}	664.1 (±84.0)^{B***}

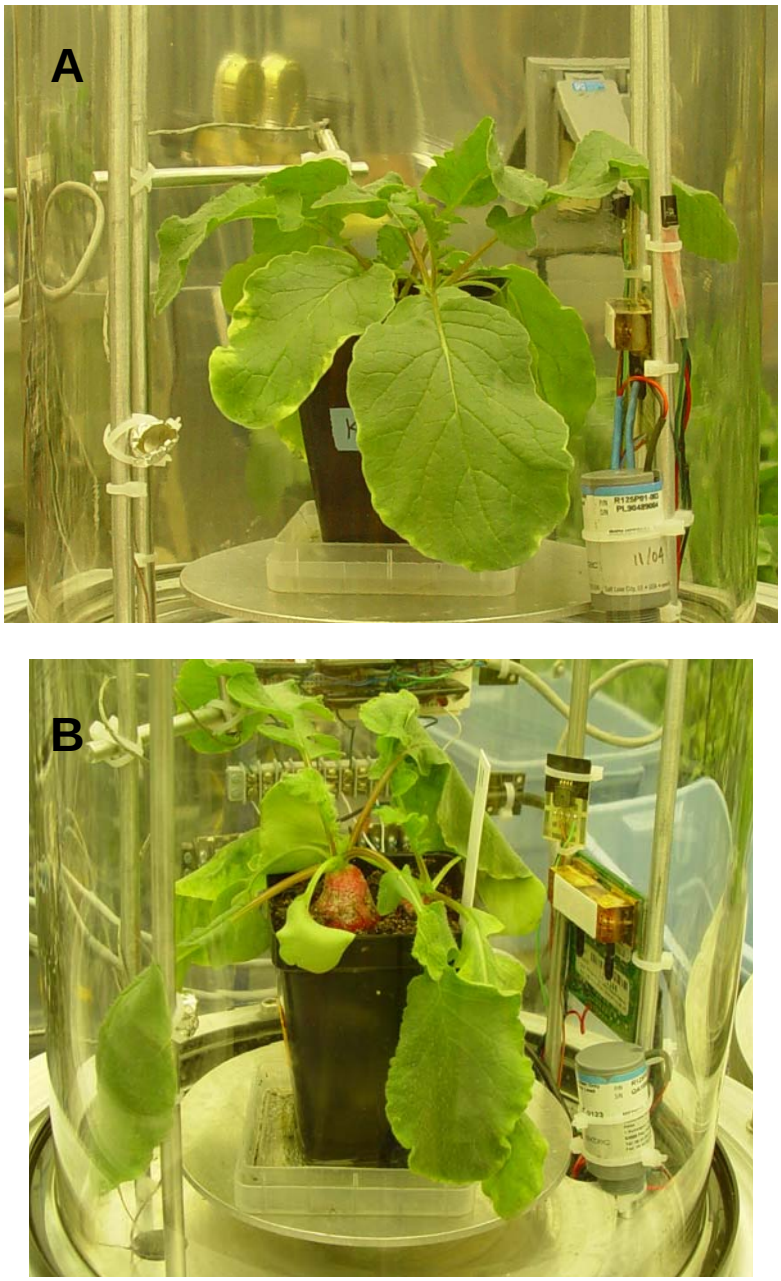

Figure 4-3. Visual observations of water status at 101 and 12 kPa. Photo A shows a turgid radish plant at 101 kPa inside the bell jar system. Photo B shows a radish plant 45 minutes after pressure was reduced to 12 kPa. The CO_2 concentration for the plants in both photos is 40 Pa.

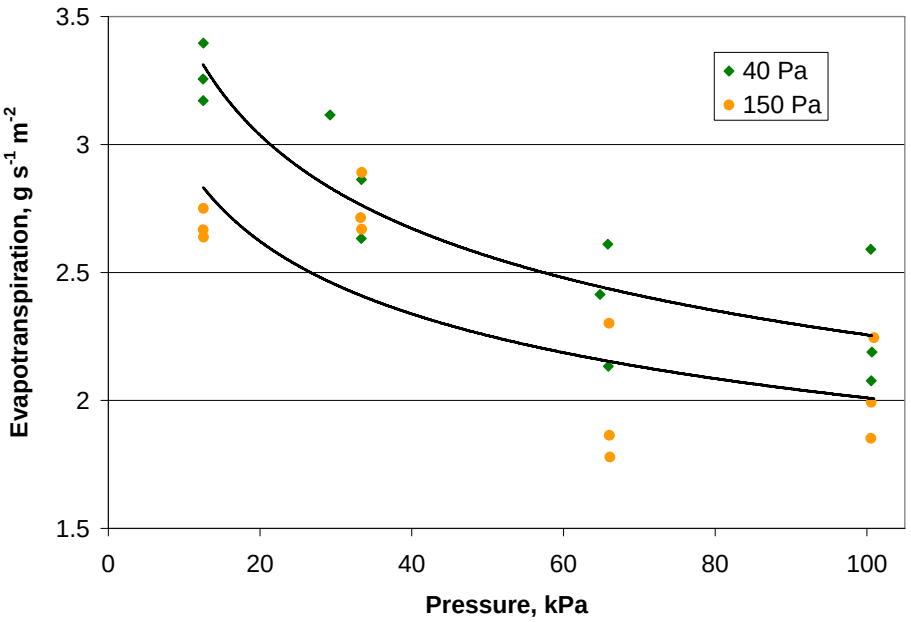

Figure 4-4. Effects of pressure and CO_2 on evapotranspiration. Evapotranspiration rates increased with decreasing pressure and CO_2 concentration. PAR was 341 µmol m^{-2} s^{-1}.

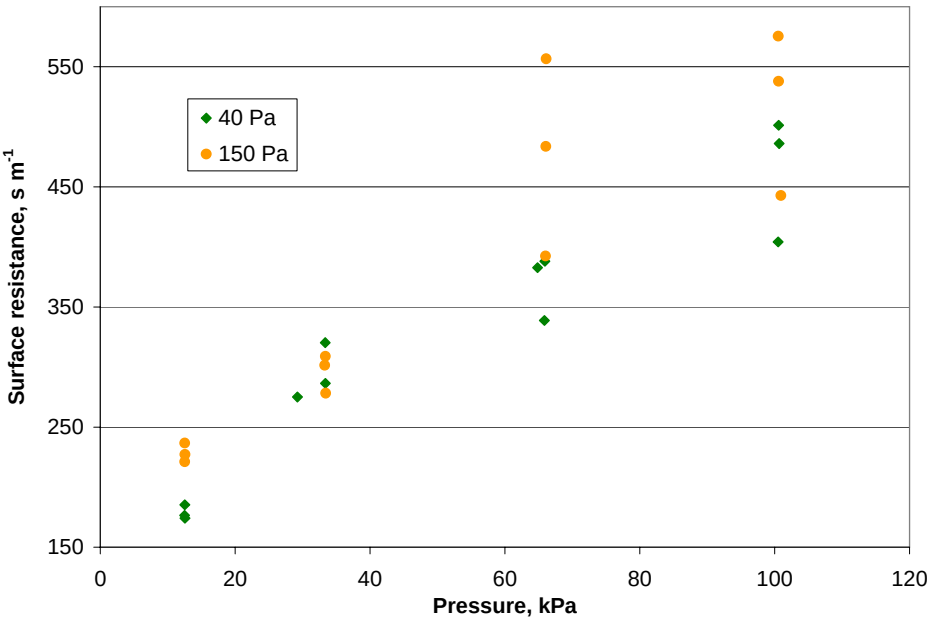

Figure 4-5. Effect of CO_2 on surface resistance. At 12 kPa, surface resistance increased somewhat when the CO_2 concentration was increased from 40 to 150 Pa. PAR was 341 µmol m^{-2} s^{-1}.

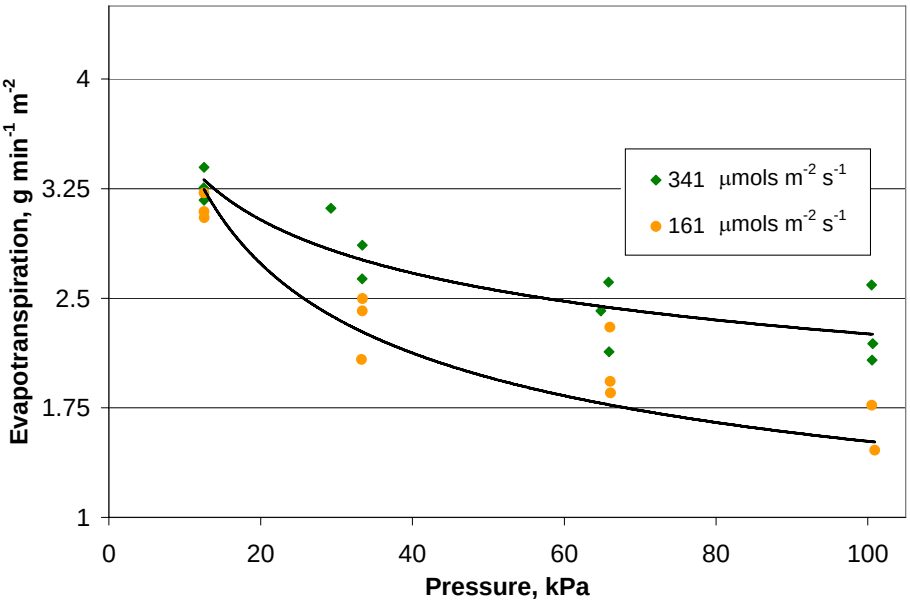

Figure 4-6. Effects of pressure and PAR on evapotranspiration. Evapotranspiration rates increased with decreasing pressure. There were no statistical differences between light levels at the lowest pressure treatment. CO_2 was 40 Pa.

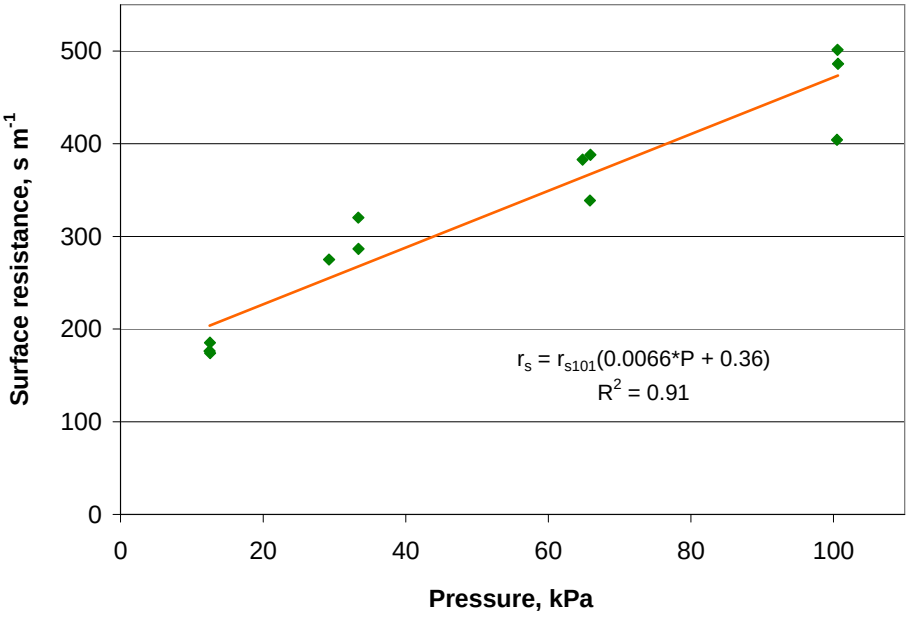

Figure 4-7. Actual and predicted values of surface resistance at 40 Pa and 341 µmol m^{-2} s^{-1}.

The root mean square error (RMSE) of the model, calculated by equation 4-8, is shown in Table 4-4 for different environmental conditions.

$$RMSE = \sqrt{\frac{1}{N}\sum_{i=0}^{N}(y_i - \hat{y}_i)^2} \quad (4\text{-}7)$$

where: N = number of predictions

$y = i^{th}$ actual value

$\hat{y} = i^{th}$ predicted value

Table 4-4. Root mean square error of surface resistance model.

Environmental conditions	**RMSE ($s\ m^{-1}$)**
CO2 = 150 Pa PAR = 341 μmol m-2 s-1	92.7
CO2 = 40 Pa PAR = 161 μmol m-2 s-1	77.3

Conclusions

Surface resistance is the resistance of the leaf surface to water vapor loss. It accounts for the effects of stomata and the leaf cuticle. Since cuticle resistance is constant, changes in surface resistance can be used to understand stomatal control in response to environmental conditions. Surface resistance for mature radish plants, calculated from measured values of evapotranspiration, increased significantly with increasing pressure while evapotranspiration decreased. An empirical model developed to predict r_s as a function of pressure and a reference value determined at standard pressure performed well. There was also a significant effect of CO_2 on stomata. Surface resistance increased and ET decreased when CO_2 rose from 40 to 150 Pa for all pressure treatments. Decreasing PAR from 340 to 160 μmol m^{-2} s^{-1} had little effect on r_s or ET.

CHAPTER 5
EVAPOTRANSPIRATION MODEL PERFORMANCE IN MARS GREENHOUSE CONDITIONS

The evapotranspiration models described in Chapter 1 provides a way to calculate the water loss rate of a crop of plants. It accounts for the physical environment as well as physiological control of plant stomata to limit water loss. Because water stress is anticipated to be a limiting factor in growing plants in a low pressure Mars greenhouse, understanding the effects of environmental parameters on evapotranspiration rate is important in designing the structure and control system.

Thorough analysis of a mathematical model provides a great deal of information. The sensitivity of the prediction to each parameter identifies the parameters with the most influence. To reduce water stress of plants in a Mars greenhouse, more attention should be focused on those parameters that have the strongest affect on the rate of water loss. Design decisions regarding parameters with little influence on ET can be based solely on other factors besides plant water stress.

Error analysis quantifies the performance of the model. One method to quality error is to calculate the anticipated error of the prediction resulting from error in the estimation or measurement of parameters. Another method of error analysis is validation of the prediction in comparison with actual data. Strong correlation of the model with actual data establishes confidence in the model predictions.

Objectives

The objective of this chapter is to evaluate the performance of the Penman-Monteith model including the resistance models of Chapters 3 and 4 to predict evapotranspiration rate of radish plants in Mars greenhouse conditions.

Materials and Methods

The sensitivity of evapotranspiration rate predictions to pressure, air velocity, surface resistance, temperature of surroundings, and incident radiation was determined by varying one parameter at a time with remaining parameters held constant. The parameters evaluated and their reference values are listed in Table 5-1. Evapotranspiration rate was calculated by equation 1-3 for air velocity, surface resistance, and incident radiation varied by -90, -50, +50, and +100% of the reference value. Pressure was varied -90, -25, -50, and -75% and $VPD_{leaf\text{-}air}$ -90, -50, +50 % from their reference values. The percent change in evapotranspiration was calculated by equation 5-1 for each parameter perturbation.

$$\%\ change = \frac{ET - ET^{o}}{ET^{o}} \tag{5-1}$$

where ET = evapotranspiration rate with one parameter varied, g m^{-2} s^{-1}

ET^{o} = evapotranspiration calculated at reference parameters, g m^{-2} s^{-1}

Table 5-1. Parameter descriptions and reference values.

Parameter	Description	Reference value
P	Atmospheric pressure	101 kPa
u_{∞}	Air velocity	1.3 m s^{-1}
r_s	Surface resistance	464 s m^{-1}
$VPD_{leaf\text{-}air}$	Leaf-to-air vapor pressure deficit	2.65 kPa

The error of the evapotranspiration model was evaluated in two ways. First, the propagation of error from environmental measurements to predicted evapotranspiration

was calculated by equation 5-2 (Dally et al., 1993). Errors associated with measurement of pressure, air velocity, incident radiation, temperature of surroundings and estimation of surface resistance were included in the calculation of evapotranspiration error.

$$dET = \sqrt{\left(\frac{\partial ET}{\partial p_1} dp_1\right)^2 + \left(\frac{\partial ET}{\partial p_2} dp_2\right)^2 + \cdots + \left(\frac{\partial ET}{\partial p_i} dp_i\right)^2} \quad (5\text{-}2)$$

where $\frac{\partial ET}{\partial p_i}$ =change in ET per unit change in parameter p_i

dp_i = error in estimation of p_i

The unit change in ET per unit of each parameter was determined by sensitivity analysis. The errors associated with P, u_∞, and $VPD_{leaf\text{-}air}$ were estimated as typical errors for that particular type of sensor. Surface resistance error was estimated as the standard error of the regression model in Chapter 4.

The second method for evaluating the error of the evapotranspiration model was by validation using independent data. Two sets of the evapotranspiration experiments described in Chapter 4 were performed with three replications each. One set was used to develop the surface resistance model and the other was for validation of the evapotranspiration model. The model was validated by computing the RMSE of the model compared to the actual data for different environmental conditions.

Results and Discussion

Evapotranspiration rate was predicted as a function of atmospheric pressure above 10 kPa in Figure 5-1 for the reference conditions. The model predicted a gradual increase in ET as pressure dropped from 101 to approximately 35 kPa and a more significant increase in ET at pressures below 35 kPa. The actual data shown in Figure 5-1 were also used to develop surface resistance model in Chapter 4.

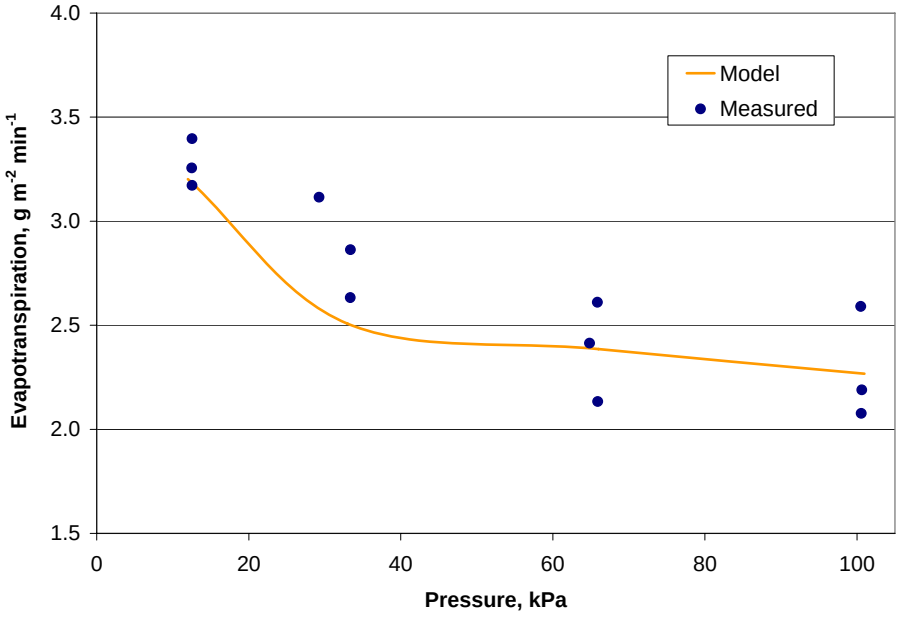

Figure 5-1. Predicted and measured evapotranspiration rate as a function of pressure.

Sensitivity Analysis

The change in evapotranspiration rate for the parameters in Table 5-1 varied one at a time is given in Table 5-2. Predicted ET and the percent change from the ET at reference conditions calculated by equation 5-1 are shown. Predicted ET when all parameters were at reference values was 2.22 g m^{-2} min^{-1}.

Air velocity was negatively proportional to the external resistance to sensible heat transfer. Increasing air velocity decreased the resistance to heat transfer. When air velocity was increased by 50%, ET increased to 2.26 g m^{-2} min^{-1}, 1.8% of the reference ET. Surface resistance was also negatively proportional to ET. With pressure held constant, increasing the surface resistance by 50% from 464 to 696 s m^{-1} decreased ET by 31%. Conversely, decreasing r_s by 90% increased ET four-fold. At constant pressure,

changes in surface resistance were caused by other environmental parameters such as CO_2 concentration and PAR availability (see chapter 4).

Table 5-2. Sensitivity analysis of the evapotranspiration model for Mars greenhouse conditions. Given are the evapotranspiration rate and percent change from reference conditions when only one parameter is varied. The evapotranspiration rate at the reference conditions was 2.47 g m^{-2} min^{-1}.

Parameter	**ET g m^{-2} min^{-1}**	**% change**
Pressure		
10.1 kPa	3.02	36
50 kPa	2.60	17
Air velocity		
0.13 m s^{-1} (r_h = 146.2 s m^{-1})	1.87	-16
0.65 m s^{-1} (r_h = 66.8 s m^{-1})	2.14	-4
1.95 m s^{-1} (r_h = 38.6 s m^{-1})	2.26	1.8
2.60 m s^{-1} (r_h = 33.4 s m^{-1})	2.28	2.7
Surface resistance		
46.4 s m^{-1}	12.23	451
232 s m^{-1}	4.07	83
696 s m^{-1}	1.53	-31
928 s m^{-1}	1.16	-47.7
$VPD_{leaf-air}$		
0.27 kPa	0.23	-90
1.3 kPa	1.09	-51
4.0 kPa	4.00	81

Error Analysis

The expected error in predicted evapotranspiration rate caused by error in parameter estimation was calculated by equation 5-2. Table 5-3 lists the change in ET per unit change in each parameter and error for estimation of each parameter. Error in the estimation of pressure, air velocity, incident radiation, and surrounding temperature are typical errors for sensors for that particular parameter. The estimation error for surface resistance is the RMSE error of the model in Chapter 4 for reference conditions. The expected error in prediction of evapotranspiration rate was 0.36 g m^{-2} min^{-1}.

Table 5-3. Change in evapotranspiration rate and estimated error of parameters for overall error calculation.

Parameter	**$\partial ET/\partial p_i$**	**dp_i**
Pressure, kPa	-0.009	0.5 kPa
Air velocity, m s^{-1}	0.46 (< 2.5 m s^{-1}) 0.172 (≥ 2.5 m s^{-1})	0.1 m s^{-1}
Surface resistance, s m^{-1}	-0.011	35 s m^{-1}
$VPD_{leaf\text{-}air}$	0.84	0.1 kPa

Performance of the evapotranspiration model was validated by comparison to independent data. Equation 4-7 was used to calculate the root mean square error of the model at 12, 33, 66, and 101 kPa. The model was validated (Figures 5-2, 5-3, and 5-4) for the reference conditions (CO_2 = 40 Pa; PAR = 340 µmol m^{-2} s^{-1}), elevated CO_2 (CO_2 = 150 Pa; PAR = 340 µmol m^{-2} s^{-1}); and reduced PAR (CO_2 = 40 Pa; PAR = 160 µmol m^{-2} s^{-1}). The RMSE error was 0.2 g m^{-2} min^{-1} in reference conditions, 0.4 g m^{-2} min^{-1} in elevated CO_2, and 0.3 g m^{-2} min^{-1} in reduced PAR.

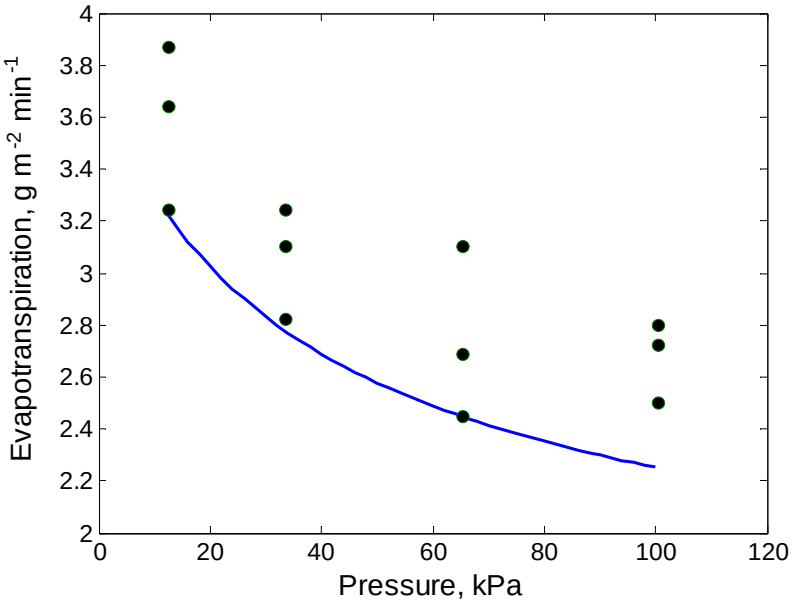

Figure 5-2. Model performance at reference conditions. Carbon dioxide concentration was 40 Pa and PAR was 340 µmol m^{-2} s^{-1}.

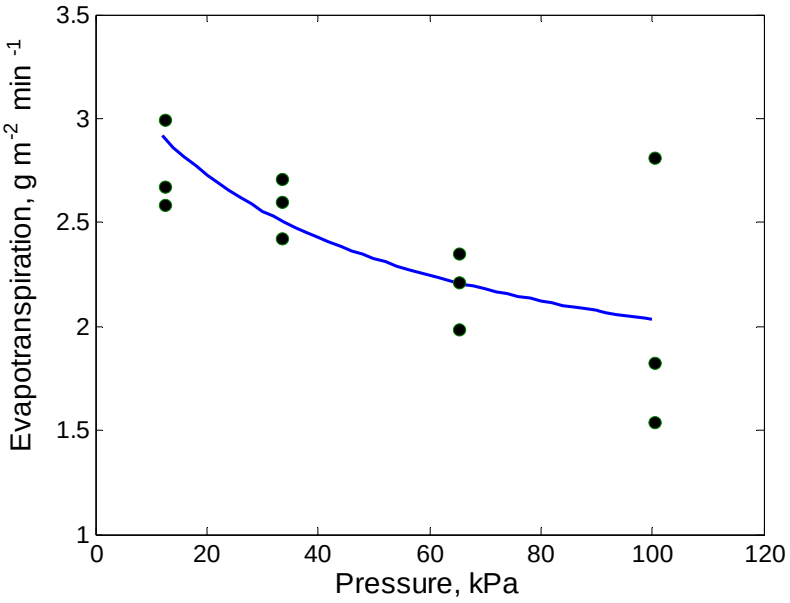

Figure 5-3. Model performance in elevated CO_2. Carbon dioxide concentration was 150 Pa and PAR was 340 μmol m^{-2} s^{-1}.

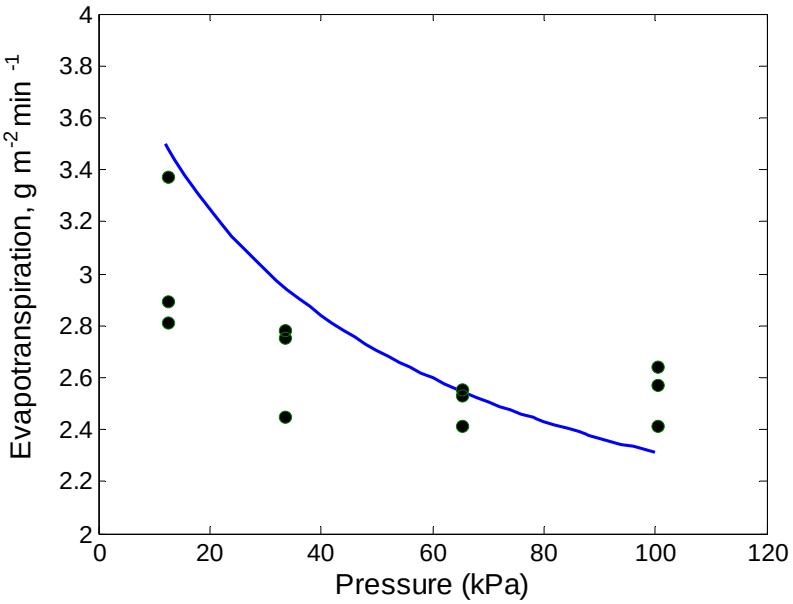

Figure 5-4. Model performance in low PAR conditions. Carbon dioxide concentration was 40 Pa and PAR was 160 μmol m^{-2} s^{-1}.

Conclusions

The evapotranspiration model incorporating the external and surface resistance models developed in this research performed well to predict evapotranspiration rate of mature radish plants in Mars greenhouse conditions. The value of the predicted evapotranspiration was close to the independent evapotranspiration rate measurements. The root mean square error of the model compared to independent data was less than 0.5 g m^{-2} min^{-1} for all conditions tested.

CHAPTER 6
LEAF TEMPERATURE IN A MARS GREENHOUSE

Leaf temperature is an important component of the leaf energy balance. Leaf temperature influences the rate of the evapotranspiration, convection and radiation heat fluxes. High rates of evapotranspiration at low pressures and the extremely cold environment in a Mars greenhouse may cause leaf temperatures below typical values on Earth. This chapter examines the impacts of reduced pressures on leaf temperature and how this affects evapotranspiration.

Literature Review

The temperature of a leaf is determined by the leaf heat balance (equation 1-1). If the rate of heat gain is greater than the rate of heat loss leaf temperature will rise. Conversely, if the rate of heat loss exceeds heat gains, the leaf temperature will decrease. The primary modes of heat transfer for a crop canopy are radiation, convection, and latent heat loss by evapotranspiration.

The vapor pressure deficit between the crop canopy and ambient air ($VPD_{crop\text{-}air}$) is the driving force for evapotranspiration (Zolnier et al., 2000). Accurate calculation of the $VPD_{crop\text{-}air}$ requires that the temperature of the leaf is known to calculate the vapor pressure of the saturated surface of the leaf. A simplification in the derivation of the Penman-Monteith model described in chapter 1 assumes that the leaf temperature is approximately equal to the air temperature. This simplification introduces a new variable, Δ, which is the slope of the saturation vapor pressure curve (see Figure 1-2). The slope is evaluated at the air temperature and is assumed to provide a good

approximation of leaf temperature. This simplification eliminates the need to measure leaf temperature in order to predict evapotranspiration rates. For many situations in Earth greenhouses the difference between leaf and air temperature is small and this assumption is reasonable (Stanghellini, 1987; Zolnier et al., 2000).

The rate of radiation heat transfer to or from a leaf is driven by the difference between the leaf and the temperature of its surroundings. In a subalpine environment in the mountains of Wyoming, frost was observed on plants even when air temperature was above freezing (Jordan and Smith, 1995). Long wave radiation heat transfer from the leaf to the night sky during clear conditions accounted for 30% of the frost events. Leaf temperature depressions (T_{leaf}-T_{air}) of up to -5 ^{o}C were observed in response to radiative cooling.

Several factors of a Mars greenhouse environment may cause leaf temperatures less than those commonly observed in Earth greenhouse conditions. It was shown in Chapter 4 that, depending on the CO_2 concentration, higher rates of evapotranspiration (ET) can be expected at lower atmospheric pressures. It is hypothesized that these higher rates of ET will cool the leaf causing the temperature to drop. Radiative cooling is also expected between the interior surface of the Mars greenhouse structure and the leaf. The average temperature on the surface of Mars is -63 ^{o}C (NASA, 2005). If the greenhouse structure is assumed to be in equilibrium with the outside environment, the direction of radiation heat transfer will be away from the plant canopy.

Objectives

The objectives of this chapter were to examine how the components of the leaf energy balance would be affected in a greenhouse on Mars. Specifically, the effects of high rates of evapotranspiration and radiative cooling on leaf temperature were examined.

Materials and Methods

The effects of reduced pressure on leaf temperature were determined via the use of evapotranspiration experiments. Evapotranspiration rate and leaf temperature were measured during a series of experiments in the pressure controlled chambers described in chapter 2.

Leaf temperature experiments were performed in conjunction with the surface resistance experiments of chapter 4. Leaf temperature was measured by non-contact infrared thermocouples (OS36SM-K-140F, Omega, Stamford, CT) directed at the underside of a leaf. Each bell jar chamber contained one infrared thermocouple (IRt/c). Replacement of the analog input module used to read the IRt/c sensors from bell jars 2 and 3 solved the interference problem, but a new module was not available until the end of the experiments.

Performance of the infrared thermocouples was compared with fine gauge type-T thermocouples during a preliminary study. Leaf temperature of a single radish plant was measured by two IRt/c sensors, one above and one below a leaf, and three type-T thermocouples inserted in the midvein of leaves. Three replications were performed at each of three pressure treatments: 10, 25, and 50 kPa.

The potential effects of the cold surfaces of a Mars greenhouse on the leaf energy balance were determined by a theoretical model. A model to predict the leaf-to-air temperature difference was derived from the energy balance of equation 1-1. Equations 1-1, 1-2, and 1-8 were combined and simplified to give equation 6-1.

$$T_{Leaf} - T_{air} = \frac{\dfrac{(r_s + r_h)R_n}{\rho_a c_p} - \dfrac{VPD_{air}}{\gamma}}{1 + \dfrac{\Delta}{\gamma} + \dfrac{r_s}{r_h}} \qquad (6\text{-}1)$$

Results and Discussion

Infrared Thermocouple Performance

As shown in Table 6-1, the average difference between the mean reading of the infrared thermocouples and the mean of the type-T thermocouples over a two-hour period (one minute sampling interval) was only 0.4 ^{o}C. This is within the error of the IRt/c reading (including analog input module) of 0.8 ^{o}C. T-tests performed on the mean data sets confirmed that there was no difference between the average of the infrared thermocouples and the average of the type-T thermocouples. Figure 6-1 shows data from a single replication at 25 kPa. The infrared temperature readings matched closely with the type-T thermocouple readings. Al-Faraj et al. (1994) recommended the use of infrared thermometry for measuring leaf temperature. They argued that thermocouple measurements are more affected by local air and lead wire temperatures than by the leaf temperature.

Table 6-1. Comparison of temperature sensors for leaf temperature measurement. There was no statistical difference in leaf temperature data measured by non-contact infrared thermocouples and type-T thermocouples inserted in a radish leaf.

Pressure (kPa)	mean IR (^{o}C)	mean TC (^{o}C)	Difference (^{o}C)
10	17.9	18.5	0.5
10	15.8	16.5	0.6
10	16.7	15.8	0.9
25	16.9	17.0	0.1
25	16.9	17.3	0.5
25	16.7	16.8	0.1
50	18.5	18.7	0.2
50	18.4	18.9	0.4
50	18.8	18.4	0.4

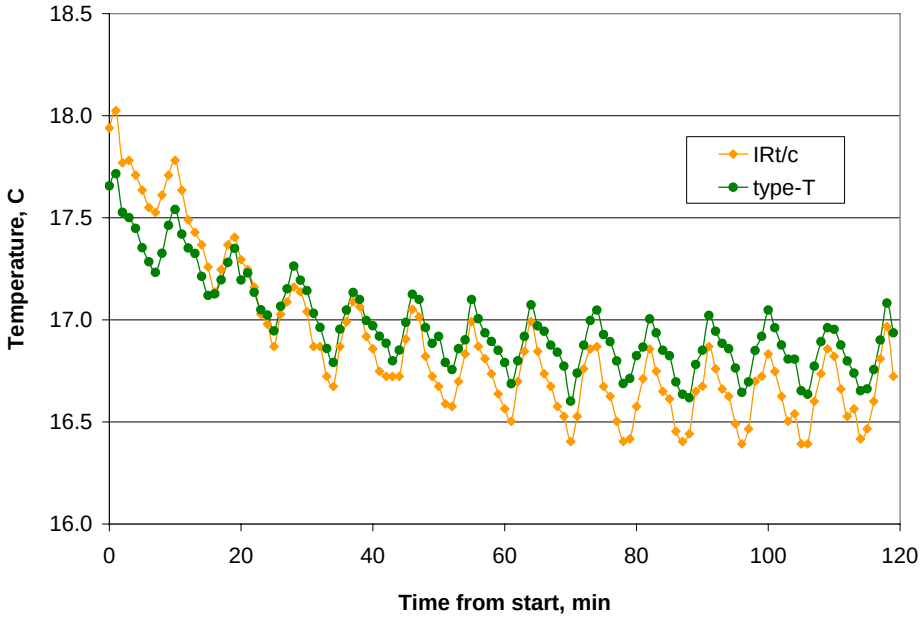

Figure 6-1. Leaf temperature measurement at 25 kPa. Leaf temperature readings from infrared and type-T thermocouples were similar over the course of a two-hour 25 kPa treatment.

Effects of Evapotranspiration at Reduced Pressures on Leaf Temperature

The average values of evapotranspiration, leaf temperature, and leaf-to-air temperature difference for each pressure treatment in bell jar 1 are given in Table 6-2. The data presented here included both levels of CO_2 and PAR treatments. As first shown in chapter 4, there was no change in the rate of evapotranspiration at 33, 66, and 101 kPa. Evapotranspiration at 12 kPa was 3.6 g m^{-2} min^{-1}, significantly higher than at higher pressures.

Higher rates of evapotranspiration at 12 kPa caused the lowest leaf temperature, 19.3 ^{o}C, and the largest leaf-to-air temperature difference, -5.3 ^{o}C. Note that negative leaf-to-air temperature differences occurred when leaf temperature was less than air

temperature. Leaves were cooler than air at all pressures except 101 kPa, when leaves were an average of 1.1 ^{o}C warmer than air.

Figures 6-2 and 6-3 show leaf-to-air temperature difference as a function of pressure and evapotranspiration rate, respectively. The relationship between pressure and leaf-to-air temperature difference ($R^2 = 0.57$) was a bit stronger than it was for evapotranspiration rate ($R^2 = 0.30$). This suggested that there were other modes of heat flux away from the leaf in addition to evaporative cooling.

Table 6-2. Effects of pressure on evapotranspiration rate and leaf temperature. Shown in the table below are the average values (± standard deviation) for all eight measurements made in bell jar 1 at each pressure. Different superscripts indicate statistical difference (α=0.05).

Pressure (kPa)	**ET ($g\ m^{-2}\ min^{-1}$)**	**T_{leaf} (^{o}C)**	**$T_{leaf} - T_{air}$ (^{o}C)**
12	3.6 (±1.0)^{A}	19.3 (±3.3)^{A}	-5.3 (±2.8)^{A}
33	2.5 (±0.6)^{B}	22.6 (±2.0)^{B}	-1.9 (±1.6)^{B}
66	2.1 (±0.27)^{B}	23.5 (±1.8)^{BC}	-1.1 (±1.6)^{BC}
101	2.5 (±0.6)^{B}	25.6 (±2.7)^{C}	1.1 (±2.3)^{C}

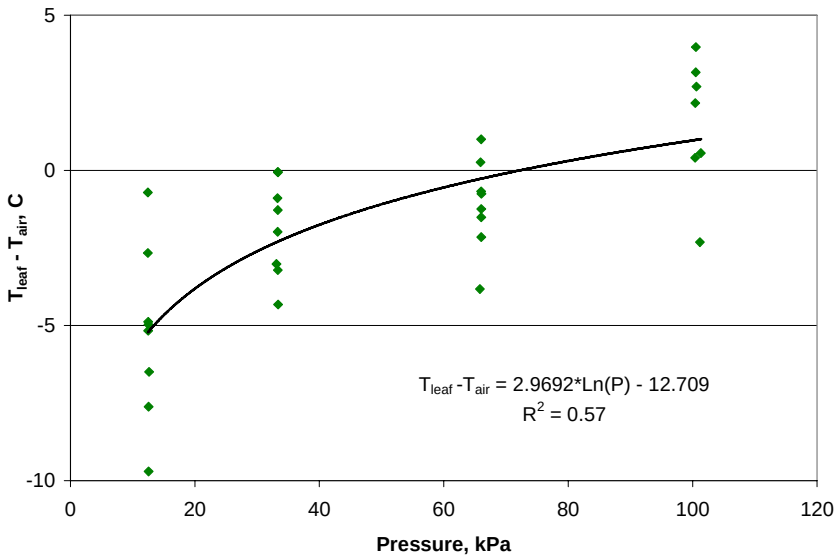

Figure 6-2. Effect of pressure on leaf-to-air temperature difference. The largest differences between leaf and air temperatures occurred at 12 kPa when leaves were always cooler than air.

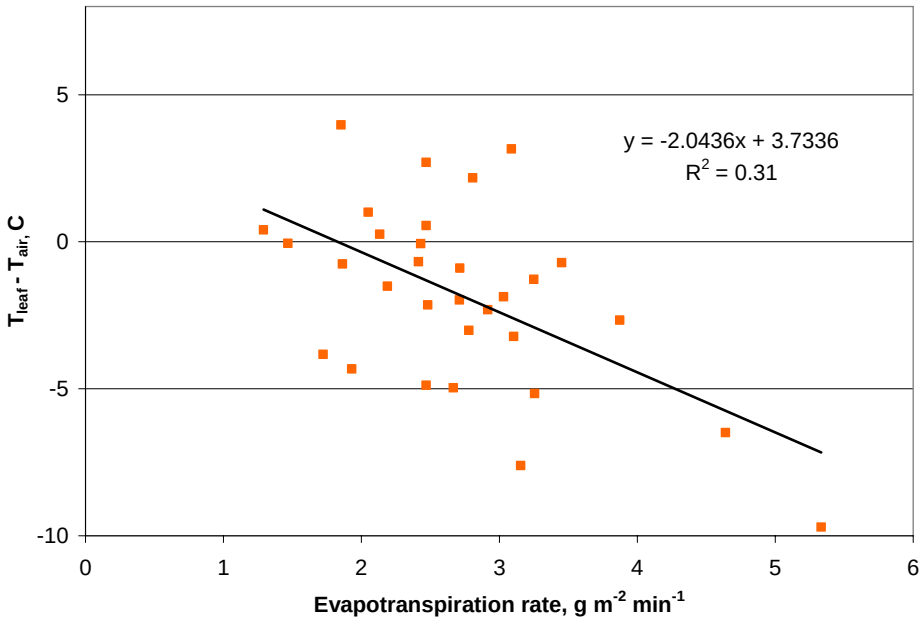

Figure 6-3. Effect of evapotranspiration rate on leaf-to-air temperature difference. Higher rates of evapotranspiration led to leaf temperatures several degrees below the ambient air.

Leaf Temperature in a Mars Greenhouse

Figure 6-4 shows the leaf-to-air temperature difference predicted by equation 6-1 as a function of the temperature of surrounding surfaces for 12, 33, 66, and 101 kPa. Surface resistance was estimated by the model in chapter 4 with a reference value, r_{sref}, of 75 s m^{-1}. Canopy external resistance was estimated by the model in chapter 3 for air velocity equal to 1.3 m s^{-1} and a leaf area index of 1. Net radiation was estimated using equation 4-7 with an incoming short wave radiation of 150 W m^{-2}, reflectance of 0.27, and emissivity of 0.9. Leaf temperature was held constant and the temperature of the surroundings ranged from -70 ^{o}C (R_n = -180 W m^{-2}) to 20 ^{o}C (R_n = 110 W m^{-2}). At the lowest values of net radiation, estimates of latent heat flux, equation 1-8, were negative. Because evapotranspiration can only be a heat loss, not a gain, these values were replaced with LE = 0. The heat balance was then reduced to equation 6-2.

$$R_n - H = 0 \tag{6-2}$$

Substitution of equation 1-2 into 6-2 and rearranging gave equation 6-3 for leaf-to-air temperature difference when evapotranspiration was zero.

$$T_{Leaf} - T_{air} = \frac{R_n r_h}{\rho_a c_p} \tag{6-3}$$

In Figure 6-4, the sharp decrease in leaf-to-air temperature difference occurred when LE = 0. Table 6-3, gives the predicted latent and sensible heat fluxes and the leaf-to-air temperature difference for range of T_{sur} values from -70 to 20 ^{o}C. At the colder T_{sur}, leaves had no latent heat loss and all heat gained by convection from the warmer air surrounding the canopy, was lost by radiation heat transfer to the cold surroundings. The sensible heat loss decreased the temperature of the leaf. When T_{sur} was warmer, a portion of the heat gain by convection was lost by evaporative cooling during transpiration.

The magnitude of the difference between leaf and air temperatures increased as pressure decreased. For the conditions applied in the model for Figure 6-4 and Table 6-3, the only mode of heat gain was convection from the warmer ambient air. At lower pressures the decrease in air density reduces the effectiveness of convection heat transfer. Evapotranspiration and radiation become the dominant heat transfer modes, thereby cooling the leaves. For example, when T_{sur} was -40 ^{o}C net radiation for both 12 and 101 kPa was -117 W m^{-2} and there was no latent heat loss. The resistance to sensible heat transfer by convection was higher for 101 kPa, 47 versus 16.5 s m^{-1}. Therefore, although the magnitude of sensible heat loss was the same for both pressures, the smaller resistance at 12 kPa resulted in a lower predicted leaf temperature than at 101 kPa.

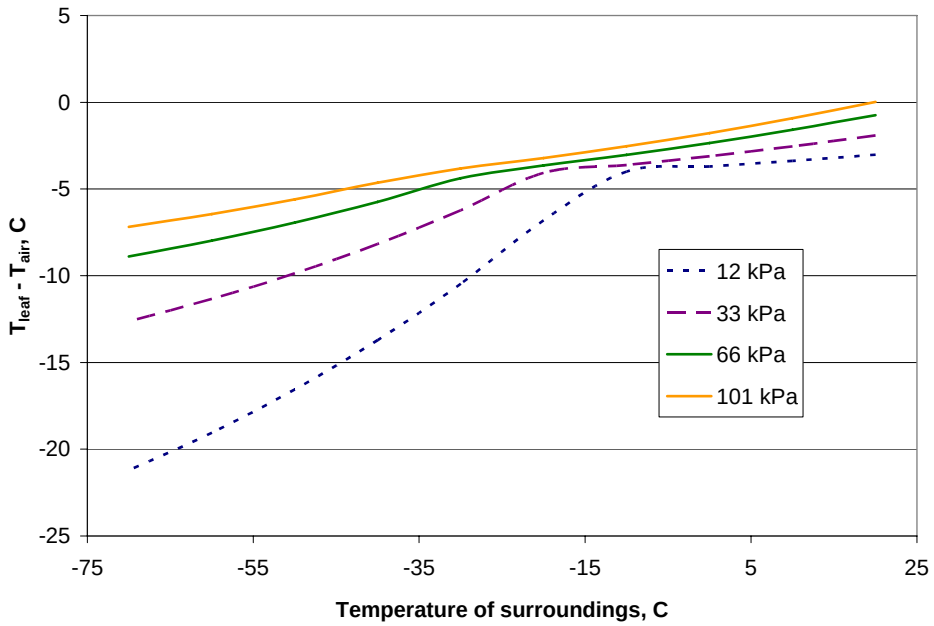

Figure 6-4. Effects of net radiation on leaf-to-air temperature difference. Leaf-to-air temperature difference was predicted by equation 6-1 as a function of net radiation for 12, 33, 66, and 101 kPa. Net radiation varied from -180 W m^{-2} when the temperature of the surroundings was -70 ^{o}C, as on Mars, to 110 W m^{-2} at 20 ^{o}C.

Table 6-3. Leaf temperature model results for 12 and 101 kPa. Shown below are the latent and sensible heat fluxes and the leaf-to-air temperature differences predicted by the Penman-Monteith model for radiation heat exchange between leaves and surroundings as cold as -70 ^{o}C.

		12 kPa			101 kPa		
T_{sur} (^{o}C)	R_n (W m^{-2})	LE (W m^{-2})	H (W m^{-2})	$T_{Leaf} - T_{air}$ (^{o}C)	LE (W m^{-2})	H (W m^{-2})	$T_{Leaf} - T_{air}$ (^{o}C)
20	110	135	-26	-3.0	109	0.4	0.0
0	17	48	-32	-3.7	61	-44.6	-1.8
-10	-23	11	-34	-4.0	41	-63.7	-2.5
-40	-117	0	-117	-13.7	0	-117	-4.6
-70	-180	0	-180	-21.2	0	-180	-7.2

As previously mentioned, a simplification was employed in the derivation of the Penman-Monteith evapotranspiration model to eliminate leaf temperature as an independent variable. This simplification required the assumption that the slope of the saturation vapor pressure curve at the leaf temperature was approximately equal to the slope at air temperature. This assumption was valid for cases when the absolute value of

the leaf-to-air temperature difference was less than 10 ^{o}C (Jones, 1992). For the conditions applied to the leaf temperature model for Figure 6-4, at 12 kPa this assumption was valid for T_{sur} as low as -30 ^{o}C. If the temperature of the interior surface of a Mars surrounding the plant canopy is much less than freezing, this assumption should be reevaluated. For it is likely that the slope of the vapor pressure curve at the leaf temperature would be significantly different than the slope at the air temperature.

Another consequence of very low leaf temperatures is chilling injury. Sensitive plant species show signs of wilting or inhibited growth and reproduction when tissue temperature is lowered about 10 ^{o}C (Jones, 1992). Long term exposure to conditions causing leaf temperatures lower than plants were adapted for could significantly reduce productivity. The effects of environmental conditions on leaf temperature should be considered in the design of a greenhouse on Mars.

Conclusions

The heat balance for a plant in a Mars greenhouse will be much different than for a plant on Earth. It is anticipated that the pressure inside a Mars greenhouse will be less than 30 kPa. At these low atmospheric pressures, evapotranspiration will occur faster than on Earth causing more latent heat loss and cooler leaf temperatures. Leaves will also lose heat by radiation to the cold greenhouse structure. In fact, it is likely that more heat will be lost than gained by radiation. In this case, sensible heat transfer by convection will be the only mode of heat gain. Since, convection heat transfer is less effective at reduced pressures; the leaf temperature in a low pressure Mars greenhouse will be significantly lower than air temperature. This could invalidate some of the assumptions made during the derivation of the Penman-Monteith model. Low leaf temperatures could also cause chilling injury in plants adapted for warmer conditions.

CHAPTER 7
CONCLUSIONS AND FUTURE RESEARCH

When astronauts embark on a long-term exploration mission to Mars, they will need reliable, efficient life-support systems. Plants will play important roles in these systems as sources of food and oxygen production and waste treatment. Plant growth and development, and thus, performance of a biological life-support system are highly dependent on plant environmental responses. Therefore, it is critical that the interaction between plants and the environment of a Mars greenhouse is well understood.

The constraints of building a structure on the Martian surface to withstand interior air pressures equal to that of earth make it essential to develop crop production systems capable of operating at pressures as low as 0.1 to 0.3 atm (10 – 30 kPa). Recent research has shown that plants are capable of surviving in such environments; however, they experience increased rates of evapotranspiration. The enormous costs associated with launching a manned mission to Mars make it critical that plants be not only capable of survival, but also of producing fruit and seed. Even slight environmental stress throughout the life of a plant can greatly affect growth, quality, and reproduction. The effect of the environment on the rate of plant water loss should be considered in the design of a Mars greenhouse.

In this research, water loss of mature radish plants in response to their environment was evaluated by application of a mathematical model. An evapotranspiration model was used to predict the rate of evapotranspiration of 18-to-24-day-old radish plants in

response to changes in pressure, CO_2 concentration, and photosynthetically active radiation (PAR). A system of three low-pressure bell jar based controlled environment chambers were designed and built for this research. The system provided control of pressure, CO_2 concentration, air temperature, and relative humidity and measured plant weight and leaf temperature.

The rate of convection heat transfer is an important component of the canopy energy balance and the evapotranspiration model. The effects of reduced pressure and air velocity on convection were determined by comparison of a theoretical model for the external resistance to sensible heat transfer with empirical values calculated from the rate of cooling for a thin, heated sheet. Theoretical versus empirical data were compared for four levels of pressure (12, 33, 66, and 101 kPa) and four air velocities (still air, 1.9, 2.8, and 5.8 m s^{-1}). The theoretical model fit the empirical data well with an average error of only 2.6 m s^{-1}. As predicted by the model, external resistance was proportional to both pressure and air velocity.

Another important parameter in the evapotranspiration model was the resistance to water loss by the canopy surface. The rate of water evaporation from the interior of the leaf is inhibited by the cuticle and stomata. The surface resistance accounts for this effect and is influenced mostly by the opening and closing of stomata. Changes in surface resistance can be interpreted as the stomatal response to environmental conditions. A model was developed to predict surface resistance as a function of pressure for elevated CO_2 and reduced PAR. The model calculated surface resistance as a reference value (taken at standard pressure) for particular levels of CO_2 and PAR multiplied by an empirically determined function. The predicted values of surface resistance were

compared with values calculated from measured rates of evapotranspiration. At 12 kPa there was a more significant decrease in resistance and corresponding increase in evapotranspiration. There was also a significant effect of CO_2 on stomatal control. When CO_2 rose from 40 to 150 Pa surface resistance increased and evapotranspiration decreased. In fact, the decrease in evapotranspiration rate for elevated CO_2 at 12 kPa was significant enough to prevent wilting. Decreasing PAR from 340 to 160 μmol m^{-2} s^{-1} had little effect on surface resistance or evapotranspiration.

The resistance models accounting for the effects of pressure and other environmental variables on convection heat transfer and stomatal control were built into the evapotranspiration model. The overall model performed adequately well with a root mean square error compared to independent data of less than 0.5 g m^{-2} min^{-1}.

The heat balance for a plant in a greenhouse on Mars will be much different than for a plant on Earth. Evapotranspiration will occur faster and plants may lose heat rather than gain it by radiation. The result will likely be leaf temperatures much lower than typically faced by plants on earth. These lower leaf temperatures will invalidate some of the underlying assumptions made in the derivation of the Penman-Monteith model with regard to leaf temperature. Parameters often taken at air temperature should be taken at leaf temperature to improve model accuracy. Chilling injury may also occur in plants adapted for warmer conditions.

Application of an evapotranspiration model for Mars greenhouse conditions was useful for understanding how plants will respond in those conditions with regard to the rate of water loss by evapotranspiration. Reduced pressure increases the rate of evapotranspiration by decreasing resistances to sensible and latent heat loss as well as

reducing the effectiveness of convection. However, selecting appropriate values for other environmental parameters may enable plants to withstand very low pressures. For example, in elevated CO_2 concentrations plants close their stomata. This increases surface resistance and, consequently, evapotranspiration decreases. The structure itself may also reduce the rate of water loss. In a Mars greenhouse the cold interior surface temperature will cool leaves by radiation heat transfer. This cooling will also reduce the rate of evapotranspiration. Properly selecting environmental parameters will make it possible to grow plants at super low pressures; however, they will be much more dependent on the performance of the environmental control system. If, for example, the CO_2 control system fails, plants growing in pressures below 25 kPa will wilt within a half hour of a decrease in CO_2. In other words, at super low pressures failure of the control system will almost definitely result in failure of the crop.

The model applied in this research was useful for better understanding how plants will respond to environmental conditions in a Mars greenhouse. Yet more research is needed to develop a more reliable evapotranspiration model that can be incorporated into the Mars greenhouse control system. In particular, the model for surface resistance should be expanded to include more crops and environmental parameters. Only mature radish plants were used in this research. The effect of reduced pressures on development should also be examined. It is hypothesized that stomatal density of plants grown in reduced pressures will be less than plants grown at standard pressure. Such changes in stomatal density would affect surface resistance and should be accounted for in the reference surface value. The model should also be expanded to predict surface resistance as a function of CO_2, PAR, and VPD. Such functions have already been developed for

many crops. Genetic modifications are likely for plants selected for the Mars greenhouse to improve their ability to withstand stressful conditions such as low temperatures. Any changes in stomatal control as a result of genetic modification should be accounted for in the surface resistance model.

LIST OF REFERENCES

Al-Faraj, A., G. E. Meyer, and J. B. Fitzgerald. 1994. Simulated Water Use and Canopy Resistnace of New Guinea Impatiens (*Impatiens X hb.)* in Single Pots Using Infrared Heating. *Transactions of the ASAE* 37(6): 1973-1980.

Andre, M. and D. Massimino. 1992. Growth of Plant at Reduced Pressures: Experiments in Wheat-Technological Advantages and Constraints. *Advances in Space Research* 12(5): 97-106.

American Society of Heating, Refrigeration, and Air-Conditioning Engineers (ASHRAE). 2001. *ASHRAE Handbook: Fundamentals.* Atlanta, GA: ASHRAE.

Assmann, S. M. 1999. The Cellular Basis of Guard Cell Sensing of Rising CO_2. *Plant, Cell, and Environment* 22(6): 629-637.

Aubinet. M., J. Deltour, and D. DeHalleux. 1989. Stomatal Regulation in Greenhouse Crops: Analysis and Simulation. *Agricultural and Forest Meteorology* 48:21-44.

Bailey, B. J. and J. F. Meneses. 1995. Modelling Leaf Convective Heat Transfer. *Acta Horticulturae* 399: 191-198.

Baille, M., A. Baille, and J. C. Laury. 1994. Canopy Surface Resistances to Water Vapour Transfer for Nine Greenhouse Pot Plant Crops. *Scientia Horticulturae* 57: 143-155.

Bakker, J. C. 1991. Effects of Humidity on Stomatal Density and its Relation to Leaf Conductance. *Scientia Horticulturae* 48: 205-212.

Brown, D. L. 2002. *A Distributed Control System for Low-Pressure Plant Growth Chambers*. M.S. thesis. College Station, TX: Texas A&M University, Department of Biological and Agricultural Engineering.

Bucklin, R. A., P. A. Fowler, V. Y. Rygalov, R. M. Wheeler, Y. Mu. I. Hublitz, and E. G. Wilkerson. 2004. Greenhouse Design for the Mars Environment: Development of a Prototype, Deployable Dome. *Acta Horticulturae* 659: 127-134.

Comstock, J. P. 2002. Hydraulic and Chemical Signalling in the Control of Stomatal Conductance and Transpiration. *Journal of Experimental Botany.* 53(367): 195-200.

Corey, K. A., D. J. Barta, and D. L. Henninger. 1997. Photosynthesis and Respiration of Wheat Stand at Reduced Atmospheric Pressure and Reduced Oxygen. *Advances in Space Research* 20(10): 1869-1877.

Corey, K. A., D. J. Barta, and R. M. Wheeler. 2002. Toward Martial Agriculture: Responses of Plants to Hypobaria. *Life Support & Biosphere Science* 8: 103-114.

Dally, J. W., W. F. Riley, and K. G. McConnell. 1993. *Instrumentation for Engineering Measurements,* Second Edition. New York, NY: John Wiley and Sons, Inc.

Daunicht, H. J. and H. J. Brinkjans. 1992. Gas Exchange and Growth of Plants Under Reduced Pressure. *Advances in Space Research* 12(5): 107-114.

Ferl, R. J., A. C. Schuerger, Paul A., W. B. Gurley, K. Corey, and R. A. Bucklin. 2002. Plant Adaptation to Low Atmospheric Pressures: Potential Molecular Responses. *Life Support & Biosphere Science* 8: 93-101.

Fowler, P. A., V. Y. Rygalov, R. A. Bucklin, and R. M. Wheeler. 2001. Design and Control of Interior Climate of Martian Greenhouses. *ASAE Paper No FL01104 American Society of Agricultural Engineers, St Joseph, MI.*

Gay, A. P. and R. G. Hurd. 1975. Influence of Light on Stomatal Density in Tomato. *New Phytologist* 75(1): 37-46.

Goto, E., K. Iwabuchi, and T. Takakura. 1995. Effect of Reduced Total Air Pressure on Spinach Growth. *Journal of Agricultural Meteorology* 51(2): 139-145.

Goto, E., H. Ohta, K. Iwabuchi, and T. Takakura. 1996. Measurement of Net Photosynthetic and Transpiration Rates of Spinach and Maize Plants under Hypobaric Condition. *Journal of Agricultural Meteorology* 52(2): 117-123.

Goto, E., Y. Arai, and K. Omasa. 2002. Growth and Development of Higher Plants Under Hypobaric Conditions. *2002 International Conference of Environmental Systems Meeting Paper No 2002-01-2439 Society of Automotive Engineers, San Antonio, TX.*

Hanan, J. J. 1998. *Greenhouses: Advanced Technology for Protected Horticulture*. Boca Raton, FL: CRC Press.

Henderson, S. M., R. L. Perry, and J. H. Young. 1997. *Principles of Process Engineering,* Fourth Edition. St. Joseph, MI: ASAE.

Incropera, F. P. and D. P. DeWitt. 1996. *Fundamentals of Heat and Mass Transfer,* Fourth Edition. New York, NY: John Wiley and Sons, Inc.

Jarvis, P. G. 1976. The Interpretation of the Variations in Leaf Water Potential and Stomatal Conductance Found in Canopies in the Field. *Phil Trans R Soc Lond B* 273: 593-610.

Jarvis, P. G. and K. G. McNaughton. 1986. Stomatal Control of Transpiration: Scaling Up from Leaf to Region. *Advances in Ecological Research* 15: 1-45.

Jones, H. G. 1992. *Plants and Microclimate: A Quantitative Approach to Environmental Plant Physiology,* Second Edition. New York, NY: Cambridge University Press.

Jones, P., L. H. Allen, J. W. Jones, and R. Valle. 1985. Photosynthesis and Transpiration Responses of Soybean Canopies to Short-Term and Long-Term CO_2 Treatments. *Agronomy Journal* 77(1): 119-126.

Jordan, D. N., and W. K. Smith. 1995. Microclimate Factors Influencing the Frequency and Duration of Growth Season Frost for Subalpine Plants. *Agricultural and Forest Meteorology* 77: 17-30.

Lhomme. J. P. 2001. Stomatal Control of Transpiration: Examination of the Jarvis-type Representation of Canopy Resistance in Relation to Humidity. *Water Resources Research* 37(3): 689-699.

Massimino, D. and M. Andre. 1999. Growth of Wheat Under one-Tenth of the Atmospheric Pressure. *Advances in Space Research* 24(3): 293-296.

Monteith, J. L. 1965. Evaporation and Environment. *Symp Soc Exp Biol* 19: 205-234.

Monteith, J. L. 1995. A Reinterpretation of Stomatal Responses to Humidity. *Plant, Cell, and Environment* 18: 357-364.

Monteith, J. L. and M. H. Unsworth. 1990. *Principles of Environmental Physics,* Second Edition. Boston, MA: Butterworth Heinemann.

Mott, K. A. and D. F. Parkhurst. 1991, Stomatal Responses to Humidity in Air and Helox. *Plant, Cell, and Environment* 14: 509-515.

Mu, Y. 2005. *A Distributed Control System for Low Pressure Plant Growth Chambers.* Ph.D. dissertation. Gainesville, FL: University of Florida, Agricultural and Biological Engineering Department.

National Aeronautics and Space Administration (NASA). 2005. Mars Fact Sheet: NASA. Available at: http://nssdc.gsfc.nasa.gov/planetary/factsheet/marsfact.html. Accessed 15 August 2005.

Nobel, P.S. 1999. *Physicochemical and Environmental Plant Physiology,* Second Edition. San Diego, CA: Academic Press.

Omega Engineering, Inc. 2005. Thermocouples - An Introduction. Available at: http://www.omega.com/thermocouples.html. Accessed 26 August 2005.

Outlaw, W. H. 2003. Integration of Cellular and Physiological Functions of Guard Cells. *Critical Reviews in Plant Science* 22(6): 503-529.

Paul A., A. C. Schuerger, M. P. Popp, J. T. Richards, M. S. Manak, and R. J. Ferl. 2004. Hypobaric Biology: Arabidopsis Gene Expression at Low Atmospheric Pressure. *Plant Physiology* 134: 215-223.

Penman, H. L. 1948. Natural Evaporation From Open Water, Bare Soil and Grass. *Proc Roy Soc London (A)* 193: 120-145.

Purswell, J. L. 2002. *Engineering Design of a Hypobaric Plant Growth Chamber*. M.S. thesis. College Station, TX: Texas A&M University, Department of Biological and Agricultural Engineering.

Rule, D. E. and G. L. Staby. 1981. Growth of Tomato Seedlings at Sub-atmospheric Pressures. *HortScience* 16(3): 331-332.

Rygalov, V. Y., P. A. Fowler, J. M. Metz, R. M. Wheeler, and R. A. Bucklin. 2002. Water Cycles in Closed Ecological Systems: Effects of Atmospheric Pressure. *Life Support & Biosphere Science* 8: 125-135.

Schoch, P. G., C. Zinsou, and M. Sibi. 1980. Dependence of the Stomatal Index on Environmental Factors during Stomatal Differentiation in Leaves of Vigna-Sinensis L. 1. Effect of Light Intensity. *Journal of Experimental Botany* 31(124): 1211-1216.

Stanghellini, C. 1987. *Transpiration of Greenhouse Crops: An Aid to Climate Management*. Ph.D. dissertation Landbousuniversiteit, Wageningen.

Stanghellini, C. and J. A. Bunce. 1993. Response of Photosynthesis and Conductance to Light, CO_2, Temperature, and Humidity in Tomato Plants Acclimated to Ambient and Elevated CO_2. *Photosynthetica* 29(4): 487-497.

Wheeler, R. M., C. L. Mackowiak, N. C. Yorio, and J. C. Sager. 1999. Effects of CO_2 on Stomatal Conductance: Do Stomata Open at Very High CO2 Concentrations? *Annals of Botany* 83: 243-251.

Woodward, F. I. 1987. Stomatal Numbers are Sensitive to Increases in CO_2 from Preindustrial Levels. *Nature* 327(6123):617-618.

Zhang, L. and R. Lemeur. 1992. Effect of Aerodynamic Resistance on Energy Balance and Penman-Monteith Estimates of Evapotranspiration in Greenhouse Conditions. *Agricultural and Forest Meteorology* 58: 209-228.

Zolnier, S., R. S. Gates, J. Buxton, and C. Mach. 2000. Psychrometric and Ventilation Constraints for Vapor Pressure Deficit Control. *Computers and Electronics in Agriculture* 26: 343-359.

Zolnier, S., R. S. Gates, R. L. Geneve, and J. W. Buxton. 2001. Surface Diffusive Resistances of Rooted Poinsettia Cuttings Under Controlled-Environment Conditions. *Transactions of the ASAE* 44(6): 1779-1787.

Zolnier, S., G. B. Lyra, R. S. Gates. 2004. Evapotranspiration Estimates for Greenhouse Lettuce Using an Intermittent Nutrient Film Technique. *Transactions of the ASAE* 47(1):271-282.

APPENDIX A
SENSOR CALIBRATIONS

All sensors used in this research to monitor radish plants and bell jar environment were calibrated within one year of all experiments. With the exception of relative humidity sensors, which were factory calibrated, all sensors and thermocouples were calibrated in place.

Pressure

Pressure sensors (Bell jars 1 and 3: MPXH6101A6U and Bell jar 2: MPXH6115A6U, Freescale Semiconductor, Inc., Austin, TX) were calibrated by linear regression analysis in comparison to a dial pressure gauge (Model CM, Heise, Stratford, CT) in line between the vacuum pump and bell jars over the range of 10 – 101 kPa. Figure A-1 shows the data, best fit line, regression coefficient, and standard error for each sensor. The standard error was less than 0.2 kPa for each sensor.

Leaf Temperature

Leaf temperature was measured using miniature infrared thermocouples (model OS36SM, Omega, Stamford, CT). These infrared thermocouples had a type-K thermocouple output, but had significantly higher internal impedances. A three-point calibration was performed by comparing the three infrared thermocouples to a precision infrared sensor (Model 4000.4GL, Everest Interscience, Inc, Tucson, AZ) with NIST traceable calibration. One by one an infrared thermocouple and the precision infrared sensor were directed at an open container of water just above the surface and the readings recorded. Some drift was observed in the offset of the calibration equation. As a result, a

one-point calibration was performed daily as described above to determine the offset. The slope of the calibration curve remained constant over the course of all experiments. Figure A-2 shows the calibration data and best fit line for infrared sensors in bell jar 1. The infrared thermocouples were read by an Optp22 SNAP-AITM analog input module. According to manufacturer's specifications, the calibrated sensor accuracy was 0.8 ^{o}C.

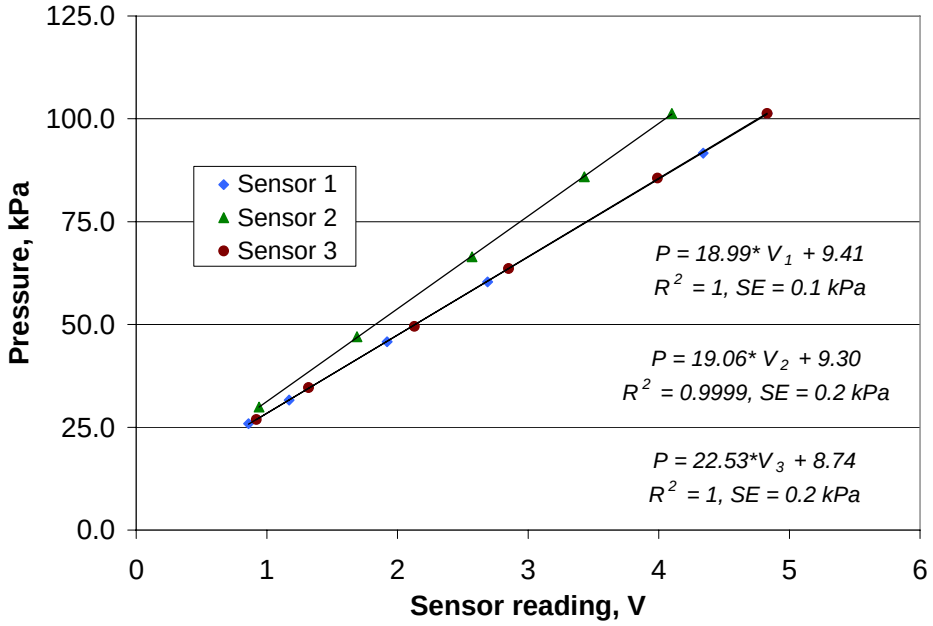

Figure A-1. Pressure sensor calibration. The microchip sensors used to monitor pressure inside the bell jars were calibrated in comparison to a vacuum gage. Linear regression analysis was used to determine the best fit lines and error for each sensor.

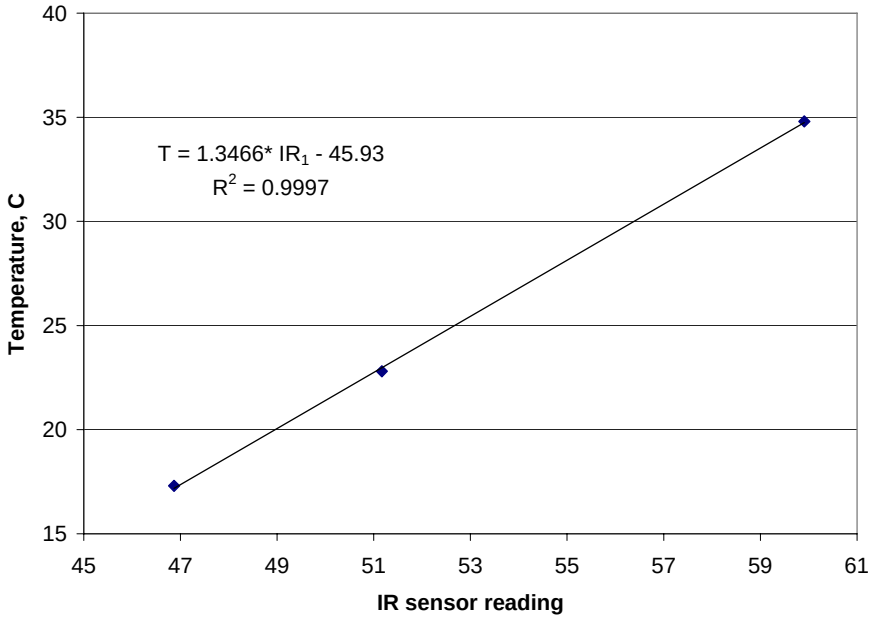

Figure A-2. Infrared sensor calibration. The data and best-fit line for a three-point calibration is shown for IR_1.

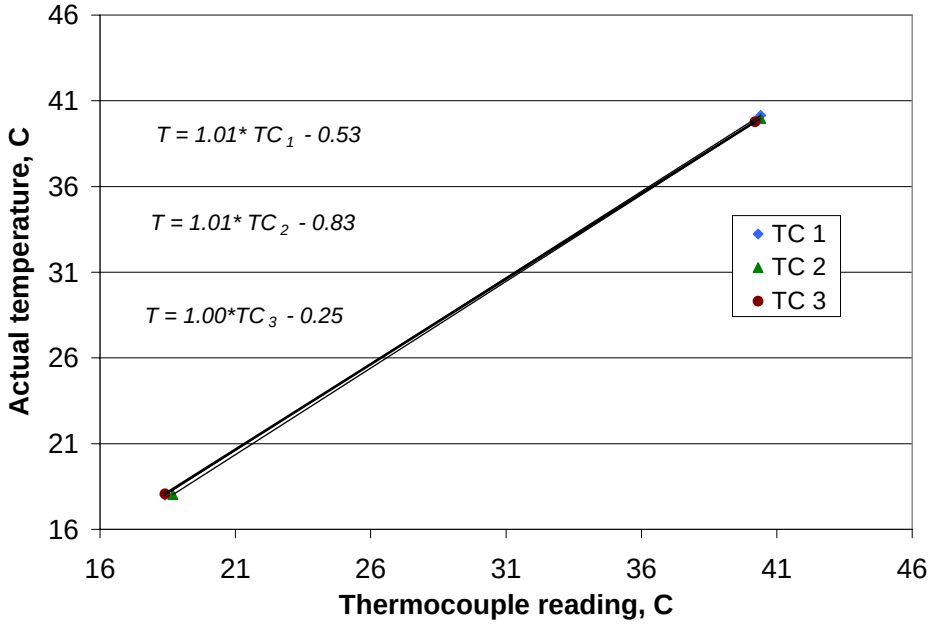

Figure A-3. Thermocouple calibration. The type-T thermocouples used to monitor air temperature inside the bell jars were calibrated using a two point temperature calibration.

Air Temperature

The temperature inside each bell jar was measured by type-T thermocouples. A two point calibration (Figure A-3) was performed using a thermocouple calibrator (TCAL, Sun Electronic Systems, Inc., Titusville, FL). Estimated error of the calibrated thermocouples was 1.0 ^{o}C (Omega, 2005).

Weight

The load cells inside each bell jar were calibrated by linear regression analysis using standard weights. Figure A-4 shows the calibration data, best fit lines, regression coefficient, and standard error for each load cell. Standard error was less than 0.2 g for all three load cells. As for the infrared thermocouples, some drift was observed in the offset of the calibration equation. As a result, a routine was added to the control program to perform a one-point calibration with no weight on the scale to zero it. The slope of the calibration curve remained constant over the course of all experiments.

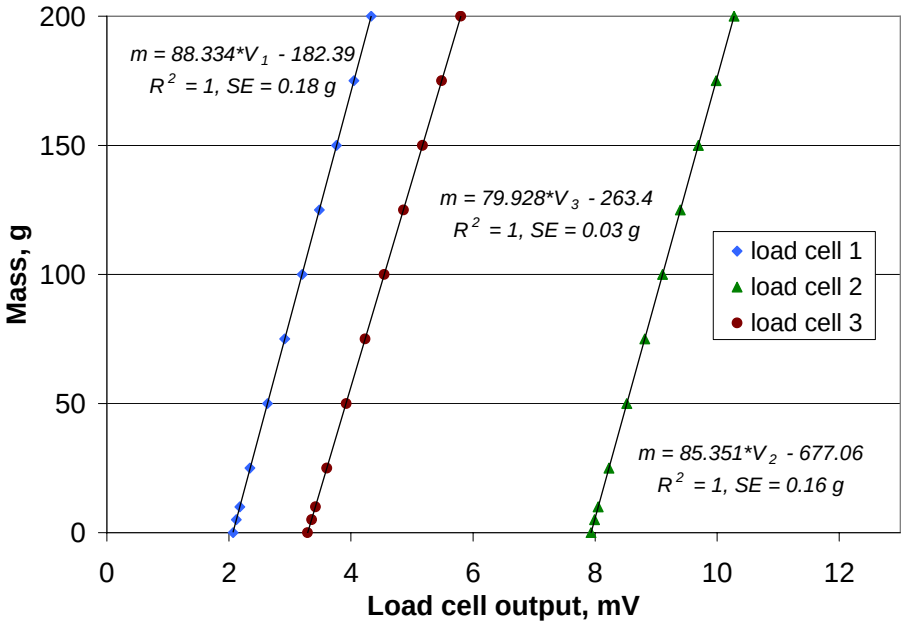

Figure A-4. Load cell calibration. The load cells were calibrated using standard weights and linear regression analysis.

Carbon Dioxide Concentration

The response of the carbon dioxide sensors used in this research was sensitive to pressure. The calibration equation developed accounted for the effect of pressure using a method similar to Mu (2005). A two point calibration was applied to each carbon dioxide sensor at approximately 10, 30, 50, 70, 90, and 101 kPa. The sensor reading was compared to the CO_2 concentration as measured by a gas chromatograph. For each sensor an equation was fit to the slopes and intercepts of the linear regression equations as a function of pressure. The form of final calibration equations is below.

$$[CO_2] = f(P) * V_{CO2} + g(P) \qquad \text{(A-1)}$$

where $[CO_2]$ = CO_2 concentration, ppm

V_{CO2} = CO_2 sensor output, V

f(P) = slope as a function of pressure (from Table A-1)

g(P) = intercept as a function of pressure (from Table A-1)

Figure A-5 shows the functions determined by linear regression analysis of CO_2 concentration as a function of sensor output for sensor 1 at six pressures. Only the plots for sensor 1 are shown. The slope and intercept equations for all three sensors are given in Tables A-1. To obtain the CO_2 concentration, these pressure dependent slope and intercept equations were plugged into equation A-1.

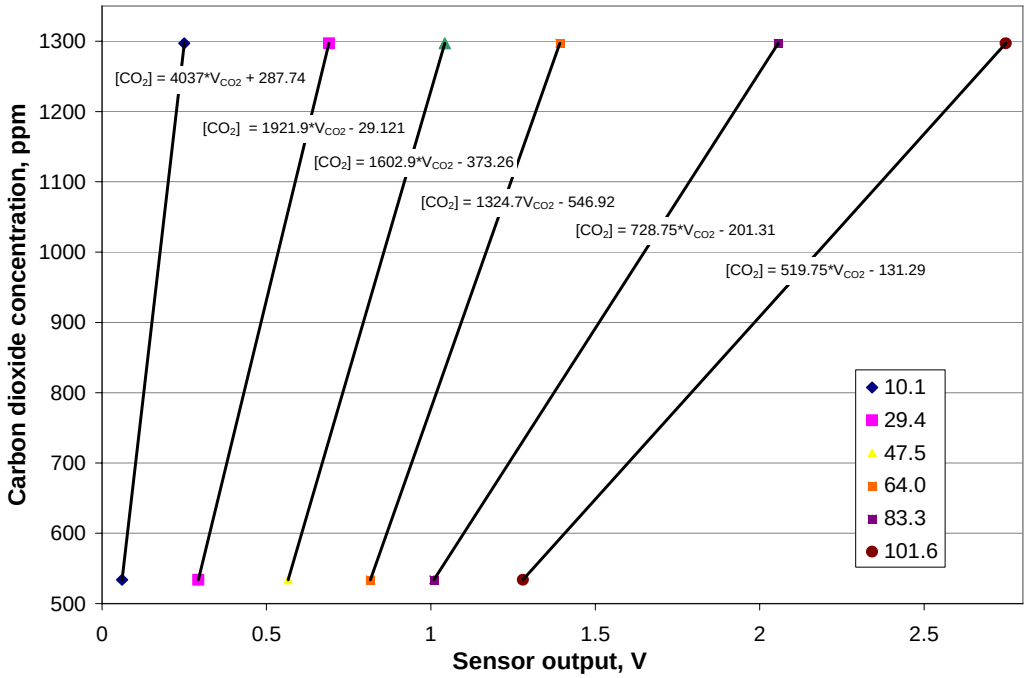

Figure A-5. Carbon dioxide sensor calibration. Linear functions determined by linear regression analysis for sensor 1 at six pressures ranging from approximately 10 to 101 kPa.

Table A-1. Slope and intercept equations for carbon dioxide sensors.

Sensor	Slope	Intercept
1	$4645e^{-0.0208*P}$	$0.2486*P^2 - 33.492*P + 656.87$
2	$2791e^{-0.0184*P}$	$0.0558*P^2 - 8.264 + 300$
3	$4547.1e^{-0.0254*P}$	$0.0857*P^2 - 11.424*P + 418.07$

The accuracy of the carbon dioxide sensors is listed by the manufacturer as ±40ppm + 3% of the reading. Since the sensor accuracy is a function of the sensor output, the accuracy of carbon dioxide readings is dependent on concentration and pressure. It ranges from 52 ppm for an ambient CO_2 concentration of 400 ppm at standard pressure to 490 ppm for a concentration of 15000 ppm at 10 kPa.

Oxygen concentration

Like the carbon dioxide sensors, the oxygen sensors used in this research were sensitive to changes in total pressure. The calibration procedure for the oxygen sensors was the same as for the CO_2 sensors. A two-point calibration was performed with one point determined by comparing the sensor output to oxygen concentration measured by a gas chromatograph. The second calibration point was obtained by assuming that the sensor output was zero volts when the oxygen concentration was zero. Table A-2 gives the slope equation for the three oxygen sensors. The assumption of zero voltage when no oxygen was present meant that there was no offset term in the calibration equation. The resulting oxygen sensor calibration equation is given below.

$$[O_2] = f(P) * V_{O2} \qquad \text{(A-2)}$$

where: $[O_2]$ = O_2 concentration, %

V_{O2} = O_2 sensor output, mV

f(P) = slope as a function of pressure (from Table A-2)

Table A-2. Slope equations for the oxygen sensors.

Sensor	Slope
1	$158.6*P^{-0.9783}$
2	$148.7*P^{-0.9892}$
3	$146.0*P^{-0.9893}$

APPENDIX B
SENSOR ERROR BUDGETS

The error budget for each measured parameter was the accumulated error of the sensor and measurement system. Total error was estimated as the root sum square error (Root SSE) calculated by the following equation (Dally et al., 1993).

$$Root \;\; SSE = \sqrt{e_s^2 + e_m^2}$$

where e_s = sensor error,

e_m = error of the measurement system

The error of each sensor and measurement system accounted for the accuracy and sources of error as appropriate. Error estimation calculations for the Opto 22 analog input modules used in this research and each environmental parameter are given here.

Voltage Input Module (SNAP-AIV-4)

- accuracy = 2.5 mV at 5 VDC
- offset temperature coefficient = 15 ppm/^{o}C
- gain temperature coefficient = 30 ppm/^{o}C

Offset drift (25 ^{o}C) = (15 x 10^{-6} ppm/^{o}C)(25 ^{o}C)(5 VDC full scale) = 1.875 mV

Gain drift (25 ^{o}C) = (30 x 10^{-6} ppm/^{o}C)(25 ^{o}C)(5 VDC full scale) = 3.75 mV

The overall root sum square error:

$$Root \;\; SSE = \sqrt{(2.5\ mV)^2 + (1.875\ mV)^2 + (3.75\ mV)^2} = \underline{\underline{4.9\ mV}}$$

Voltage Input Module (SNAP-AITM-2)

- accuracy = 0.1% at 50 mV

- offset temperature coefficient = 5 μV/^{o}C
- gain temperature coefficient = 2 μV/^{o}C

Accuracy = (0.001)(50 mV) = 0.05 mV

Offset drift (25 ^{o}C) = (5 x 10^{-6} μV/^{o}C)(25 ^{o}C) = 0.125 mV

Gain drift (25 ^{o}C) = (2 x 10^{-6} μV ^{o}C)(25 ^{o}C) = 0.05 mV

The overall root sum square error:

$$Root \;\; SSE = \sqrt{(0.05\ mV)^2 + (0.125\ mV)^2 + (0.05\ mV)^2} = \underline{\underline{0.14\ mV}}$$

Pressure

- Accuracy from calibration = 0.52 kPa
- Voltage-to-pressure relationship (from calibration) = 22.47 kPa/V
- SNAP-AIV-4 error = 4.9 mV

Input module error = (0.0049 V)(22.47 kPa/V) = 0.11 kPa

The overall root sum square error:

$$Root \;\; SSE = \sqrt{(0.52\ kPa)^2 + (0.11\ kPa)^2} = \underline{\underline{0.53\ kPa}}$$

Relative Humidity

- Sensor accuracy = 2% RH
- Linearity = 0.5% RH
- Full scale = 5 VDC
- SNAP-AIV-4 error = 4.9 mV

The sensor root sum square error:

$$Root \;\; SSE\ (sensor) = \sqrt{(2\ \%)^2 + (0.5\ \%)^2} = 2.1\%$$

Input module error = (0.0049 V) (1/5 V) = 0.1 % RH

The overall root sum square error:

$$Root\ \ SSE = \sqrt{(2.1\,\%)^2 + (0.1\,\%)^2} = \underline{\underline{2.1\,\%}}$$

Oxygen

- Sensor accuracy = 1.0 % full scale at constant temperature and pressure
- SNAP – AITM-2 accuracy = 0.14 mV
- Voltage-to-oxygen relationship (theoretical) = 1.67 % O_2/mV
- Full scale = 59.9 mV

Sensor accuracy = (1.0 %) (59.9 mV) = 0.6 mV

The overall root sum square error:

$$Root\ \ SSE = \sqrt{(0.6\ mV)^2 + (0.14\ mV)^2} = 0.62\ mV = \underline{\underline{1.0\,\%\ O_2}}$$

Carbon Dioxide

- Sensor accuracy = 40 ppm + 3% of reading
- Voltage-to-carbon dioxide response (theoretical) = 500 ppm/V
- SNAP-AIV-4 accuracy = 4.9 mV

Sensor accuracy (at 2000 ppm) = 40 ppm + (0.03)(2000 ppm) = 100 ppm = 0.2 V

Sensor accuracy (at 1000 ppm) = 40 ppm + (0.03)(1000 ppm) = 70 ppm = 0.14 V

The overall root sum square error (at 2000 ppm):

$$Root\ \ SSE = \sqrt{(0.2\,V)^2 + (0.0047\,V)^2} = 0.2\,V = \underline{\underline{100\ ppm}}$$

The overall root sum square error (at 1000 ppm):

$$Root\ \ SSE = \sqrt{(0.14\,V)^2 + (0.0047\,V)^2} = 0.14\,V = \underline{\underline{70\ ppm}}$$

Leaf temperature

Module and calibrated sensor accuracy (SNAP-AITM module specifications) = $\underline{\underline{0.8\ ^oC}}$

Air temperature

Module and calibrated sensor accuracy (SNAP-AITM2 module specifications) =2.0 ^{o}C

APPENDIX C
BELL JAR BASE DRAWINGS

As part of this research new bell jar bases were designed to house the cooling coil, fans, humidifier, and wiring connections below the bell jar itself to maximize space for the plants. The bases were constructed out of aluminum by machinists at the Kennedy Space Center prototype shop. The following figures show the actual dimensions and details of the bell jar bases.

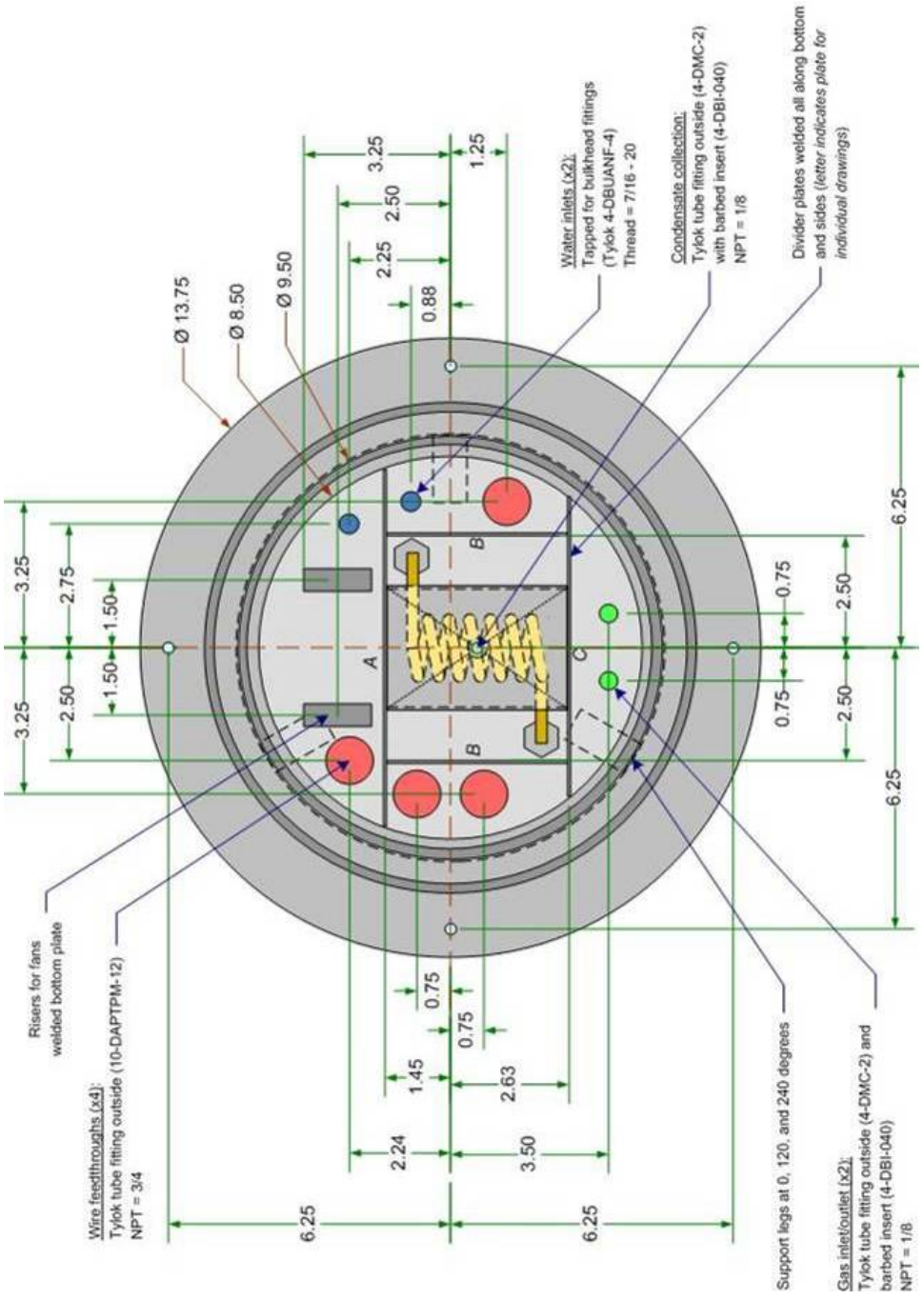

Figure C-1. Top view of bell jar base. All dimensions are in inches (not to scale).

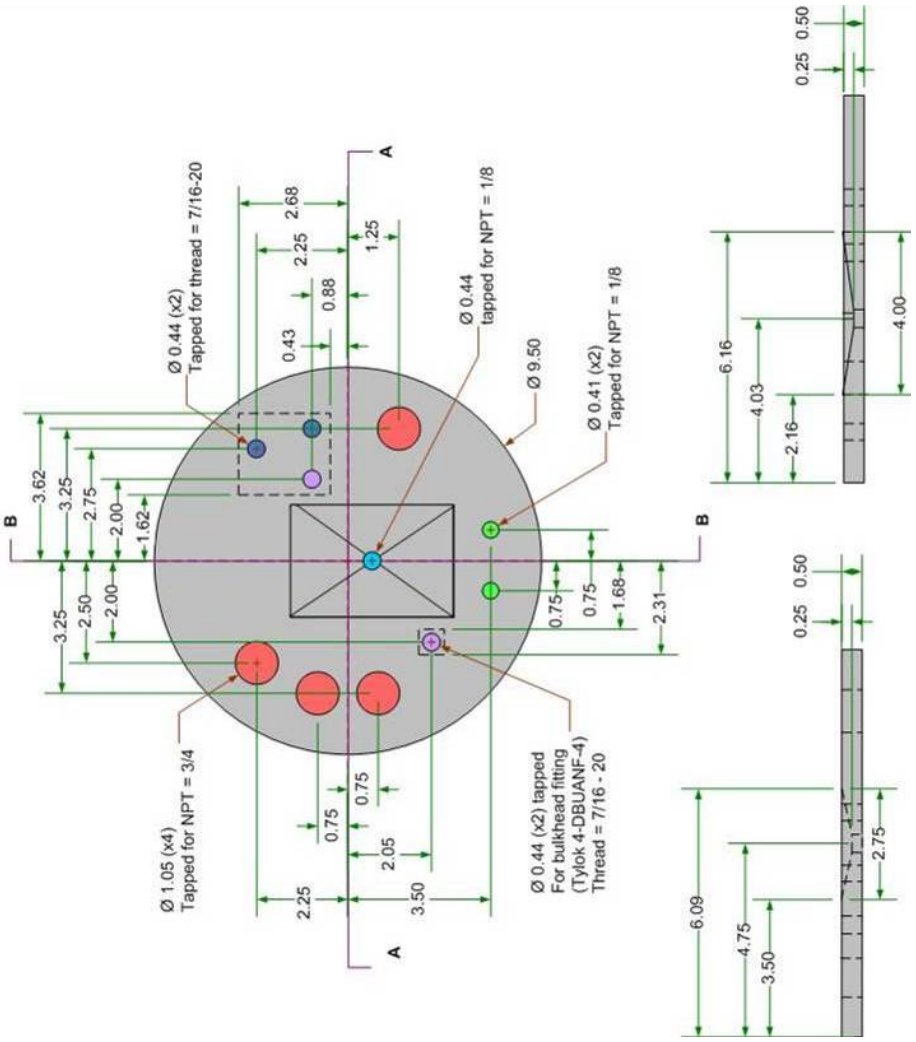

Figure C-2. Bottom view of bell jar base. All dimensions are in inches (not to scale).

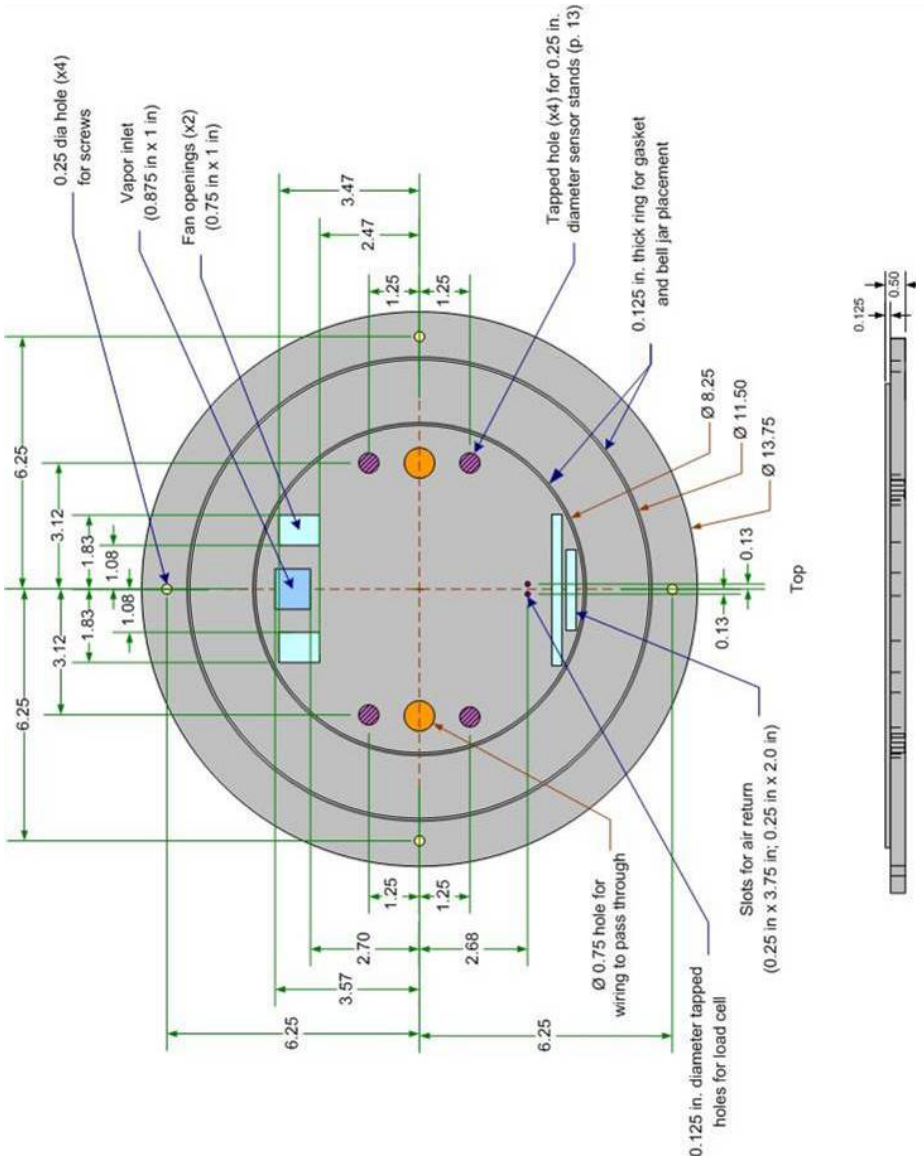

Figure C-3. Bell jar base top plate. All dimensions are in inches (not to scale).

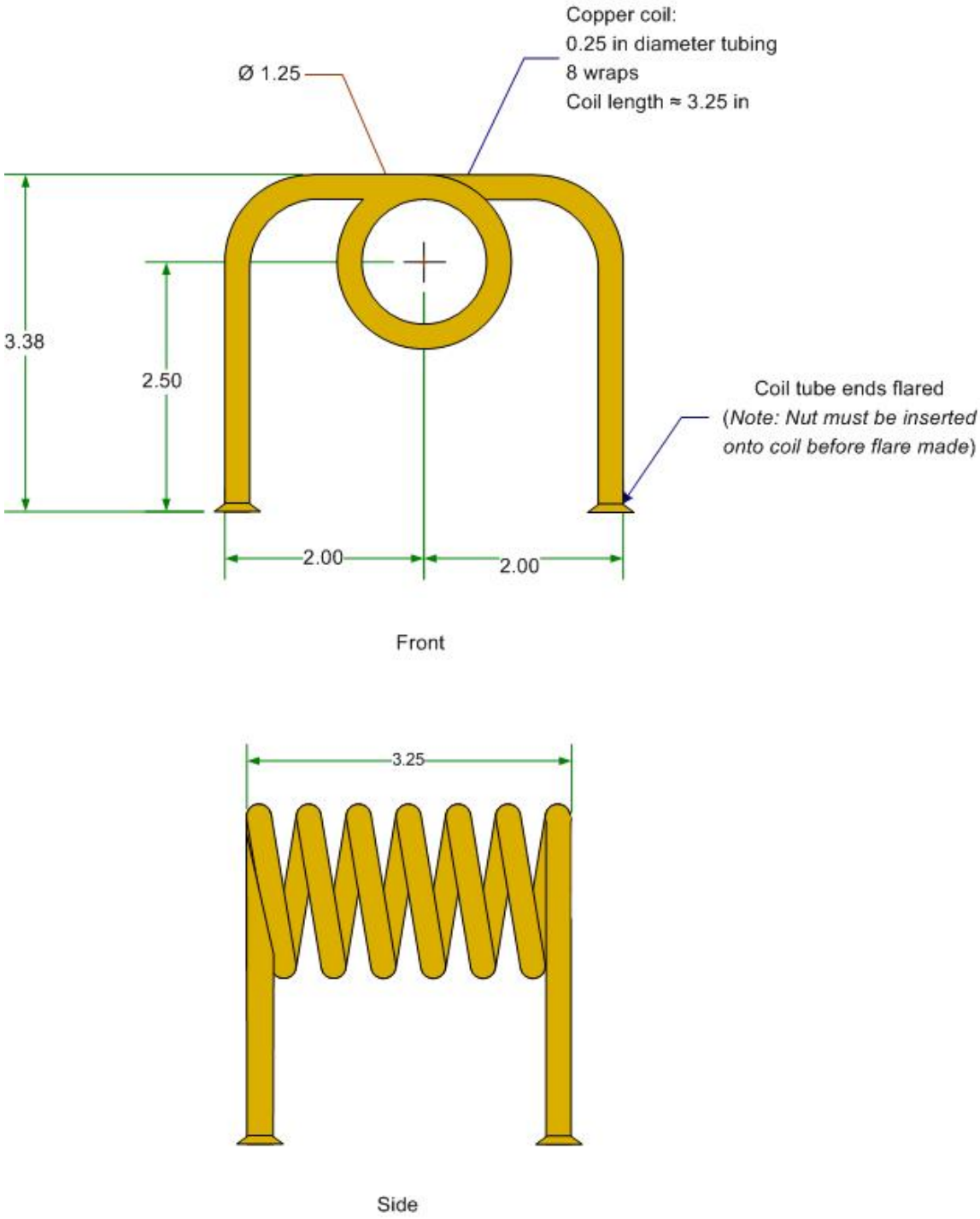

Figure C-4. Cooling coil. All dimensions are in inches (not to scale).

APPENDIX D
BELL JAR CONTROL ALGORITHM

An Opto 22 system was used for data acquisition and control for the bell jar chambers. The control program, written in *ioControl 6.*0, is shown below. *ioControl* is a flowchart based software. The flowchart for each routine is shown followed by the instructions and code for each block of the chart. The user interface, written in *ioDisplay 6.0*, is also included.

Data Buffer Routine

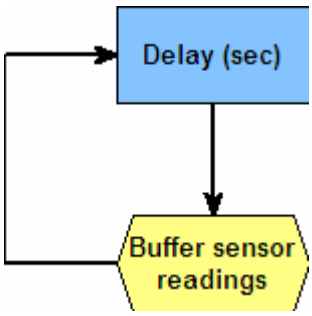

Action Block: Delay (sec) (Id: 0)
Exit to: Buffer sensor readings (Id: 9)
Delay variable buffer
Delay (mSec) 500

OptoScript Block: Buffer sensor readings (Id: 9)
Exit to: Delay (sec) (Id: 0)

```
// Get sensor readings
for k = 1 to 10 step 1

// Bell jar 1

TC1 = TC_0; // thermocouple
IR1 = IR_0;   // IR thermocouples
rh1 = rh_0;   //Relative humidity sensor
```

```
prsr1= prsr_0;   //Pressure sensor
co21 = co2_0;   //Carbon dioxide sensor
o21 = o2_0;   //Oxygen sensor
lc1 = lc_0;   //Load cell

// Bell jar 2
TC2 = TC_1; // thermocouple
IR2 = IR_1;   // IR thermocouples
rh2 = rh_1;   //Relative humidity sensor
prsr2= prsr_1;   //Pressure sensor
co22 = co2_1;   //Carbon dioxide sensor
o22 = o2_1;   //Oxygen sensor
lc2 = lc_1;   //Load cell

 // Bell jar 3
 TC3 = TC_2; // thermocouple
 TC4 = TC_3;
 IR3 = IR_2;   // IR thermocouples
 rh3 = rh_2;   //Relative humidity sensor
 prsr3= prsr_2;   //Pressure sensor
 co23 = co2_2;   //Carbon dioxide sensor
 o23 = o2_2;   //Oxygen sensor
 lc3 = lc_2;   //Load cell

// Ignore out of range load cell readings
 if (lc1>1000) then
   lc1 = 0;
 elseif (lc1<0) then
   lc1 = 0;
 endif

 if (lc2>1000) then
   lc2 = 0;
 elseif (lc2<0) then
   lc2 = 0;
  endif

 if (lc3>1000) then
   lc3 = 0;
 elseif (lc3<0) then
   lc3 = 0;
 endif

// Buffer sensor readings to eliminate noise

// Bell jar 1
```

```
TC1_sum = TC1_sum + TC1; // thermocouple
IR1_sum = IR1_sum + IR1;   // IR thermocouples
rh1_sum = rh1_sum + rh1;   //Relative humidity sensor
prsr1_sum = prsr1_sum + prsr1;   //Pressure sensor
co21_sum = co21_sum + co21;   //Carbon dioxide sensor
o21_sum = o21_sum + o21;   //Oxygen sensor
lc1_sum = lc1_sum + lc1;   //Load cell

// Bell jar 2
TC2_sum = TC2_sum + TC2; // thermocouple
IR2_sum = IR2_sum + IR2;   // IR thermocouples
rh2_sum = rh2_sum + rh2;   //Relative humidity sensor
prsr2_sum = prsr2_sum + prsr2;   //Pressure sensor
co22_sum = co22_sum + co22;   //Carbon dioxide sensor
o22_sum = o22_sum + o22;   //Oxygen sensor
lc2_sum = lc2_sum + lc2;   //Load cell

// Bell jar 3
TC3_sum = TC3_sum + TC3; // thermocouple
TC4_sum = TC4_sum + TC4;
IR3_sum = IR3_sum + IR3;   // IR thermocouples
rh3_sum = rh3_sum + rh3;   //Relative humidity sensor
prsr3_sum = prsr3_sum + prsr3;   //Pressure sensor
co23_sum = co23_sum + co23;   //Carbon dioxide sensor
o23_sum = o23_sum + o23;
```

```
//Oxygen sensor
   lc3_sum = lc3_sum + lc3;   //Load cell

   next

   // Reset intermediate variable sums

   // Bell jar 1
   TC1_avg = TC1_sum/10; // thermocouple
   IR1_avg = IR1_sum/10;   // IR thermocouples
   rh1_avg = rh1_sum/10;   //Relative humidity sensor
   prsr1_avg = prsr1_sum/10;   //Pressure sensor
   co21_avg = co21_sum/10;   //Carbon dioxide sensor
   o21_avg = o21_sum/10;   //Oxygen sensor
   lc1_avg = lc1_sum/10;   //Load cell

   // Bell jar 2
   TC2_avg =TC2_sum/10; // thermocouple
   IR2_avg = IR2_sum/10;   // IR thermocouples
   rh2_avg = rh2_sum/10;   //Relative humidity sensor
   prsr2_avg = prsr2_sum/10;   //Pressure sensor
   co22_avg = co22_sum/10;   //Carbon dioxide sensor
   o22_avg = o22_sum/10;   //Oxygen sensor
   lc2_avg = lc2_sum/10;   //Load cell

   // Bell jar 3
   TC3_avg = TC3_sum/10; // thermocouple
   TC4_avg = TC4_sum/10; // thermocouple
   IR3_avg = IR3_sum/10;   // IR thermocouples
   rh3_avg = rh3_sum/10;   //Relative humidity sensor
   prsr3_avg = prsr3_sum/10;   //Pressure sensor
   co23_avg = co23_sum/10;   //Carbon dioxide sensor
   o23_avg = o23_sum/10;   //Oxygen sensor
   lc3_avg = lc3_sum/10;   //Load cell

   // Bell jar 1
   TC1_sum = 0; // thermocouple
   IR1_sum = 0;   // IR thermocouples
   rh1_sum = 0;   //Relative humidity sensor
   prsr1_sum = 0;   //Pressure sensor
   co21_sum = 0;   //Carbon dioxide sensor
   o21_sum = 0;   //Oxygen sensor
   lc1_sum = 0;   //Load cell

   // Bell jar 2
   TC2_sum = 0; // thermocouple
```

```
IR2_sum = 0;   // IR thermocouples
rh2_sum = 0;   //Relative humidity sensor
prsr2_sum = 0;   //Pressure sensor
co22_sum = 0;   //Carbon dioxide sensor
o22_sum = 0;   //Oxygen sensor
lc2_sum = 0;   //Load cell

// Bell jar 3
TC3_sum = 0; // thermocouple
TC4_sum = 0;
IR3_sum = 0;   // IR thermocouples
rh3_sum = 0;   //Relative humidity sensor
prsr3_sum = 0;   //Pressure sensor
co23_sum = 0;   //Carbon dioxide sensor
o23_sum = 0;   //Oxygen sensor
lc3_sum = 0;   //Load cell
```

Variable Update Routine

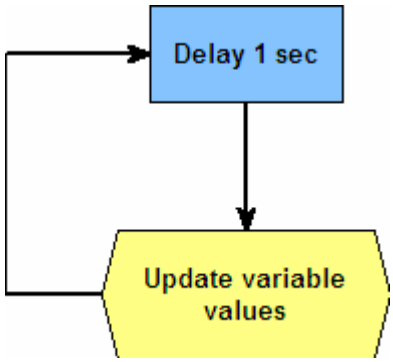

Action Block: Delay 1 sec (Id: 0)
Exit to: Update variable values (Id: 1)
variable update delay
Delay (mSec) 1000

OptoScript Block: Update variable values (Id: 1)
Exit to: Delay 1 sec (Id: 0)

```
// This block assigns sensor readings to variables

//For bell jar 1, if online
if (bJar1 == 1) then
```

```
   Ta[0] = 1.01* TC1_avg – 0.53;
   Tl[0] = 1.35* IR1_avg-21.96;   // Leaf temperature, IR sensors
   RH[0] = 23.9* rh1_avg-21.96; //Relative humidity
   Prsr[0] = prsr1_avg * 18.99 + 9.41;  //Pressure
   CO2[0] = 4645 * RaiseEToPower(-0.0208 * Prsr[0]) * co21_avg + (0.2486 * Prsr[0] *
        Prsr[0] - 33.492 * Prsr[0] + 656.87);   //Carbon dioxide
   O2[0] = 158.6 * power(Prsr[0],-0.9783) * o21_avg;   //Oxygen
   weight[0] = 88.334 * (1000 * lc1_avg) - 182.39 + offset[0];   //Plant weight
 else
   Ta[0] = 0;   // Air temperatures, T thermocouples
   Tl[0] = 0;   // Leaf temperature, IR thermocouples
   RH[0] = 0; //Relative humidity
   Prsr[0] = 0;  //Pressure
   CO2[0] = 0;   //Carbon dioxide
   O2[0] = 0;   //Oxygen
   weight[0] = 0;   //Plant weight
endif

//For bell jar 2, if online
if (bjar2 == 1) then
  Ta[1] = 1.01 * TC2_avg - 0.88;   // Air temperatures, T thermocouples
  Tl[1] = IR2_avg * 1.29 + IRoffset_2;   // Leaf temperature, IR sensors
  RH[1] = rh2_avg* 23.7 - 21.9; //Relative humidity
  Prsr[1] = prsr2_avg * 19.06 + 9.30;  //Pressure
  CO2[1] = 2791 * RaiseEToPower(-0.0184 * Prsr[1]) * co22_avg + (0.05586 * Prsr[1]
        * Prsr[1]-8.2642 * Prsr[1]+300);   //Carbon dioxide
  O2[1] = 148.7 * power(Prsr[1],-0.9872) * o22_avg;   //Oxygen
  weight[1] = 85.351 * (1000 * lc2_avg) - 677.06 + offset[1];   //Plant weight
else
  Ta[1] = 0;   // Air temperatures, T thermocouples
  Tl[1] = 0;   // Leaf temperature, IR thermocouples
  RH[1] = 0; //Relative humidity
  Prsr[1] = 0;  //Pressure
  CO2[1] = 0;   //Carbon dioxide
  O2[1] = 0;   //Oxygen
  weight[1] = 0;   //Plant weight
endif

//For bell jar 3, if online
if (bjar2 == 1) then
  Ta[2] = TC3_avg - 0.25;   // Air temperatures, T thermocouples
  Tc[2] = TC4_avg;   // Coil temperature, T thermocouples
  Tl[2] = IR3_avg * 1.2696 + IRoffset_3;   // Leaf temperature, IR sensors
  RH[2] = rh3_avg* 23.9 - 21.4; //Relative humidity
  Prsr[2] = prsr3_avg * 22.53+8.74;  //Pressure
  CO2[2] = 4547 * RaiseEToPower(-0.0254 * Prsr[2]) * co23_avg + (0.0857 * Prsr[2] *
```

```
        Prsr[2]- 11.429 * Prsr[2]+418.1);   //Carbon dioxide
  O2[2] = 146.0 * power(Prsr[2],-0.9893) * o23_avg;   //Oxygen
  weight[2] = 79.928 * (1000 * lc3_avg) - 263.4 + offset[2];   //Plant weight
else
  Ta[2] = 0;   // Air temperatures, T thermocouples
  Tl[2] = 0;   // Leaf temperature, IR thermocouples
  RH[2] = 0; //Relative humidity
  Prsr[2] = 0;  //Pressure
  CO2[2] = 0;   //Carbon dioxide
  O2[2] = 0;   //Oxygen
  weight[2] = 0;   //Plant weight
endif
```

Fan Control Routine

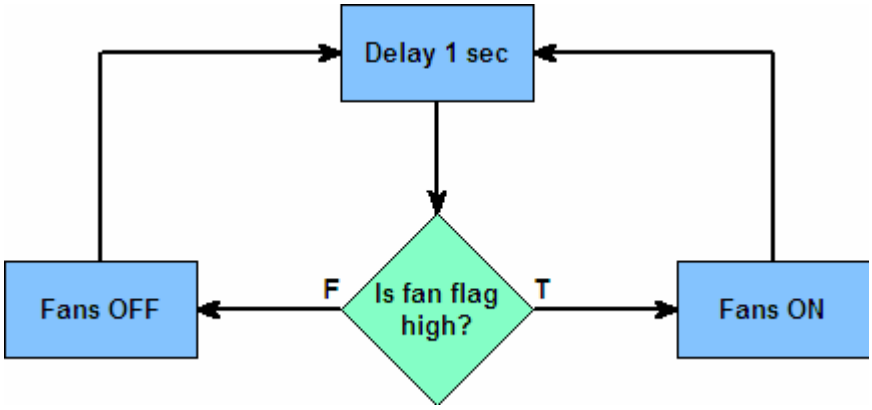

Action Block: Delay 1 sec (Id: 0)
Exit to: Is fan flag high? (Id: 3)
Delay (Sec) 1.0

Action Block: Fans OFF (Id: 7)
Exit to: Delay 1 sec (Id: 0)
turn fans off
Turn Off doFans

Action Block: Fans ON (Id: 2)
Exit to: Delay 1 sec (Id: 0)
turn fans on
Turn On doFans

Condition Block: Is fan flag high? (Id: 3)
Operator Type: AND

TRUE Exit to: Fans ON (Id: 2)
FALSE Exit to: Fans OFF (Id: 7)

Is bFans
Variable True?

Carbon Dioxide and Pressure Control

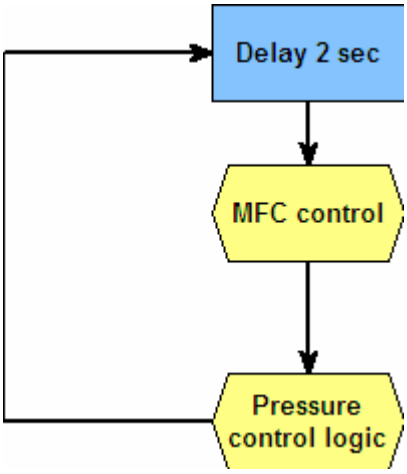

Action Block: Delay 2 sec (Id: 0)
Exit to: MFC control (Id: 4)
Delay (Sec) 2.0

OptoScript Block: MFC control (Id: 4)
Exit to: Pressure control logic (Id: 27)

// If CO2 addition needed, turn on MFC for calculated time

```
////// Bell jar 1 //////
if (bJar1) then
  if (hasdowntimerexpired(dtdiffusion_0)) then
    if (CO2_set[0] - CO2[0] > 40) then
      // Toggle flags for user interface
      bCO2[0] = 1;    // Raise CO2 flag for bell jar 1
      bMFC = 1;     // Raise mass flow controller flag
      // Set MFC flow rate and timer
      Q = (Prsr[0]/10) * 5;
      // If CO2 setpoint is 160 ppm or more > actual CO2,
      //only try to fill to 90%
      if (CO2_set[0] - CO2[0] > 160) then
```

```
      MFCtime[0] = (CO2_set[0] - CO2[0])*0.9/40;
     else
      MFCtime[0] = 1.0;
     endif
    // Open appropriate solenoids and start mass flow
    //controller and timer
    turnon(doBJsol_0);   // Open bell jar solenoid
    setdowntimerpreset(MFCtime[0] , dtMFC_0); // Set timer
    turnon(doCO2);    // Open CO2 solenoid
    aoMFC = Q/10;    // Turn on MFC at specified flow rate
    starttimer(dtMFC_0);  // Start timer
    // Wait while timer counts down
    while (not hasdowntimerexpired(dtMFC_0))
     delaymsec(100);
    wend
    // Close solenoids and turn off MFC after timer
    //expires
    aoMFC = -1.0;  // Turn off MFC
    turnoff(doCO2);  // Close CO2 solenoid
    turnoff(doBJsol_0);  // Close bell jar solenoid
    bCO2[0] = 0;
    bMFC = 0;
    // Set down timer to allow for CO2 diffusion before
    //adding more
    setdowntimerpreset(60.0, dtdiffusion_0);
    starttimer(dtdiffusion_0);
   endif
  endif
 endif

////// Bell jar 2 //////
if (bJar2) then
 if (hasdowntimerexpired(dtdiffusion_1)) then
  if (CO2_set[1] - CO2[1] > 40) then
   // Toggle flags for user interface
   bCO2[1] = 1;    // Raise CO2 flag for bell jar 2
   bMFC = 1;     // Raise mass flow controller flag
   // Set MFC flow rate and timer
   Q = (Prsr[1]/10) * 5;
   // If CO2 setpoint is 160 ppm or more > actual CO2,
   //only try to fill to 90%
   if (CO2_set[1] - CO2[1] > 160) then
    MFCtime[1] = (CO2_set[1] - CO2[1])*0.9/40;
   else
    MFCtime[1] = 1.0;
   endif
```

```
   // Open appropriate solenoids and start mass flow
   //controller and timer
   turnon(doBJsol_1);   // Open bell jar solenoid
   setdowntimerpreset(MFCtime[1], dtMFC_1);  // Set timer
   turnon(doCO2);    // Open CO2 solenoid
   aoMFC = Q/10;    // Turn on MFC at specified flow rate
   starttimer(dtMFC_1);  // Start timer
   // Wait while timer counts down
   while (not hasdowntimerexpired(dtMFC_1))
     delaymsec(100);
   wend
   // Close solenoids and turn off MFC after timer expires
   aoMFC = -1.0;  // Turn off MFC
   turnoff(doCO2);  // Close CO2 solenoid
   turnoff(doBJsol_1);  // Close bell jar solenoid
   bCO2[1] = 0;
   bMFC = 0;
   // Set down timer to allow for CO2 diffusion before
   //adding more
   setdowntimerpreset(60.0, dtdiffusion_1);
   starttimer(dtdiffusion_1);
  endif
 endif
endif

////// Bell jar 3 //////
if (bJar3) then
 if (hasdowntimerexpired(dtdiffusion_2)) then
  if (CO2_set[2] - CO2[2] > 40) then
   // Toggle flags for user interface
   bCO2[2] = 1;    // Raise CO2 flag for bell jar 3
   bMFC = 1;     // Raise mass flow controller flag
   // Set MFC flow rate and timer
   Q = (Prsr[2]/10) * 5;
   // If CO2 setpoint is 160 ppm or more > actual CO2,
   //only try to fill to 90%
   if (CO2_set[2] - CO2[2] > 160) then
   MFCtime[2] = (CO2_set[2] - CO2[2])*0.9/40;
  else
   MFCtime[2] = 1.0;
  endif
   // Open appropriate solenoids and start mass flow
   //controller and timer
   turnon(doBJsol_2);   // Open bell jar solenoid
   setdowntimerpreset(MFCtime[2], dtMFC_2);   // Set timer
   turnon(doCO2);    // Open CO2 solenoid
```

```
  aoMFC = Q/10;    // Turn on MFC at specified flow rate
  starttimer(dtMFC_2);  // Start timer
  // Wait while timer counts down
  while (not hasdowntimerexpired(dtMFC_2))
    delaymsec(500);
  wend
  // Close solenoids and turn off MFC after timer expires
  aoMFC = 0;  // Turn off MFC
  turnoff(doCO2);  // Close CO2 solenoid
  turnoff(doBJsol_2);  // Close bell jar solenoid
  bCO2[2] = 0;
  bMFC = 0;
  // Set down timer to allow for CO2 diffusion before
  //adding more
  setdowntimerpreset(60.0, dtdiffusion_2);
  starttimer(dtdiffusion_2);
 endif
endif
endif
```

OptoScript Block: Pressure control logic (Id: 27)
Exit to: Delay 2 sec (Id: 0)

```
// Turn on vacuum pump if pressure greater than setpoint

////// Bell Jar 1 //////
if (bJar1) then
  repeat
  if (prsr[0] > prsr_set[0] + 3) then
    turnon(doBJsol_0);    // Open solenoids for bell jars
    //if pressure too high
    bVac = 1;   // Raise vacuum pump control
    bVacSol[0] = 1; // Raise vacuum flags for user
    //interface
  elseif (prsr[0] < prsr_set[0]) then
    turnoff(doBJsol_0);   // Close solenoids for bell
          //jars if pressure too high
    bVacSol[0] = 0;
    bVac = 0;
  endif

  // Turn vacuum pump ON if needed
  if (bVac) then
    turnon(doVacSol);     // Open vacuum pump solenoid
    turnon(doPump);     // Vacuum pump
```

```
  endif

  until (not bVac);
  //If bell jar is offline, close solenoids
 elseif (not bJar1) then
  turnoff(doBJsol_0);
  bVacSol[0] = 0;
 endif

 // Turn OFF vacuum pump and lower flags when no longer
 //needed

 turnoff(doPump);    // Vacuum pump
 bVacSol[0] = 0;  // Vacuum solenoid flags for user
 //interface
 bVac = 0;  // Vacuum pump control flag


 ////// Bell Jar 2 //////
 if (bJar2)then
  repeat

  if (prsr[1] > prsr_set[1] + 3) then
   turnon(doBJsol_1);    // Open solenoids for bell jars
   //if pressure too high
   bVac = 1;   // Raise vacuum pump control
   bVacSol[1] = 1;   // Raise vacuum flags for user
   //interface
  elseif (prsr[1] < prsr_set[1]) then
   turnoff(doBJsol_1);   // Close solenoids for bell
   //jars if pressure too high
   bVacSol[1] = 0;
   bVac = 0;
  endif

  // Turn vacuum pump ON if needed
  if (bVac) then
   turnon(doVacSol);     // Open vacuum pump solenoid
   turnon(doPump);     // Vacuum pump
  endif

  until (not bVac);

  //If bell jar is offline, close solenoids
elseif (not bJar2) then
    turnoff(doBJsol_1);
```

```
    bVacSol[1] = 0;
endif

// Turn OFF vacuum pump and lower flags when no longer
//needed

turnoff(doPump);    // Vacuum pump
bVacSol[1] = 0;  // Vacuum solenoid flags for user
//interface
bVac = 0;  // Vacuum pump control flag


////// Bell Jar 3 //////
if (bJar3)then
  repeat

  if (prsr[2] > prsr_set[2] + 3) then
    turnon(doBJsol_2);    // Open solenoids for bell jars
    if pressure too high
      bVac = 1;   // Raise vacuum pump control
      bVacSol[2] = 1;   // Raise vacuum flags for user
      //interface
    elseif (prsr[2] < prsr_set[2]) then
      turnoff(doBJsol_2);   // Close solenoids for bell
      //jars if pressure too high
      bVacSol[2] = 0;
      bVac = 0;
    endif

    // Turn vacuum pump ON if needed
    if (bVac) then
      turnon(doVacSol);     // Open vacuum pump solenoid
      turnon(doPump);     // Vacuum pump
    endif

    until (not bVac);

    //If bell jar is offline, close solenoids
elseif (not bJar3) then
    turnoff(doBJsol_2);
    bVacSol[2] = 0;
endif

// Turn OFF vacuum pump and lower flags when no longer
//needed
```

turnoff(doPump); *// Vacuum pump*
bVacSol[2] = 0; *// Vacuum solenoid flags for user*
//interface
bVac = 0; *// Vacuum pump control flag*
turnoff(doVacSol); *// Close vacuum pump solenoid*

Temperature and Relative Humidity Control

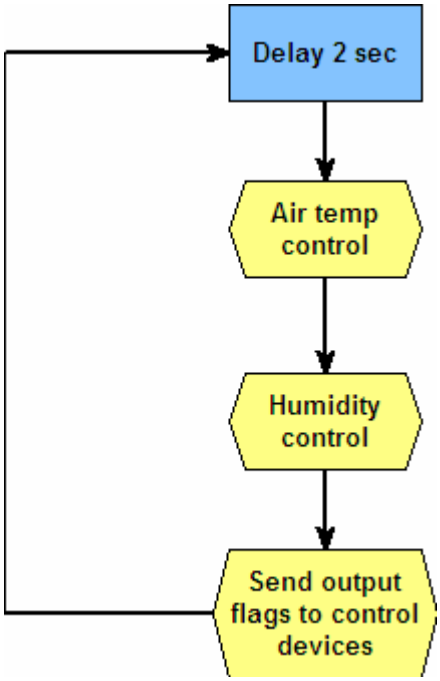

Action Block: Delay 2 sec (Id: 0)
Exit to: Air temp control (Id: 14)
Control delay
Delay (Sec) 2.0

OptoScript Block: Air temp control (Id: 14)
Exit to: Humidity control (Id: 20)

// If Tair greater than setpoint temp, turn cooling coil ON
bCoil = 0;

for j = 0 to 2 step 1

if (Ta[j] > T_set[j] + 0.5) then
  bCoil = 1;
endif

```
next

// If Tair less than setpoint temp, turn heater ON
for j = 0 to 2 step 1

if (Ta[j] < T_set[j] - 0.5) then
  bHeater[j] = 1;
elseif (Ta[j] > T_set[j]) then
  bHeater[j] = 0;
endif

next
```

OptoScript Block: Humidity control (Id: 20)
Exit to: Send output flags to control devices (Id: 21)

```
// If RH greater than setpoint RH, turn cooling coil ON

for j = 0 to 2 step 1

if (RH[j] > RH_set[j] + 4) then
  bCoil = 1;
endif

next

// If RH less than setpoint RH, turn humidifier ON

for j = 0 to 2 step 1

if (RH[j] < RH_set[j] - 4) then
  bHumidifier[j]=1;
else
  bHumidifier[j]=0;
endif

next
```

OptoScript Block: Send output flags to control devices
Exit to: Delay 2 sec (Id: 0)

```
if (bManual == 0) then
  // Automatic cooling coil and heater control

  if (bJar1 or bJar2 or bJar3) then
    // Turn coil ON/OFF as needed
```

```
if (bCoil) then
  turnon(doCoil);
else
  turnoff(doCoil);
endif

// If bell jar is ON, turn heaters and humidifiers
//ON/OFF as needed

//// Bell Jar 1 ////
// Heater control
if (bJar1) then
  if (bHeater[0]) then
    turnon(doHeater_0);
  else
    turnoff(doHeater_0);
  endif

  // Humidifier control
  if (bHumidifier[0]) then
    turnon(doHumidifier_0);
  else
    turnoff(doHumidifier_0);
  endif

endif

//// Bell Jar 2 ////
// Heater control
if (bJar2) then
  if (bHeater[1] and not bHeater[0]) then
    turnon(doHeater_1);
  else
    turnoff(doHeater_1);
  endif

  // Humidifier control
  if (bHumidifier[1]) then
    turnon(doHumidifier_1);
  else
    turnoff(doHumidifier_1);
  endif
endif

//// Bell Jar 3 ////
// Heater control
```

```
  if (bJar3) then
    if(bHeater[2]and not bHeater[0]and not bHeater[1])
      then
      turnon(doHeater_2);
    else
      turnoff(doHeater_2);
    endif

    // Humidifier control
    if (bHumidifier[2]) then
      turnon(doHumidifier_2);
    else
      turnoff(doHumidifier_2);
    endif
  endif

 endif

else

// Manual override of cooling coil, humidifiers, and eaters

 if (bCoil_man) then
  turnon(doCoil);
 else
  turnoff(doCoil);
 endif

 if (bHumidifier_man[0]) then
  turnon(doHumidifier_0);
 else
  turnoff(doHumidifier_0);
 endif

 if (bHumidifier_man[1]) then
  turnon(doHumidifier_1);
 else
  turnoff(doHumidifier_1);
 endif

 if (bHumidifier_man[2]) then
  turnon(doHumidifier_2);
 else
  turnoff(doHumidifier_2);
 endif
```

```
  if (bHeater_man[0]) then
    turnon(doHeater_0);
  else
    turnoff(doHeater_0);
  endif

  if (bHeater_man[1]) then
    turnon(doHeater_1);
  else
    turnoff(doHeater_1);
  endif
  if (bHeater_man[2]) then
    turnon(doHeater_2);
  else
    turnoff(doHeater_2);
  endif

endif


// Turn off heater and humidifier if bell jar is offline
if(not bJar1) then
  turnoff(doHeater_0);
  turnoff(doHumidifier_0);
endif

if(not bJar2) then
  turnoff(doHeater_1);
  turnoff(doHumidifier_1);
endif

if(not bJar3) then
  turnoff(doHeater_2);
  turnoff(doHumidifier_2);
endif

if (not bJar1 or not bJar2 or not bJar3) then
  turnoff(doCoil);
endif
```

APPENDIX E
EVAPOTRANSPIRATION MODEL

The evapotranspiration model, including calculation of external and surface resistance, was implemented in Matlab (Release 13, Mathworks, Natick, MA).

Following is the code for the evapotranspiration model.

```
clc
clear

% Input variables
LAI = 1.0;       % Leaf area index
L = 0.127;     % Characteristic length of leaf, m
Patm = 10:5:101; % Atmospheric pressure, kPa
Ri = 95;       % Incident radiation, W/m^2
Ta = 25 + 273.15; % Ambient temperature, K
Tsur = 24 + 273.15; % Temperature of surroundings, K
VPD = 0.75;    % Air vapor pressure deficit, kPa
u = 1.3;       % Air velocity, m/s
rsref = 28;    % Reference rs at low PAR, s/m

% Constant air properties
mu = 184.6e-7;   % Dynamic viscosity, N s/ m^2
k = 0.0263;      % Thermal conductivity of air, W/m K
Cp = 1.007;      % Specific heat of air constant P, kJ/kg K
R = 287.05;      % Gas constant, J/kg K
g = 9.81;        % Gravitational constant, m/s^2

for i = 1:length(Patm)

% Estimate leaf temperature
Tl(i) = (0.0634.*Patm(i)+19.34) + 273.15;  % Leaf temp, K

%%%%% Calculate canopy external resistance %%%%%

% Calculate pressure and temperature dependent air
```

```
% properties
rho(i) = (Patm(i)*1000)/(R*Ta);  % Air density, kg/m^3
v(i) = mu/rho(i);            % Kinematic viscosity, m^2/s
alpha(i) = k/(rho(i)*Cp*1000); % Thermal diffusivity, m^2/s
beta = 1/Ta;      % Coefficient of thermal expansion, K^-1

% Calculate dimensionless numbers
Re(i) = rho(i)*u*L/mu;  % Reynold's number
Pr(i) = v(i)/alpha(i);  % Prandtl number
Gr(i) = g*beta*abs(Tl(i)-Ta)*L^3./(v(i)^2); %Grashof number
Ra(i) = Gr(i)*Pr(i);  % Rayleigh number

% Does forced or free convection dominate? Free = 0; Forced % = 1; Mixed = 2
   check(i) = Gr(i)/Re(i)^2;
   x(i) = abs(1-check(i));
   if x(i) > 0.9
      if check(i) > 1
         conv(i) = 0;
      else
         conv(i) = 1;
      end
   else
      conv(i) = 2;
   end

% Calculate Nusselt number based on dominate HT mode
   if conv(i) == 1
      % Forced convection dominates
                  % Average Nusselt number for laminar flow
       Nu(i) = 0.664*Re(i)^(1/2).*Pr(i)^(1/3);
   elseif conv(i) == 0
      % Free (natural) convection dominates
      L = 0.0105;
      Nu(i) = 0.59*Ra(i)^0.25;  % Nusselt number for
       % upper surface of a heated plate (from
                  % Incropera and DeWitt, 1996)
   else
      % Mixed convection dominates
      Nu(i) = 0.37.*(Gr(i)+6.92.*Re(i).^2)^(0.25);
            % Stanghellini (1987)
   end

% Calculate external resistance
rh_leaf(i) = L/(alpha(i)*Nu(i));
rh(i) = rh_leaf(i)/(2*LAI);
```

```
%%%%% Calculate surface resistance %%%%%
rs(i) = rsref.*Patm(i)./101.3;

%%%%% Calculate rate of ET %%%%%

% Psychrometric parameters
lambda = 2442; % Latent heat of vaporization at 25 C, kJ/kg
delta = 184; %Slope sat vapor pressure curve at 25 C, Pa/C
gamma(i) = 1000*Patm(i).*Cp./(0.622.*lambda);
% Psychrometric constant, Pa/C

% Calculate net radiation
Rn(i) = (1-0.27).*Ri + 5.67e-8.*0.9.*(Tsur.^4-Tl(i).^4);

% Calculate LE, W/m^2
LE(i) = (delta.*Rn(i) + 1000^2.*rho(i).*Cp.*VPD./rh(i))./(delta + gamma(i).*(1 +
  rs(i)./rh(i)));

% Calculate ET, g/m^2/min
ET(i) = LE(i).*60./lambda;

end

% Plot model vs. actual data
Pact = [12 12 12 33 33 33 66 66 66 101 101 101];
ETact = [3.37 2.81 2.89 2.78 2.75 2.45 2.41 2.53 2.55 2.64 2.57 2.41];
plot(Patm,ET, Pact, ETact, 'o'), xlabel('Pressure (kPa)'), ylabel('Evapotranspiration (g m^-
2 min^-1)')

% Display results on screen
```

BIOGRAPHICAL SKETCH

Erin Georgette Wilkerson was born on March 15, 1977, in East Tennessee. She is the daughter of George and Lawana Wilkerson. Erin and her younger brother, Wesley, grew up on their family's beef and tobacco farm in Union County, Tennessee. Since 2004 the Wilkerson family has operated a 40-cow dairy farm near their home.

Erin was valedictorian of the Class of 1995 at Horace Maynard High School. She earned a B.S. degree in agricultural engineering from the University of Tennessee in 1999 and a M.S. degree in biosystems and agricultural engineering from the University of Kentucky in 2002.